Photoelectron Spectroscopy of Reactive Intermediates

Thesis by

Gary Hermann Kruppa

In Partial Fulfillment of the Requirements

for the Degree of

Doctor of Philosophy

California Institute of Technology

Pasadena, California

1988

(Submitted March 31, 1988)

ACKNOWLEDGEMENTS

First and foremost I would like to thank my advisor, Jack Beauchamp for his financial and moral support during the work that went into this thesis. His friendly management style, understanding of my cycling habit, and constant barrage of crazy and not-so-crazy ideas for research made the stay here interesting, stimulating and fun.

The Beauchamp group, present and past has been great fun to be a part of, and I thank everyone for the helpful discussions and fun that I've had with them over the years. In particular I'd like to thank Maggie Tolbert and all her sisters, Karl "Krazy Man" Irikura, Seung-Koo "Sleepy" Shin, David Dearden, and Bob Sweeney, mainly because they're still here and will expect to see their names in the acknowledgements.

I'd also like to thank the Southern California cycling community for providing me with an activity that helped keep me sane during the work here. Rick Denman, Alan Purnell, Chris Johnston, Sam Stavros and many others were a lot of fun to train and talk with.

Finally I'd like to thank my parents, without whose love and support I would never have gotten this far.

For my mother and father.

ABSTRACT

Photoelectron Spectroscopy (PES) has been used to investigate the structure and thermochemistry of a number of alkyl radicals and their corresponding carbonium ions. The radicals have been produced by flash vacuum pyrolysis of alkyl nitrites. The shape of the first band in the photoelectron spectrum of a free radical is related to the structural changes that take place in forming the carbonium ion from the radical. The ionization potentials obtained from the photoelectron spectra of the radicals are combined with gas phase ion thermochemistry data to obtain alkyl radical heats of formation. The thermochemical data thus obtained is used to discuss substituent and structural effects on the stability of radicals and carbonium ions. In many cases the thermolytic decomposition pathways of the alkyl radicals have been elucidated using PES. The application of the PES technique to the analysis of reactive intermediates present in heterogeneous thermolysis mixtures is also discussed.

Chapter 1 presents an introduction to the technique employed in these studies, and a review of the studies performed in this laboratory. Chapter 2 presents results on the thermochemistry and structure of the 1- and 2-adamantyl radicals. The tricyclic 1-adamantyl radical and carbonium ion are important as model bridgehead compounds, and the question of the amount of strain energy caused by the non-planarity of the radical and ion center has been of great interest. The first bands in the photoelectron spectra of the *o*-, *m*- and *p*-methylbenzyl radicals are presented in Chapter 3. The methyl substituent effects on the stabilities of the radicals and ions are discussed.

In Chapter 4 results on investigations of heterogeneous processes in Chemical Vapor Deposition (CVD) systems using the chlorosilanes as feed gases are discussed. $SiCl_2$ is found to be the major silicon containing reactive intermediate produced by surface reactions at 600 - 1100 ^{o}C in CVD systems using dichlorosilane and trichlorosilane as feed gases.

Chapter 5 presents the spectra of the 1- and 2-methylnaphthyl radicals. The relative stabilities of the radicals and carbonium ions are discussed based on proton affinities determined by Fourier transform mass spectrometric equilibrium studies, combined with ionization potentials obtained from photoelectron spectra of the radicals.

TABLE OF CONTENTS

CHAPTER 1
INTRODUCTION

Photoelectron Spectroscopic Studies of the Structure and Energetics of Carbon Centered Radicals and their Corresponding Carbonium Ions.

G. H. Kruppa and J. L. Beauchamp

Carbon centered free radicals and carbonium ions are important intermediates in a wide variety of organic reactions.[1a] Also, many important organic reactions are thought to involve transition states with a large degree of radical or ion character.[1b] The kinetics and product structures of reactions involving free radicals and carbonium ions are determined by the structure and thermochemistry of the intermediates. This account will focus on studies performed in our laboratory over the past decade on the use of photoelectron spectroscopy (PES) to investigate structure, reactivity, thermochemistry and unimolecular reactions of free radicals and their related carbonium ions.

INTRODUCTION

PES of Free Radicals . The apparatus employed in these studies, shown in Figure 1, was designed with special features to facilitate the study of free radicals produced by flash vacuum pyrolysis, some of which are discussed below. The instrument has been described in detail previously,[2] and only the salient features of the PES experiment will be described here. In the typical photoelectron experiment[3] (equations 1 and 2) a monochromatic photon beam from a HeI resonance lamp ($h\nu$ = 21.2 eV) is used to ionize a gaseous sample at pressures ranging from 10^{-4} to 10^{-3} torr. The kinetic energies $E_K(e^-)$ of the ionized electrons are measured and related to the ionization potential (IP) by equation 2. The lowest kinetic energy electrons observed in the photoelectron spectrum of a radical usually correspond to the adiabatic ionization potential (IP_a) of the

$$R\cdot + h\nu \rightarrow R^+ + e^- \qquad (1)$$

$$E_K(e^-) = h\nu - IP \qquad (2)$$

radical. The Franck-Condon principle applies to the photoionization process, which means that the most probable ionization process corresponds to a

Figure 1. (a) Diagram of the PES employed in these studies. Special features incorporated for the study of alkyl radicals are the differential pumping on the source chamber (via the 2" diffusion pump), which reduces the time between radical production and detection, and the pyrolyzer inlet. (b) Detail of the flash vacuum pyrolyzer. Ref. 14a.

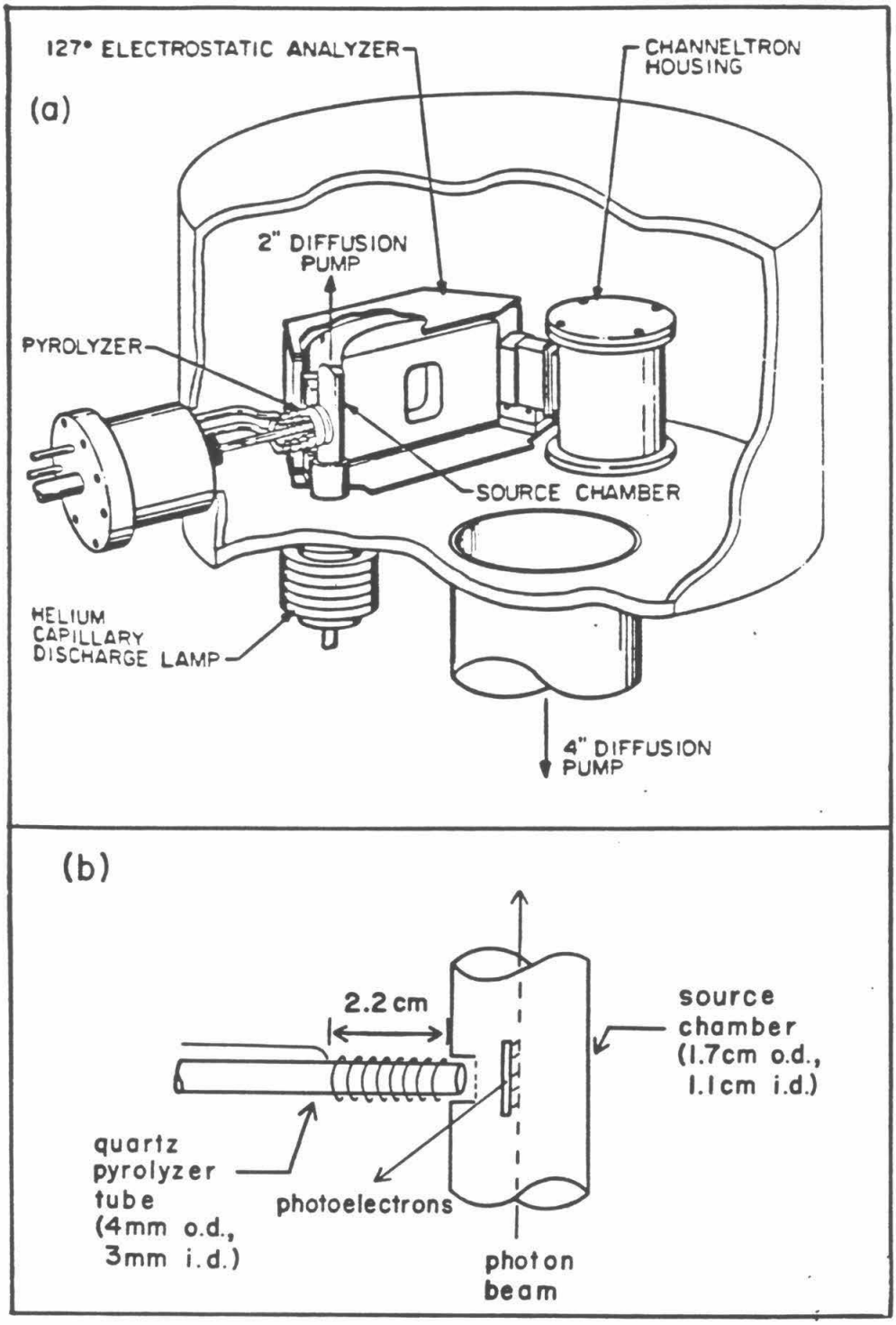
127° ELECTROSTATIC ANALYZER
CHANNELTRON HOUSING
(a)
2" DIFFUSION PUMP
PYROLYZER
SOURCE CHAMBER
HELIUM CAPILLARY DISCHARGE LAMP
4" DIFFUSION PUMP
(b)
2.2 cm
source chamber (1.7cm o.d., 1.1cm i.d.)
quartz pyrolyzer tube (4mm o.d., 3mm i.d.)
photoelectrons
photon beam

transition to an ionic state with geometry close to that of the radical ground state. The energy of this most probable process is known as the vertical ionization potential (IP_v). If the ground state of the radical and the carbonium ion have similar geometries, then the adiabatic and vertical ionization potentials coincide, and a single sharp peak is observed for the first band in the photoelectron spectrum of the radical (Figure 2, curve a). As an example of this type, Figure 2a also shows the photoelectron spectrum of the methyl radical.[4] Since the radical and carbonium ion have the same planar geometries[5] the photoelectron spectrum consists mainly of a single sharp peak. The weak vibrational structure is due to the difference in C-H bond force constants between the radical and ion, and the spectrum is discussed more fully in the section on radical geometries below.

If the ground state of the carbonium ion has a different geometry than the radical, then the vertical ionization potential will correspond to transitions to excited vibrational levels in the ion (Figure 2, curve b). In these cases a broad peak, often with resolved vibrational structure, is observed for the first band of the radical photoelectron spectrum. The most intense vibrational progressions observed in the photoelectron band will be those that correspond to the change in equilibrium geometry upon ionization. If an alkyl radical is non-planar, and the corresponding carbonium ion is planar, then the out-of-plane umbrella bending mode should be observed in the phototelectron spectrum of the radical. As an example, the photoelectron spectrum of the *tert*-butyl radical is shown in Figure 2b.[6] The *tert*-butyl radical is pyramidal, while the carbonium ion is planar.[6] The band is much broader than the methyl radical spectrum (the vibrational structure has been assigned to C-C vibrations and the out-of-plane umbrella mode) and is discussed fully in the section on radical geometries below.[7] In large alkyl radicals C-C and C-H bond lengths and bond angles may

Figure 2. Potential energy curves for a vibrational coordinate in a radical and ion, showing how vibrational modes are excited upon photoionization. Curve a illustrates a case where the radical and ion have the same equilibrium geometries, resulting in a sharp peak with little or no vibrational excitation. As an illustration of this case, the spectrum of the methyl radical is plotted next to curve a.[4,5] Curve b shows how the most probable transitions are to several vibrationally excited ionic states if the radical and ion have different equilibrium geometries. For an alkyl radical, several coordinates may change their equilibrium geometries, resulting in several vibrational progressions on a single band. The *tert*-butyl radical is pyramidal, while its carbonium ion is planar. The *tert*-butyl radical PES[6,7] is shown next to curve b, with vibrational structure discussed in the text.

(b)

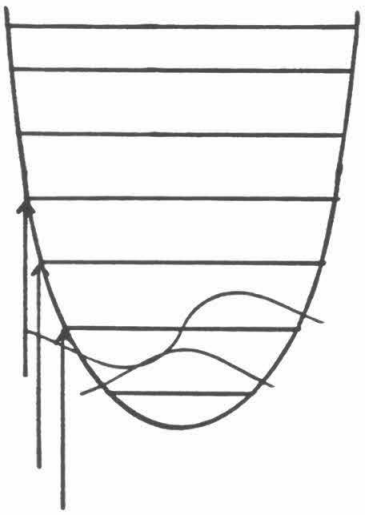

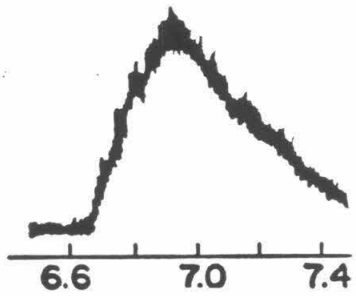

Ionization Potential (eV)

(a)

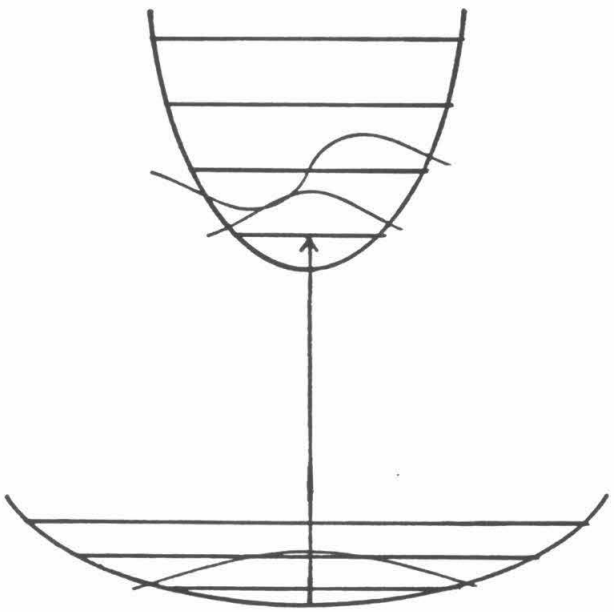

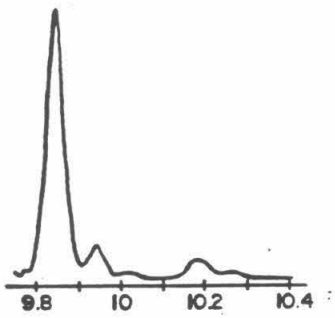

Ionization Potential (eV)

change in forming the equilibrium ion geometry from the radical geometry, causing excitation of stretching and bending modes that can overlap. The resolution in our PES instrument is 30 meV (242 cm^{-1}) at best, so that the overlapping vibrational modes expected in photoelectron spectra of large alkyl radicals often cannot be resolved, resulting in a smooth envelope for the photoelectron band. For smooth unresolved first photoelectron bands, useful information about the geometrical relationship between the radical and ion may still be extracted from the band shape.[3] Hence for the general ionization process 1, the spectrum of electron kinetic energies corresponding to ionization to the ground electronic state of R^+ contains information about the changes in geometry and force constants that occur in forming R^+ from $R\cdot$.

Finally, it should be noted that if the carbonium ion and radical have very different structures, then the Franck-Condon factor for ionization to the ground vibrational state of the ion will be small. The signal for processes resulting in the formation of ions that have structures rearranged from the radical structure will be unobservably weak. Therefore PES gives a "snapshot" of only those ion geometries which are close to the radical geometry before extensive rearrangement occurs. In cases where rearranged ion structures are possible, the information obtained by PES is often complementary to that obtained from photoionization and electron impact mass spectrometric appearance potential studies, where facile rearrangements occur in the time between ion formation and detection.[8] For example, the 1-butyl carbonium ion cannot be detected in the gas phase using mass spectrometry or in superacid media, because it rearranges spontaneously and without activation energy to the 2-butyl carbonium ion. Activation barriers for free radical rearrangements are generally higher than for carbonium ion rearrangements, so that radical precursors to the high energy

primary carbonium ions can be observed, both by ESR in solution and in the gas phase.[8] While the primary 1-butyl carbonium ion has never been observed in the gas phase or superacid media, it does exist as a *local* minimum in theoretical calculations of the C_4H_9+ energy surface (*tert*-butyl carbonium ion is the *global* minimum on the $C_4H_9^+$ energy surface),[9] and its heat of formation has been calculated. In PES the Franck-Condon factor for the formation of the 2-butyl carbonium ion from the 1-butyl radical would be extremely small, so IP of the 1-butyl radical obtained by PES corresponds to the formation of the primary ion (which rearranges *after* the photoionization event). The PES data on the 1-butyl radical and other primary radicals can thus provide data on structures that cannot be observed by other methods for comparison with theoretical results. For radicals which generate rearranged carbonium ions after photoionization, a broad band is observed for the first band in the photoelectron spectrum, and the true adiabatic ionization potential to the ionic ground state may not be observed in the spectrum. Cases where the true adiabatic ionization potential cannot be observed by PES can often be recognized by discrepancies in radical and ionic heats of formation calculated using the adiabatic IP (see discussion below), and theoretical predictions of ground state carbonium ion structures that are isomers of the radical structures.[9]

The photoelectron spectrum also yields the thermochemical relationship between the radical and ion. ΔH°_{298} for reaction 3 is simply IP_a derived from the first band of the photoelectron spectrum. In radical spectra with resolved

$$R\cdot \rightarrow R^+ + e^- \qquad (3)$$

vibrational progressions, the first vibrational peak is identified as the $0 \rightarrow 0$ transition and taken as IP_a. For bands with no resolved vibrational structure, IP_a is taken as the point where signal due to the radical first rises above the noise

level. If the heat of formation of the carbonium ion is known, the heat of formation of the radical can be calculated using IP_a. Carbonium ion heats of formation are often available from a variety of mass spectrometric techniques, such as photoionization appearance potential measurements.[10] Very accurate relative radical heats of formation can be determined from IP_a of the radicals if relative hydride affinities for the corresponding carbonium ions are available from mass spectrometric equilibria experiments.[11] This is shown by equations 4, 5 and 6. ΔH°_{298} for reaction 4 is the difference in IP_a of the two radicals which can be determined to within 0.5 kcal mol^{-1} by PES. ΔH°_{298} for reaction 5 is the difference in hydride affinities determined by mass spectrometry, typically with

$$R_1^+ + R_2\cdot \rightarrow R_1\cdot + R_2^+ \qquad (4)$$

$$R_1H + R_2^+ \rightarrow R_1^+ + R_2H \qquad (5)$$

$$R_1H + R_2\cdot \rightarrow R_1\cdot + R_2H \qquad (6)$$

error limits of 0.5 to 1.0 kcal mol^{-1}.[11] Adding equations 4 and 5 yields equation 6 which gives the relative C-H bond energies and, using the hydrocarbon heats of formation, the relative radical heats of formation to within 1 to 2 kcal mol^{-1}.

Photoelectron spectroscopy allows the *direct* detection of free radicals making it a useful technique to apply to the study of radical intermediates in thermolysis systems. In many studies of thermolytic decomposition pathways the reactive intermediates in the decomposition mechanism must be inferred from the observed stable products. Free radical scavengers and mass spectrometric sampling of thermolysis systems have been used to identify radicals that are important in thermolytic mechanisms.[12] In many cases the intermediates in thermolytic decompositions can be observed directly by photoelectron spectroscopy, thus confirming the mechanisms inferred from product analysis and radical scavenging methods. As will be shown below, PES can differentiate

isomeric radicals of the same mass, which is difficult to do using mass spectrometric sampling for the detection of radicals. PES has also been used to detect the gas phase radicals in heterogeneous catalysis, yielding information about the reactive intermediates in catalytic mechanisms.[13] Radicals produced by isomerization or decomposition of the nascent radical products are often observed in the photoelectron spectrum, resulting in data on the unimolecular reactions of free radicals. After a brief description of the methods used to produce radicals for study by PES, examples of the information about structure, thermochemistry, and reactions of carbon centered free radicals obtained by PES will be presented.

Free Radical Production by Flash Vacuum Pyrolysis. A detail diagram of the pyrolyzer employed in these studies is shown in Figure 1b. A quartz tube (3 mm i.d.) is wound noninductively with heater wire to give a region 2 cm in length that can be heated to 900 °C. The pressure in the quartz tube ranges from 1.0 to 100 millitorr, and the contact time of the gases with the heated region is about 1 msec. Most of the radicals studied were produced by pyrolysis of the appropriate alkyl nitrite (reactions 7 and 8). The alkyl nitrite pyrolysis proceeds efficiently at temperatures from 400 to 600 °C. Under these conditions, thermal activation of

$$RCH_2ONO \rightarrow RCH_2O\cdot + NO \quad (7)$$

$$RCH_2O\cdot \rightarrow R\cdot + CH_2O \quad (8)$$

the nitrite precursor results mainly from contact with the hot pyrolyzer walls. While the residence time in the pyrolyzer is short, and pressures are low, some of the initial radicals produced can suffer further energizing collisions on the surface or in the gas phase prior to intersecting the HeI photon beam, resulting in decomposition of the nascent radical products. At higher temperatures (500-750 °C) the yield of the nascent radical product is reduced and radical decomposition

product yields increase. The nascent radical product concentration is limited by radical recombination processes, and at higher temperatures by decomposition of the nascent radical product. The NO and CH_2O products give sharp peaks in the photoelectron spectrum that can be used for calibration, and to confirm that the pyrolysis is occurring as expected.

Detection Limits and Excited States of Carbonium Ions. Radicals have lower ionization potentials than stable molecules, so that their first photoelectron bands appear at higher kinetic energies than the precursor nitrites or other stable decomposition products. Because the radical signals occur in the low-noise high kinetic energy region of the photoelectron spectrum, small concentrations (1.0 - 0.1%) of radicals in complex mixtures can be detected. Since most free radicals have doublet ground states, removal of an electron can access *both* low lying singlet and triplet states of the corresponding carbonium ion. Bands due to ionization of the radicals to excited electronic states of the carbonium ion appear at lower electron energies (higher ionization potentials). Unfortunately these bands are often obscured by undecomposed precursor and stable pyrolysis products. Figure 3 shows a typical alkyl radical photoelectron spectrum, the benzyl radical,[2] produced by pyrolysis of phenethylnitrite, with bands due to NO and CH_2O identified. The feature at 9.60 eV is tentatively assigned to the $^3B_1$ state of the benzyl carbonium ion.

RADICAL AND CARBONIUM ION GEOMETRIES

The radicals studied to date in this laboratory are listed in Table 1.[14] The bonding at a Carbonium ion center typically involves sp^2 hybridization, and a preference for a planar geometry. In most cases the structure of the first photoelectron band of an alkyl radical is due to the changes in bond lengths and angles as the geometry changes to the planar sp^2 carbonium ion geometry upon

Figure 3. The photoelectron spectrum of the benzyl radical, showing the NO and CH_2O products from pyrolysis. The band marked $^3B_1$ is tentatively assigned to the $^3B_1$ excited state of the benzyl carbonium ion. Ref. 14a.

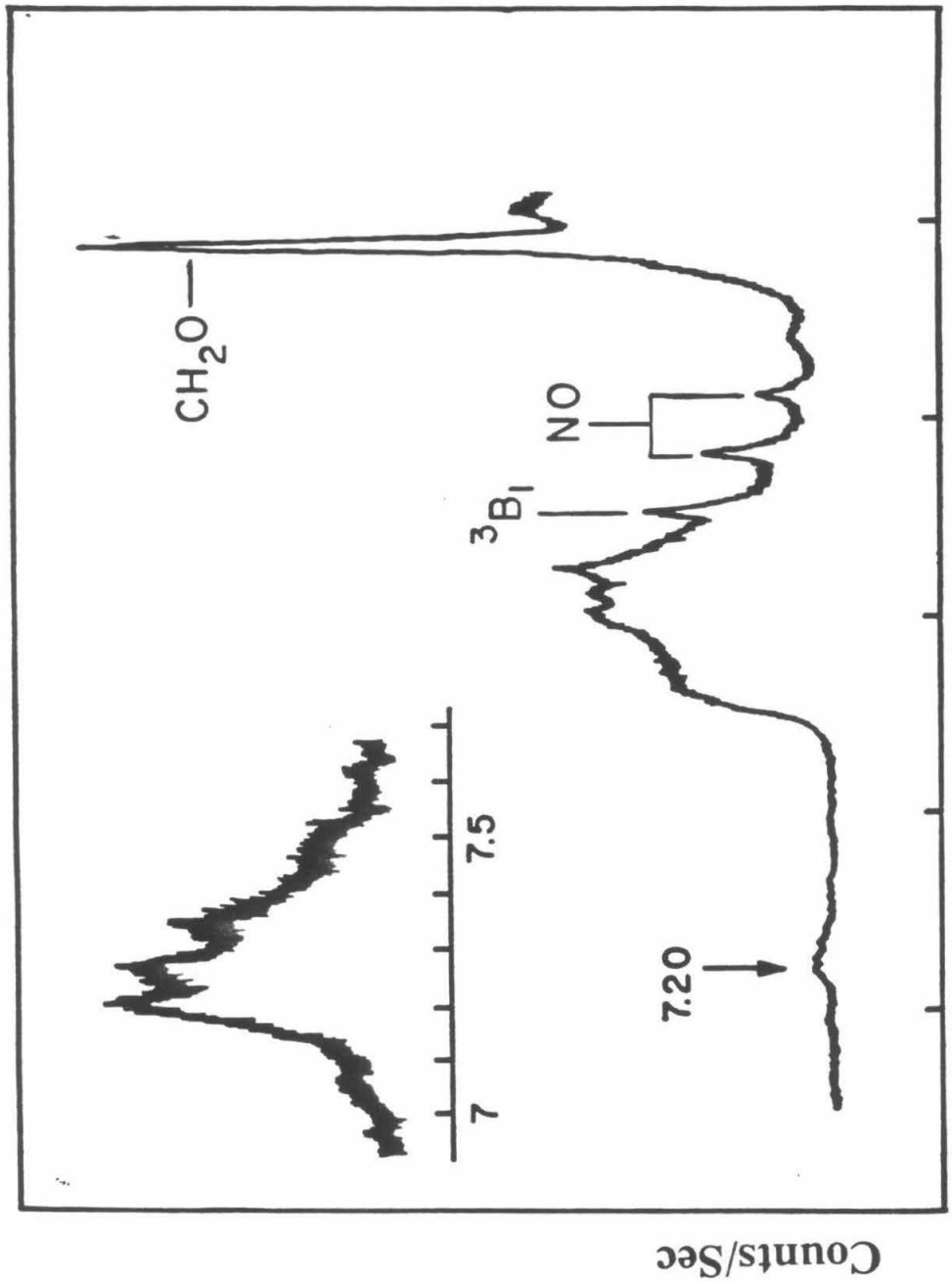
Counts/Sec
Ionization Potential (eV)
7
8
9
10
11
7.20
7
7.5
$^3B_1$
NO
CH_2O

Table 1. Thermochemical Data for Alkyl Radicals and Carbonium Ions Derived from PES.[a]

R	IP_a(eV) A	V	Vibrational Structure(cm^{-1})	$\Delta H_{f,298}^{o}[R]$	$\Delta H_{f,298}^{o}[R^+]$	$D^{o}_{298}[R\text{-}H]$	$D^{o}_{298}[R^+H^-]$
Primary[b]							
CH_3[c]	9.84	9.84	1380	34.8[d]	261.8	104.8	314.4
CD_3[e]	9.83	9.83	1050				
CH_3CH_2[e]	8.38	8.51	--	28.4[f]	215.6[g]	100.6	270.5
CH_3CD_2[e]	8.38	8.50	--				
$CH_3CH_2CH_2$[h]	8.15	8.43	540	24.0[i]	212.0	100.9	271.5
$CH_3CH_2CH_2CH_2$[h]	8.02	8.50	--	18.4	203.4	100.9[j]	268.4
1-n-pentyl[k]	8.13	8.50[l]	--	13.7	201.2	100.9[j]	271.0
1-n-hexyl[k]	8.10	8.49[l]	--	8.9	195.7	100.9[j]	270.3
1-n-heptyl[k]	8.10	8.49[l]	--	4.0	190.7	100.9[j]	270.3
$(CH_3)_2CHCH_2$[h]	7.93[a]	8.31	--	16.4	199.3	100.9[j]	266.4
$(CH_3)_3CCH_2$[h]	7.88[a]	8.25	--	8.5	190.2	100.9[j]	265.2
$CH_2{=}CHCH_2CH_2$[m]	8.04[a]	8.47	--	48.6	234.0	100.9[j]	268.9
Secondary							
$(CH_3)_2CH$[e]	7.36	7.69	730, 970	22.3[i]	192.0	99.2	251.5
2-n-butyl[h]	7.25	7.59	--	17.0[i]	184.2	99.5	249.2
cyclobutyl[m]	7.40	7.66	990	54.7[n]	225.3	100.0	253.2
cyclopentyl[o]	7.21	7.46	--	27.5[n]	193.7	98.0	246.9
cyclohexyl[o]	7.15	7.40	--	17.4[n]	182.3	99.0	246.5
2-adamantyl[p]	6.73	6.99	--	15.3	170.5	99.0[q]	236.8

Table 1. Continued.

R	IP_a(eV) A	V	Vibrational Structure(cm^{-1})	$\Delta H_{f,298}^{o}[R]$	$\Delta H_{f,298}^{o}[R^+]$	$D^{o}_{298}[R\text{-}H]$	$D^{o}_{298}[R^+H^-]$
Secondary (Cont'd.)							
2-n-pentyl [k]	7.22	--	--	12.3	178.8	99.5[r]	248.6
2-n-hexyl [k]	7.17	7.38	--	7.5	172.8	99.5[r]	247.4
2-n-heptyl [k]	7.17	7.41	--	2.6	167.9	99.5[r]	247.4
Tertiary							
$(CH_3)_3C$ [e]	6.70	6.92	450	12.4[i]	166.9	96.9	234.0
$(C_2H_5)(CH_3)_2C$ [p]	6.64	6.91	--	7.8	160.9	96.2	232.5[s]
methylcyclohexyl[x]	6.55	6.85	--	7.7[y]	158.7	96.9	230.4
1-adamantyl [p]	6.21	6.36	--	16.7	159.9	100.4	226.2[t]
Allylic and Benzylic							
$CH_2{=}CHCH_2$ [u]	8.13	8.13	420	41.5[n]	228.9	88.7	258.7
$CH_2{=}CHCHCH_3$ [m]	7.49	7.67	--	33.0[n]	205.7	84.9	240.6
$CH_2{=}C(CH_3)CH_2$ [m]	7.90	7.95	--	41.0[n]	223.1	89.1	262.1
$PhCH_2$ [u]	7.20	7.20	560	48.8[i]	214.5	88.9	237.5
$PhCD_2$ [u]	7.22	7.22	480				
ortho-methlbenzyl [v]	7.07	7.07	480	40.2	203.2	87.7	233.6[w]
meta-methylbenzyl [v]	7.12	7.12	490	40.2	204.4	88.2	234.7[w]
para-methylbenzyl [v]	6.96	6.96	400	40.2	200.3	88.0	230.8[w]

Table 1. Continued.

[a]All quantities except the IP_a are in kcal mol^{-1}. The IP_a data are in eV. Unless otherwise noted, the error limits are ± 1.5 kcal mol^{-1}. Ionic heats of formation were calculated using the convention that the heat of formation of an electron at rest is zero at all temperatures. Therefore, $\Delta H_f^o{}_{298}[H^-]$ = 34.7 kcal mol^{-1}. In each row (except ethyl) a value for $\Delta H_f^o{}_{298}[R]$ or $\Delta H_f^o{}_{298}[R^+]$ has been taken from literature sources (given in the footnotes) or derived from other assumptions (also given in the footnotes). All other values in the row are then derived from the literature value and the IP_a, using relations given in the text. [b]For all of the primary radicals except methyl, IP_a must be considered as an upper limit due to Franck-Condon considerations (see text). [c]Refs. 4, 6, 16. [d]Wagman, D. D.; Evans, W. H.; Parker, V. B.; Schumm, R. H.; Halow, I.; Bailey, S.M.; Churney, K. L.; Nuttall, R. L. *J. Phys. Chem. Ref. Data* **1982**, *11*, suppl 2. [e]Ref. 14b. [f]Ref. 37. [g]Ref. 34. [h]Ref. 14d. [i]Ref. 35. [j]These primary C-H bonds are assumed to be the same as the primary C-H bond in n-propyl ± 1.5 kcal mol^{-1}. [k]Ref. 14h. [l]Several different primary radicals may contribute to the primary radical band shape in these cases, so the IP_v should be considered approximate, see Ref. 14h. [m]Ref. 14e. [n]Corrected from experimental values given in Ref. 32 to be consistent with the higher values used for the small alkyl radicals from Ref. 35. [o]Ref. 14c. [p]Ref. 14f. [q]The 2-adamantyl C-H bond energy is assumed to be the same as the cyclohexyl C-H bond energy ± 1.5 kcal mol^{-1}. [r]These secondary C-H bond energies are assumed to be the same as the secondary C-H bond energy in n-butane ± 1.0 kcal mol^{-1}. [s]Relative hydride affinity from Ref. 11a. [t]Ref. 11d. [u]Ref 14a. [v]Ref 14g. [w]From relative chloride affinities in Ref. 11d, and see also the discussion in Ref. 14g. [x]Ref. 14i. [y]The tertiary C-H bond energy in methylcyclohexane is assumed to be the same as the tertiary C-H bond energy in isobutane ± 1.5 kcal mol^{-1}.

ionization. The alkyl radical geometries fall into several groups and these are discussed below.

Methyl, Benzyl and Allyl Radicals. These are the simplest cases to analyze, in which the radicals and carbonium ions have similar, planar geometries resulting in sharp first photoelectron bands with $IP_a = IP_v$. The photoelectron spectrum of the methyl radical, first obtained with its vibrational structure by Golob *et al.* [15] and later confirmed by others,[16] and shown in Figure 2a is a single sharp band which is strong evidence for a planar radical structure. This result is in agreement with results from optical spectroscopy,[17] matrix isolation infrared spectroscopy,[18] photoionization of CH_3^-, [19] and high level theoretical calculations.[20] The weak vibrational structure seen in the methyl radical spectrum has been fully assigned, and is due to the change in force constants in the C-H bonds (υ = 607 cm^{-1} for the C-H stretch in the radical and 1380 cm^{-1} in the ion), which produces small Franck-Condon factors for photoionization to excited vibrational levels of the ion.[4b] Ionization from υ = 0 vibrational level in the radical to the υ = 1 vibrational level in the ion is symmetry forbidden for planar radical and ion structures. The absence of the υ = 0 to υ = 1 transition in the photoelectron spectrum provides additional unambiguous evidence for the planarity of the radical. Shown in Figure 4 are the photoelectron spectra of the allyl and benzyl radicals, two π-type radicals.[14a] Vibrational structure is resolved in both the allyl and benzyl spectra, and $IP_a = IP_v$ in both cases, showing that the radicals and their corresponding ions have similar planar geometries. This result is consistent with ESR results for the allyl and benzyl radicals which show that they are planar, delocalized π-type radicals.[21] For benzyl the frequency of the observed vibrational progression in the photoelectron spectrum shows a dependence on isotopic substitution of D for H on the methylene group (see

Figure 4. (a) Photoelectron spectrum of the allyl radical, $IP_a = IP_v$ at 8.13 eV. (b) Photoelectron spectrum of the benzyl radical, $IP_a = IP_v$ at 7.20 eV. From ref. 14a.

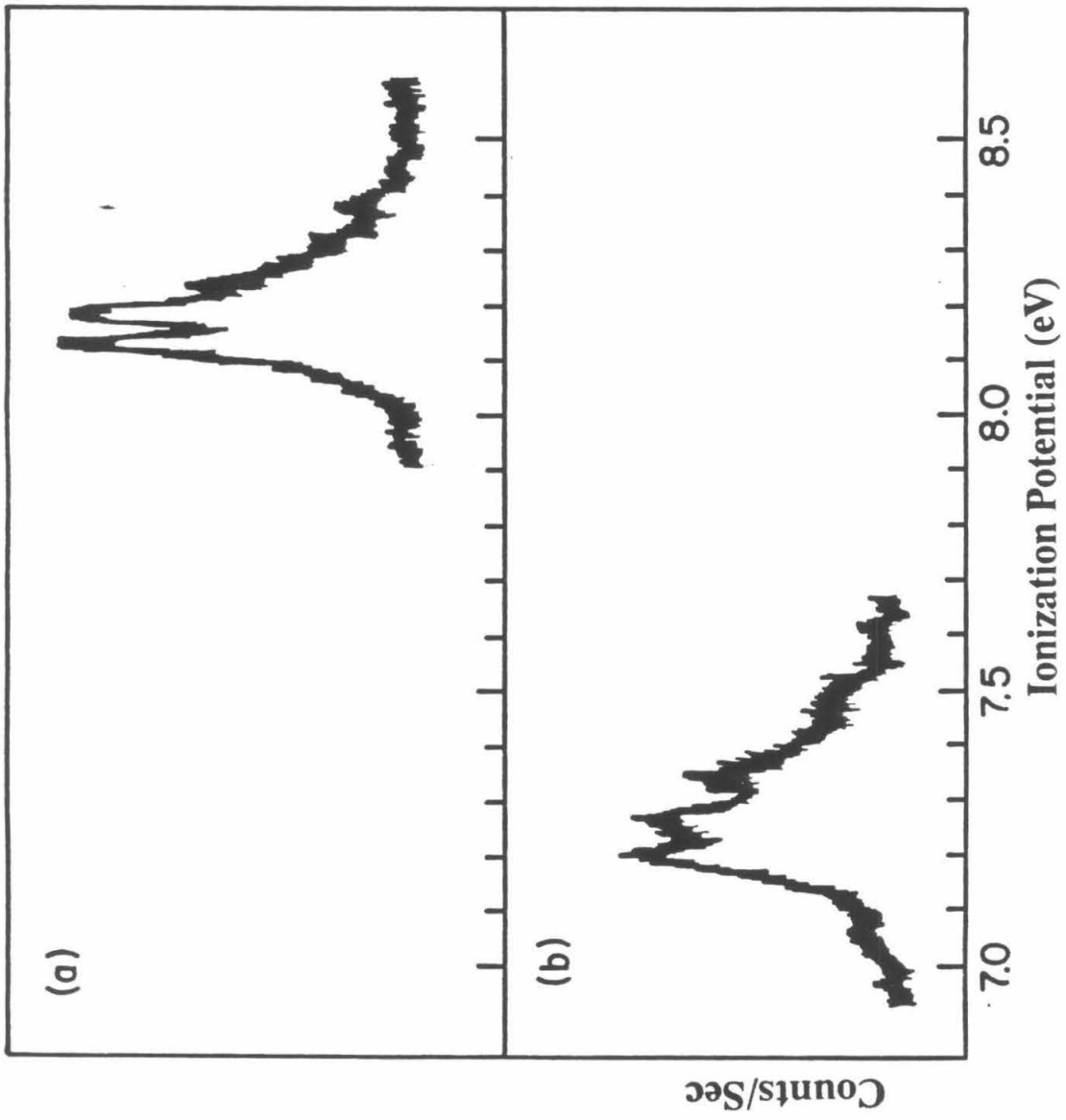
(a)
(b)
7.0
7.5
8.0
8.5
Ionization Potential (eV)
Counts/Sec

Table 1). This indicates that the vibration is probably excited by a geometry change involving the CH_2 group upon ionization. The vibrational progression was tentatively assigned to a combination of Ph-CH_2 C-C stretch and torsion modes, consistent with the planar radical and ion structures.[14a] These vibrational progressions are often difficult to assign even when IR spectroscopic data for the ions are available, and the reader is referred to the original papers for complete discussions of the observed vibrational progressions.

Ethyl and Larger Primary Radicals. Calculations and experiment have shown that the ethyl radical has a classical structure (I),[22] while calculations show that the ion has a hydrogen bridged structure (II).[9] Since the radical and ion have very different structures, the true adiabatic ionization potential may not be

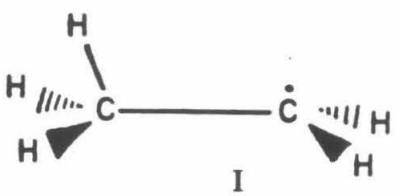

I

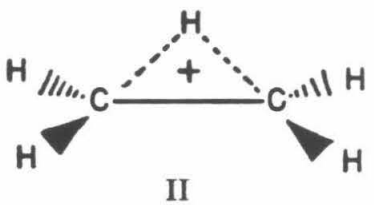

II

observed by PES. The spectra of the primary ethyl, n-propyl and n-butyl radicals are shown in Figure 5. The spectra are broad, and the true adiabatic IP is not observed in the ethyl spectrum as can be shown using thermochemical data discussed below. Reliable calculations indicate that, as for the ethyl carbonium ion, the only local minima for the primary n-propyl and n-butyl ions have non-classical hydrogen bridged structures.[9] By analogy with the ethyl radical, the adiabatic ionization potentials for all of the primary radicals listed in Table 1 must be regarded as upper limits to the true adiabatic ionization potential. Nevertheless, the photoelectron spectra of the primary radicals provide interesting insights into the ionic geometries that closely resemble the radicals and, as will be shown below, the difference in energy between the classical and

Figure 5. Photoelectron spectra of three primary radicals on identical energy scales. The adiabatic and vertical ionization potentials are indicated by arrows (values are given in Table 1). (a) Ethyl, ref. 14b. (b) 1-propyl, ref. 14d. (c) 1-n-butyl, ref. 14d.

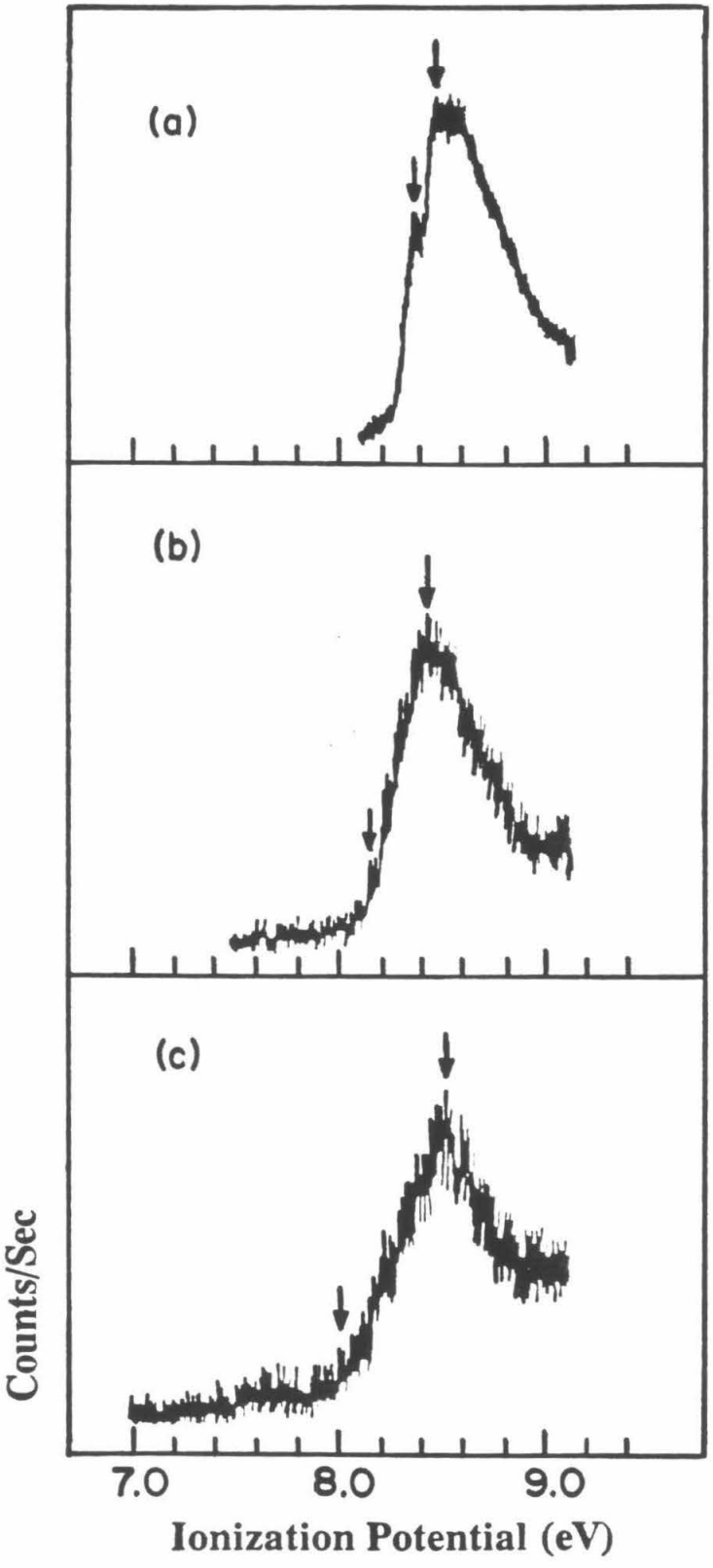
(a)
(b)
(c)
Counts/Sec
7.0
8.0
9.0
Ionization Potential (eV)

non-classical ion structures. The larger primary carbonium ions are known to rearrange spontaneously and have not been otherwise observed in the gas phase or solution.

Secondary Radicals. The secondary radicals listed in Table 1 have first photoelectron bands that are as broad as the larger primary radicals discussed above. However, in this case all available evidence indicates that IP_a derived from the PES of the secondary radicals is the true adiabatic ionization potential. As will be shown below, the adiabatic ionization potentials of the secondary radicals are consistent with the available thermochemical data for the radicals and ions. Also, theoretical calculations indicate that the isopropyl and 2-butyl cations have classical, planar structures.[9] The reason for the breadth of the first photoelectron bands of these radicals can be seen by considering the most stable conformers of the 2-butyl radical (III) and carbonium ion (IV) (the preferred radical geometry is from ESR data,[23] and the ionic geometry is from theoretical

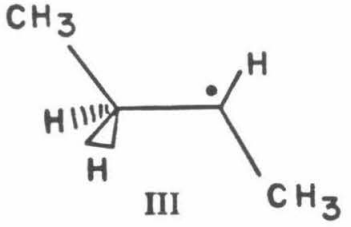

III

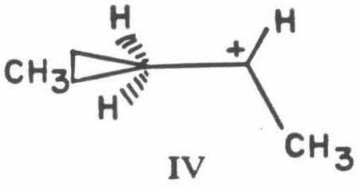

IV

results[9]). The secondary radicals generally have near planar configurations at the radical center, as do the secondary carbonium ions, but the bond lengths and angles are different between the ion and radical.[23] Therefore, even though the radical and ion have similar geometries, ionization is likely to excite a number of vibrations, including low frequency bending modes, internal rotations of the methyl groups, and the umbrella mode at the ionic center, resulting in the broad, weakly resolved vibrational envelope. Confirmation of this can be seen in Figure 6, where the isopropyl and 2-butyl radicals are plotted with the cyclohexyl and

Figure 6. Photoelectron spectra of four secondary radicals on identical energy scales. The adiabatic and vertical ionization potentials are indicated by arrows. (a) 2-propyl, ref. 14b. (b) 2-n-butyl, ref. 14d. (c) Cyclopentyl, ref. 14c. (d) 2-adamantyl, ref. 14f.

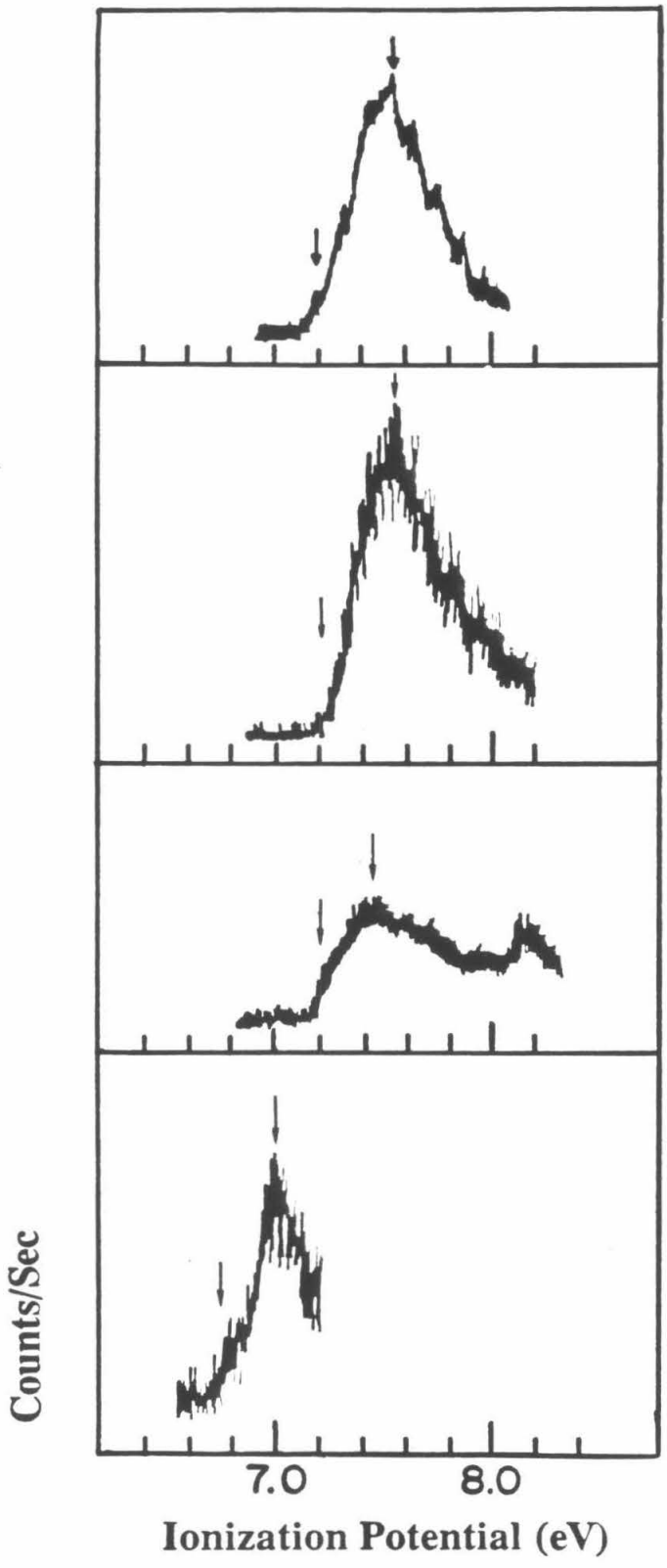
Counts/Sec
7.0
8.0
Ionization Potential (eV)

2-adamantyl radicals. Since the radicals are all nearly planar, the narrower bands (smaller difference between IP_a and IP_v) for the cyclic radicals are likely the result of the constraints of the ring which eliminate some of the bending and internal rotation modes available to the isopropyl and 2-butyl radicals and ions.

Tertiary Radicals. The spectra of three tertiary radicals are shown in Figure 7. The bands of the acyclic *tert*-butyl[14b] and *tert*-amyl[14f] radicals are somewhat narrower than the secondary radicals. The *tert*-butyl radical has been shown to be non-planar by theoretical[24] and ESR results.[25] Several measurements of the PES of the *tert*-butyl radical have been made,[14b,4a,26] and the vibrational progression on the *tert*-butyl first photoelectron band has been assigned to the umbrella bending mode and a C-C stretching vibration.[26] The constraints of the tricyclic ring system are apparent in the spectrum of the 1-adamantyl radical (V),[14f] which has a difference of only 0.15 eV between its IP_a and IP_v compared to 0.22 eV for *tert*-butyl and 0.27 eV for *tert*-amyl. The out-of-

V

plane angle is defined as the angle between the plane defined by the carbon at the radical center, C_1, with the two α-carbons, and the bond of C_1 with the remaining α-hydrogen (or carbon in the case of tertiary radicals). The smaller difference between IP_a and IP_v for the 1-adamantyl radical is primarily due to a smaller change in the out-of-plane angle upon ionization, as shown in Table 2.

The Isomeric C_4H_7 Radicals. The photoelectron spectra of the four isomeric C_4H_7 radicals are shown in Figure 8.[14e] A fifth possible isomer, the primary cyclopropylcarbinyl radical, could not be observed. Even at room

Figure 7. Photoelectron spectra of three tertiary radicals on identical energy scales. For ease of comparison of band shapes, the spectra have been plotted with the adiabatic ionization potentials aligned, and the abscissa is marked in eV above the IP_a. The adiabatic and vertical ionization potentials are indicated by arrows. (a) *tert*-butyl, ref. 14b. (b) *tert*-amyl, ref. 14f. (c) 1-adamantyl, ref. 14f.

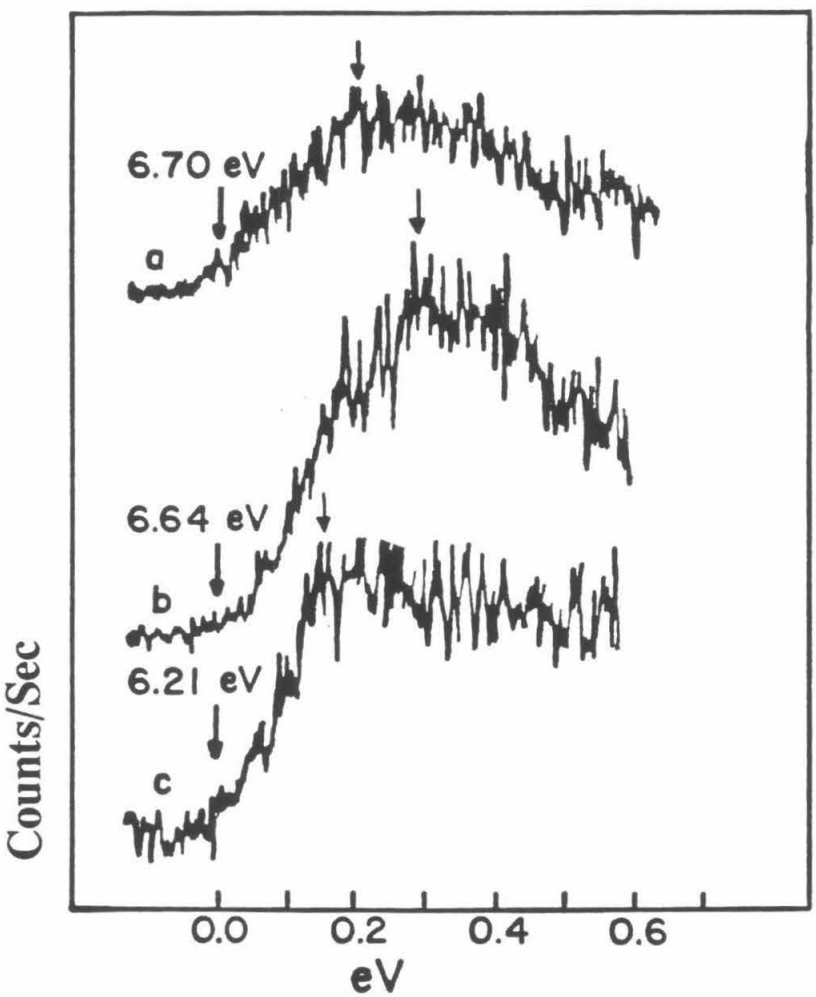
6.70 eV
a
6.64 eV
b
6.21 eV
c
Counts/Sec
0.0
0.2
0.4
0.6
eV

Table 2. Comparison of Out of Plane Angles γ for the *tert*-butyl and 1-adamantyl radicals and ions.[a]

	adamantyl	*tert*-butyl
γ(radical)	43.4°[b]	22.1°[e]
γ(ion)	29.6°[c]	0°
difference	13.8°	22.1°
$IP_a - IP_v$[f]	0.15 eV[d]	0.22 eV[g]

[a]See text on tertiary radical geometries for a definition of the out-of-plane angle γ. [b] Ref. 29. [c]Sunko, D. E.; Hirsl-Starcevic, S.; Pollack, S. K.; Hehre, W. J. *J. Am. Chem. Soc.* **1979**, *101*, 6163. [d]Ref. 14f. [e]Ref. 24. [f]The difference between the adiabatic and vertical ionization potentials for each radical. [g]Ref. 14b.

temperature the cyclopropylcarbinyl radical undergoes rapid ring opening to form the allylcarbinyl radical, which was observed when the nitrite precursor to cyclopropylcarbinyl radical was pyrolyzed.[14e] The 2-methylallyl radical (Figure 8a) shows a slight difference between IP_a and IP_v, which indicates that there is a slight geometry difference between the radical and ion. The 1-methylallyl radical (Figure 8b) is different from the rest of the π-type radicals in that it has a fairly broad band, which can arise from a number of factors. As was seen in the spectra of methyl and ethyl radicals, the addition of α methyl groups to an alkyl radical center causes the first photoelectron band to broaden due to changes in the α C-C bond length, and the methyl torsional angle upon ionization. The 1-methylallyl radical has both cis and trans isomers that would have slightly different IP_a values, and a mixture of the two isomers would also contribute to the width of the photoelectron band.[14e] The allylcarbinyl radical (Figure 8c) appears in the region typical for primary radicals, in agreement with ESR results which are typical of a primary radical also.[27] The 1-methylallyl radical, a rearrangement product of the allylcarbinyl radical, is observed in the spectrum to the low IP side of the allylcarbinyl peak. The width of the band is similar to that of the other primary radicals, and the discussion of primary radical and ion geometries above is probably appropriate for the allylcarbinyl radical and ion. ESR data on cyclobutyl radical (Figure 8d) has been interpreted as showing that both the radical center and the ring are planar.[28] Theoretical calculations predict that the ion has a puckered ring structure,[9] hence the vibrational structure may be due to a ring deformation mode excited upon ionization.[14e] The vibrational structure observed in the cyclobutyl radical spectrum also shows that the cyclobutyl structure is a local minimum on the $C_4H_7^+$ surface, in agreement with theoretical results.[9] The results from PES of the C_4H_7 radicals, when combined

Figure 8. Photoelectron spectra of the four C_4H_7 isomeric radicals. (a) Allylcarbinyl radical. (b) Cyclobutyl radical. (c) 1-methylallyl radical. (d) 2-methylallyl radical. The allylcarbinyl radical spectrum shows a small amount of 1-methylallyl radical due to rearrangement of the nascent allylcarbinyl radicals. From ref. 14e.

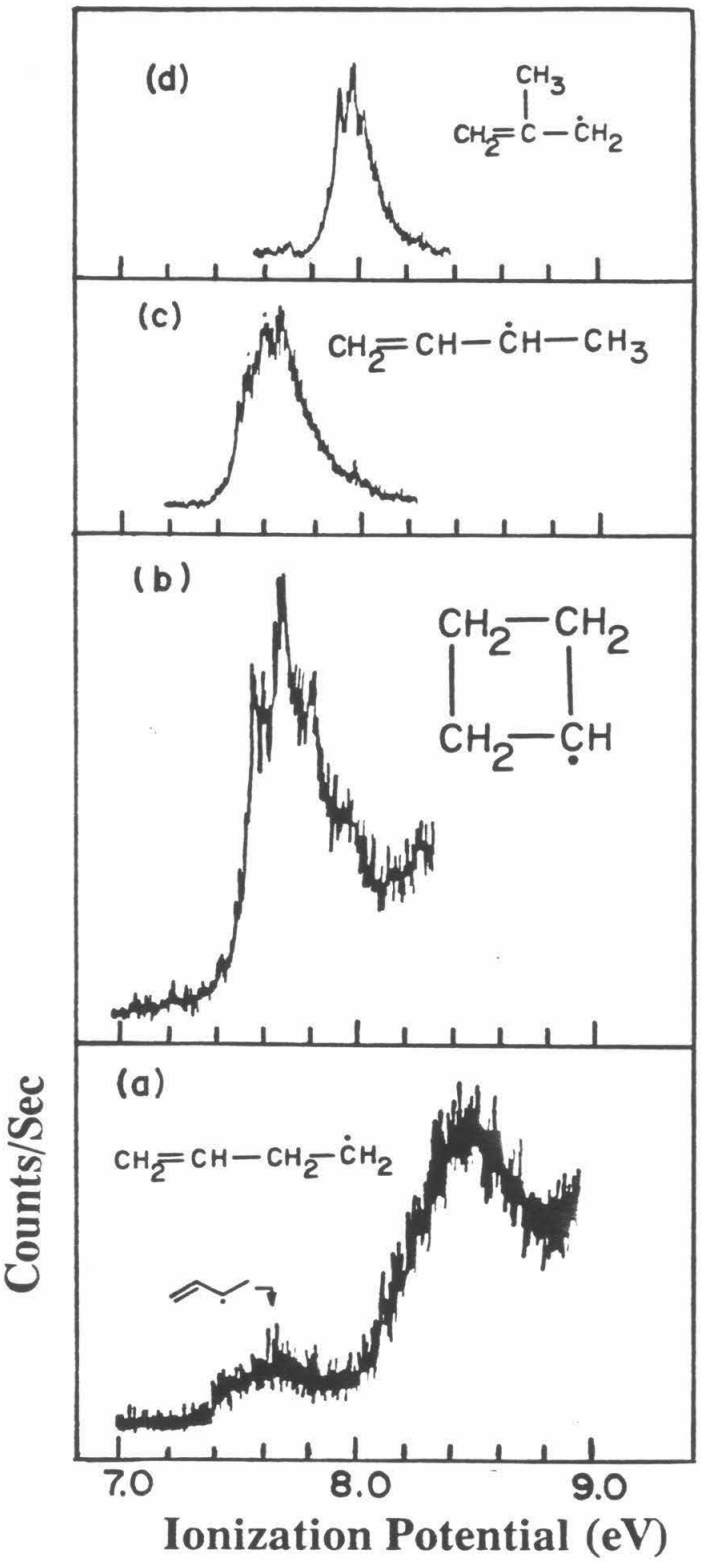
(d)
CH3
CH2=C—ĊH2
(c)
CH2=CH—ĊH—CH3
(b)
CH2—CH2
CH2—ĊH
(a)
CH2=CH—CH2—ĊH2
Counts/Sec
7.0
8.0
9.0
Ionization Potential (eV)

with gas phase ion heats of formation, provide a complete picture of the reactions and energetics relating C_4H_7 radicals, radical rearrangement products, and carbonium ions. These relationships are summarized in Figure 9.

It is interesting to note that the isomers in Figure 8 have very different ionization potentials and band shapes, and can easily be distinguished by PES. Hence the spectra shown in Figure 8 are excellent examples of the ability of PES to distinguish isomeric radicals at small concentrations in complex thermolysis mixtures.

RADICAL AND ION THERMOCHEMISTRY

The thermochemical results from the photoelectron spectra of free radicals determined to date in our laboratory are summarized in Figure 10, and Table 1. All ionic heats of formation in Table 1 were calculated using the convention that the heat of formation of an electron at rest is zero at all temperatures. As can be seen from Figure 10 and Table 1, the three types of alkyl radicals (primary, secondary, and tertiary) have adiabatic ionization potentials that fall within characteristic ranges. Figure 10 also shows that within a given class there is a good semi-quantitative correlation between the number of carbon atoms in an alkyl radical and its IP_a. This correlation is useful for distinguishing different possible radicals in a spectrum. Several examples of the types of thermochemical data that can be derived from the PES of the radicals are presented below.

Relative Bond Energies. Strain and Stabilization Energies in the 1-Adamantyl Radical. As shown above, equations 4-6 can be used to obtain very precise relative C-H bond energies (± 0.5 kcal mol^{-1}). These relative bond energies often reveal subtle substituent effects on the stabilities of radical centers that are difficult to measure by other techniques. The 1-adamantyl radical,[14f] IP_a = 6.21 eV, is a tertiary radical with a tricyclic ring structure (V). The hydride

Figure 9. Illustration of the C_4H_7 radical and carbonium ion heats of formation and C_4H_7 radical rearrangement energies. From ref. 14e.

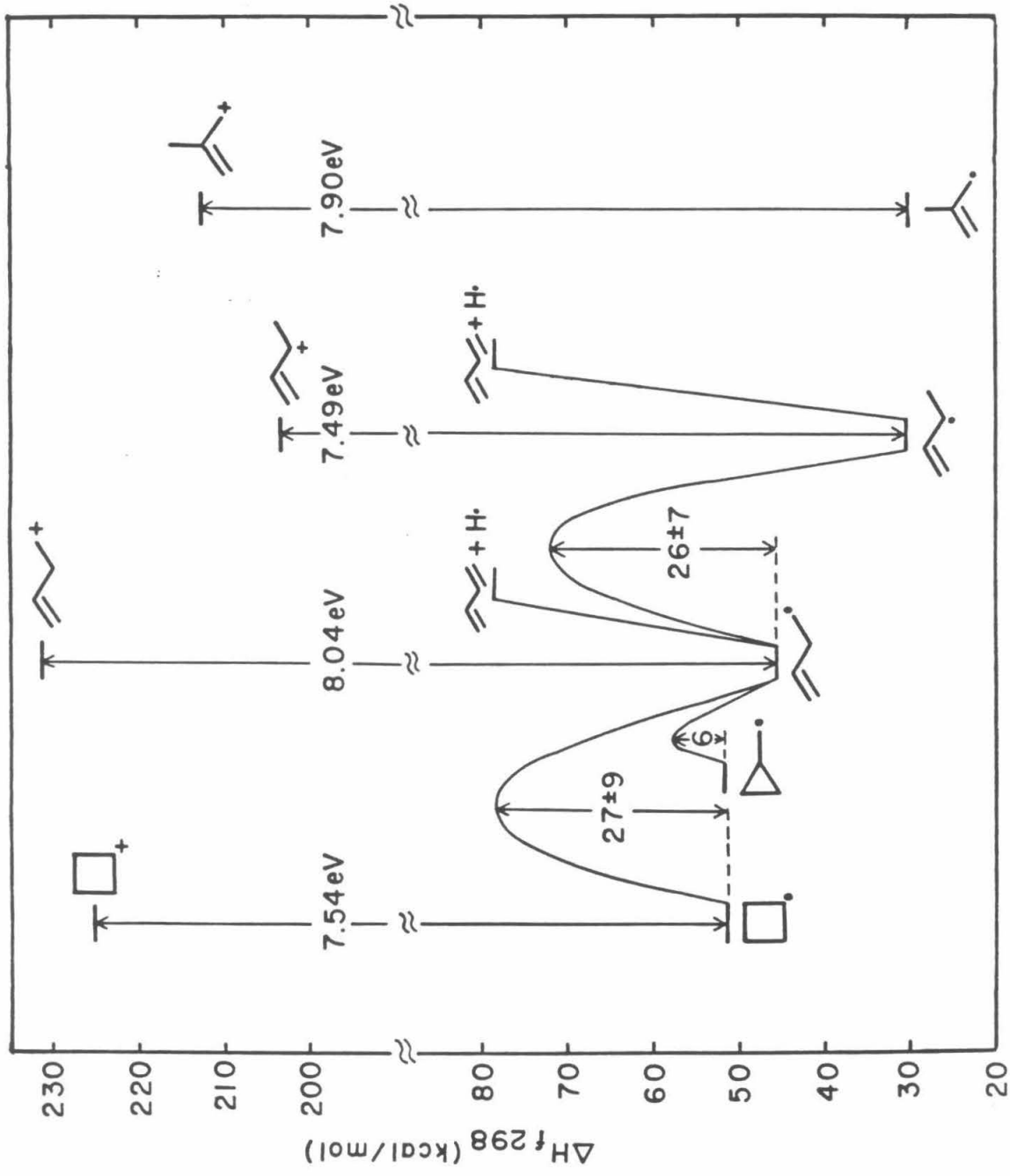
7.54eV
8.04eV
7.49eV
7.90eV
27±9
26±7
6
+H·
+H·
230
220
210
200
80
70
60
50
40
30
20
ΔH f 298 (kcal/mol)

Figure 10. Illustration of the correlation between the number of carbon atoms in a primary, secondary or tertiary radical, and its IP_a. The IP_a values plotted in Figure 10 are from ref. 14.

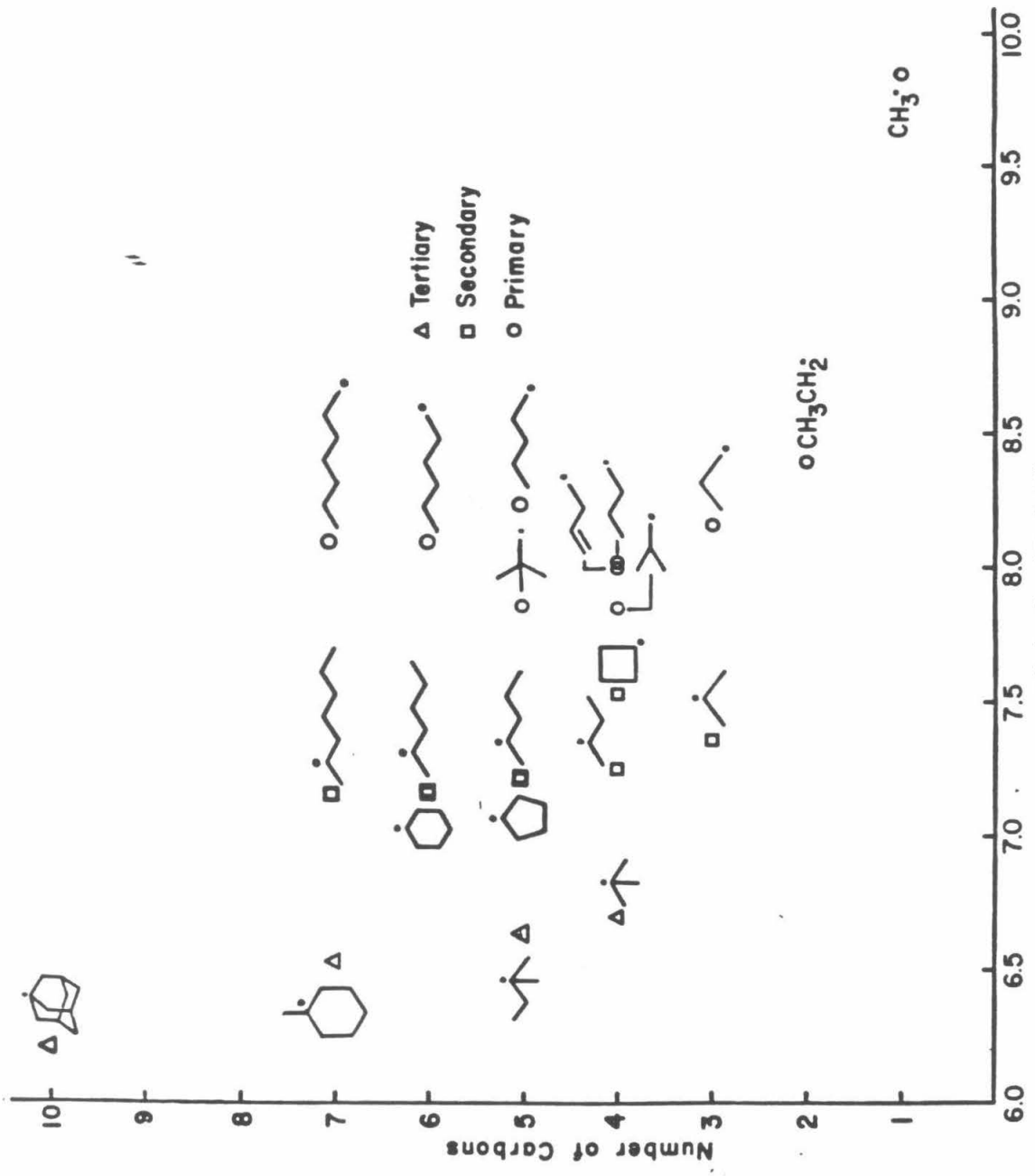
Number of Carbons
Adiabatic IP (eV)
Δ Tertiary
□ Secondary
○ Primary
○ $CH_3CH_2^{\cdot}$
$CH_3^{\cdot}$ ○

affinity of the 1-adamantyl carbonium ion relative to the *tert*-butyl ion (ΔH°_{298} for reaction 9) has been previously determined to be -7.62 ± 0.2 kcal mol^{-1}.[11d]

(9)

Combining the relative hydride affinity with the difference in ionization potentials between *tert*-butyl and 1-adamantyl radicals in equations 4-6 yields a bond energy difference of 3.7 ±1.2 kcal mol^{-1}. The surprise in this result is that the tertiary 1-adamantyl C-H bond has a bond energy 3.7 ±1.2 kcal mol^{-1} *greater* than t-butyl, making it even stronger than the bond energy for a typical *secondary* C-H bond. This result can only be explained by a larger increase in strain energy for forming the 1-adamantyl radical from adamantane than for forming the *tert*-butyl radical from isobutane. The origin of the greater increase in strain energy is most likely the difference in geometry between the two radical centers. ESR results,[25] and calculations[24] show that the *tert*-butyl radical is slightly pyramidal, while 1-adamantyl radical is nearly tetrahedral[29] (see Table 2). The greater increase in strain energy for forming 1-adamantyl radical from adamantane resulting from the pyramidal geometry is a convincing demonstration that there is a significant potential barrier for out-of-plane bending in alkyl radical centers. The unusually high tertiary C-H bond energy in adamantane, derived from the PES data, is reflected in the remarkable reactivity of the 1-adamantyl radical in processes that involve this tertiary radical as an intermediate or transition state,[30] and in the ability of 1-adamantyl radical to abstract secondary hydrogens from cyclohexane in solution.[31]

Absolute Bond Energies. Where absolute ion heats of formation are known, IP_a of a radical derived from its photoelectron spectrum can be used to obtain the absolute radical heat of formation and corresponding C-H bond energy. The C-H bond energies thus obtained can then be compared with C-H bond energies determined by kinetics methods,[32] thus providing an independent verification of the absolute ion and radical heats of formation.[33] As examples $\Delta H_{f,298}^{\circ}[PhCH_2 \cdot]$ and the somewhat controversial values of $\Delta H_{f,298}^{\circ}[(CH_3)_3C \cdot]$ and $\Delta H_{f,298}^{\circ}[(CH_3)_2CH \cdot]$ will be discussed here.

As mentioned in the introduction, absolute ion heats of formation are available from a number of techniques including photoionization appearance potential measurements and, more recently, photoion-photoelectron coincidence (PIPECO) measurements.[10] In the case of the isopropyl cation, $\Delta H_{f,298}^{\circ}[(CH_3)_2CH^+] = 191.0 \pm 1.0$ kcal mol^{-1} seems to be reasonably well established, by PIPECO and other methods.[34] Using $IP_a = 7.36$ eV for the isopropyl radical from Table 1 yields $\Delta H_{f,298}^{\circ}[(CH_3)_2CH \cdot] = 21.3 \pm 1.5$ kcal mol^{-1}, in reasonable agreement with the value of 22.3 ± 0.6 kcal mol^{-1} recommended by Tsang on the basis of reverse addition and radical recombination reaction rates,[35] but well above the value of 18.2 kcal mol^{-1} recommended in another recent review of values determined by iodination kinetics.[32] For the case of the *tert*-butyl radical and carbonium ion the situation is more complex, with a range of values for $\Delta H_{f,298}^{\circ}[(CH_3)_3C \cdot]$ from 6.6 to 12.7 kcal mol^{-1},[32,35] and values of $\Delta H_{f,298}^{\circ}[(CH_3)_3C^+]$ ranging from 161 to 169 kcal mol^{-1} reported in the literature.[10] The value for the benzyl C-H bond energy in toluene is not subject to as much uncertainty, with a value for $\Delta H_{f,298}^{\circ}[PhCH_2 \cdot] = 88.9$ kcal mol^{-1} recommended by Tsang[35] close to that preferred by Golden and others of 88.0 kcal mol^{-1}.[32] Taking 88.9 kcal mol^{-1} as the heat of formation

of the benzyl radical[35] with IP_a of benzyl = 7.20 eV from Table 1 yields an ion heat of formation of 214.8 ± 1.0 kcal mol^{-1}. Kebarle *et al.* have recently determined ΔH°_{298} for reaction 10 to be -0.5 ± 1.0 kcal mol^{-1}.[11d] Combining this result with $\Delta H_{f,298}^\circ[(CH_3)_3CCl]$ = -43.7 kcal mol^{-1} and $\Delta H_{f,298}^\circ[(CH_3)_3CCl]$ =

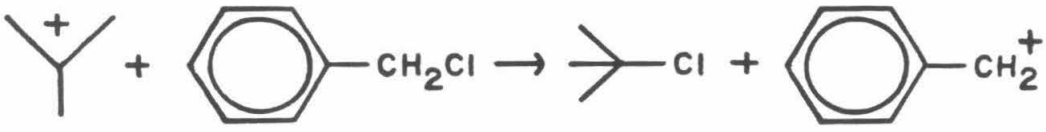

(10)

-43.7 kcal mol^{-1} and $\Delta H_{f,298}^\circ[PhCH_2Cl]$ = 4.5 kcal mol^{-1} [36] gives $\Delta H_{f,298}^\circ[(CH_3)_3C^+]$ = 167.1 ± 1.5 kcal mol^{-1}, and IP_a of *tert*-butyl radical = 6.70 eV from Table I yields $\Delta H_{f,298}^\circ[(CH_3)_3C\cdot]$ = 12.6 ± 2.0 kcal mol^{-1}. Hence the adiabatic ionization potentials of the radicals from PES, combined with the most reliable gas phase ion thermochemistry data, support the higher radical heats of formation recommended by Tsang.[35] The thermochemical data in Table 1 are an update of data that has been previously reported, using the new higher values for the radical heats of formation.[14] It should be noted that while the PES results are generally more consistent with the higher values for $\Delta H_{f,298}^\circ[(CH_3)_3C\cdot]$, the value should still be regarded as uncertain to ± 1.5 kcal mol^{-1} until a definitive absolute value for $\Delta H_{f,298}^\circ[(CH_3)_3C^+]$ is obtained, or the kinetically determined values for $\Delta H_{f,298}^\circ[(CH_3)_3C\cdot]$ are reconciled.

Thermochemistry of Classical and Non-classical Structures in Primary Ions. In the section on geometries of radicals and ions above it was noted that the true adiabatic ionization potential of the ethyl radical is not observed in the photoelectron spectrum because the geometry change from the radical structure (II) to the ground state non-classical ion structure would have a low Franck-Condon factor. Confirmation of this comes from the thermochemistry of the

radical and ion, which is well established for ethyl. The ethyl cation has a heat of formation of 215.6 ± 1.0 kcal mol^{-1} as determined by several reliable methods.[34] The ethyl radical heat of formation has been determined to be 28.4 ± 0.5 kcal mol^{-1} in several recent measurements.[37] These two numbers predict IP_a = 8.12 ± .04 eV, which is well below the value of 8.38 ± .03 eV determined from the photoelectron spectrum. Dyke *et al.* have remeasured the photoelectron spectrum of the ethyl radical using a high resolution spectrometer, and determined IP_a = 8.26 eV,[38] which is still well above the value determined from the radical and ion heats of formation. The IP_v determined in the two measurements of the photoelectron spectrum of the ethyl radical agree exactly, and the disagreement over IP_a is due in part to the interpretation of vibrational structure that Dyke *et al.* were able to resolve using their higher resolution spectrometer. IP_v of ethyl radical from the PES corresponds to ionization to a cation structure that closely resembles the radical structure. Hence IP_v (8.51 eV) minus the true adiabatic IP (8.12 eV) should give a measure of the difference in stability between the classical and hydrogen bridged structures of the ethyl cation. This difference is 9.0 kcal mol^{-1} and is close to the theoretical estimate of 7.0 kcal mol^{-1}.[9] It is not surprising that the difference between the true adiabatic IP and IP_v is higher than the theoretical estimate, because IP_v may correspond to ionization to a classical structure such as VI, which does not exist as an energy minimum in the theoretical results. The theoretical calculations were done for the ion structure VII which has a planar ion center, and is a local

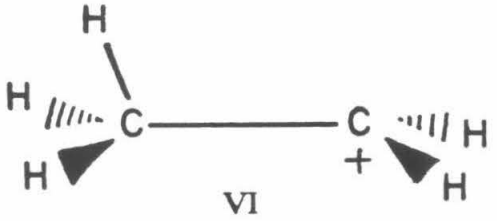

VI

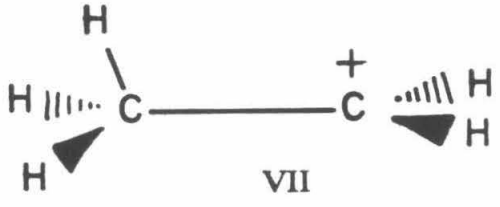

VII

minimum on the $C_2H_5^+$ surface.[9] Hence the difference between the true adiabatic IP of 8.12 eV and the vertical IP from PES must be regarded as an upper limit to the energy difference between the classical structure VII and non-classical structure II for the ethyl carbonium ion. On the basis of the above theoretical results and similar ones for the 1-propyl ion,[9] it is recommended that all IP_a values given in Table 1 for the primary radicals be regarded as upper limits.

Direct Detection of Reaction Intermediates.

PES has a high sensitivity for free radical intermediates since the radicals appear at low ionization potentials. Further, as shown in Figure 10, the primary, secondary, and tertiary radicals have IP_a values that fall within characteristic ranges, so that structural isomers can often be distinguished by PES. Hence PES allows the direct detection of free radical intermediates that can only be inferred by product analysis. Definitive structures can be assigned to the intermediates using PES, which is often difficult using mass spectrometric analysis of pyrolysis mixtures. The flash vacuum pyrolysis conditions employed in the PES studies greatly diminish the importance of bimolecular reactions subsequent to radical formation, simplifying the observed product mixture. Several examples of the utility of PES in analyzing reactive intermediates in radical decomposition and isomerization reactions, and gas phase intermediates in heterogeneous catalysis will be presented below.

Alkyl Radical Decompositions. Alkyl radicals are known to decompose primarily by β C-H and β C-C bond scission, with β C-C scission predominating when both are possible.[39] As an example, the low temperature pyrolysis photoelectron spectrum of cyclopentylmethylnitrite is shown in Figure 11a, showing the cyclopentyl radical spectrum.[14c] At higher temperature a variety of

Figure 11. Thermal decomposition of the cyclopentyl radical. (a) Spectrum at 485 °C showing predominantly the nascent pyrolysis products, cyclopentyl radical, NO, and CH_2O. (b) Spectrum at 556 °C showing the cyclopentyl radical decomposition products, allyl radical, cyclopentene and ethylene. From ref. 14c.

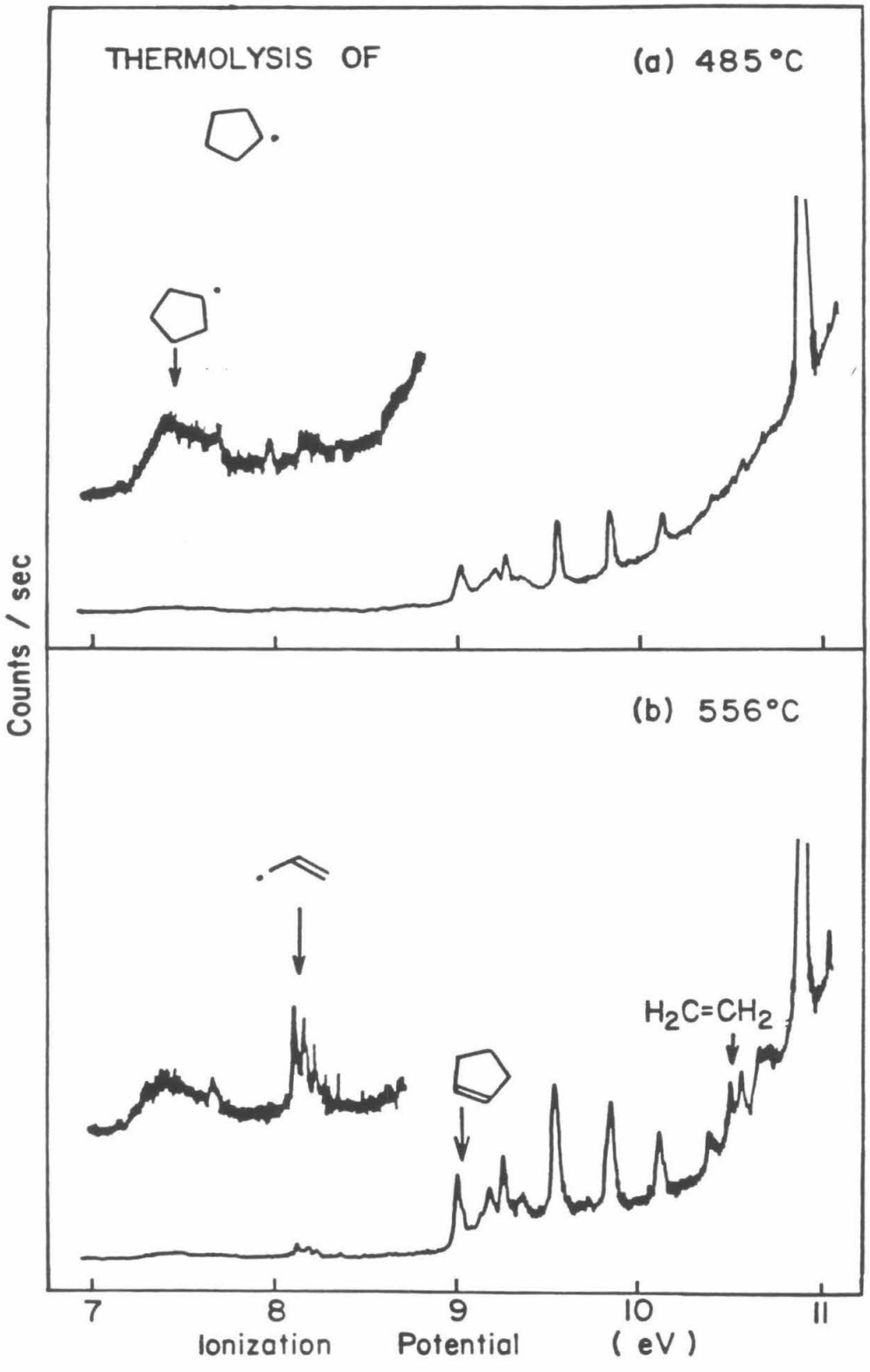
THERMOLYSIS OF
(a) 485°C
(b) 556°C
Counts / sec
H2C=CH2
7
8
9
10
11
Ionization Potential (eV)

decomposition products are apparent in the spectrum and are shown in Figure 11b. All of the products can be explained by β C-H and successive β C-C cleavages as shown in scheme 1. A wide variety of alkyl radical decomposition products have been observed by PES,[14] and in all cases the observed radical and stable products agree well with the products observed and the intermediates proposed in other kinetic studies.

Radical Isomerization Reactions. For the larger n-alkyl radicals 1,4-, 1,5-, and 1,6-H shifts are possible and will compete with the β bond scission reactions discussed above.[40] The products observed in the pyrolytic decomposition of the *n*-alkyl radicals are summarized by scheme 2. The pyrolysis products of *n*-octyl nitrite at 350 °C are shown in Figure 12a, and at 550 °C in Figure 12b. At the lower temperature both primary and secondary radicals are observed. The secondary radicals must come from intramolecular 1,4-, 1,5-, and 1,6-H shifts because bimolecular processes are not observed under these conditions. If bimolecular reactions were important 2-butyl radicals should be observed in the spectrum of 1-butyl under similar conditions, but this is not the case.[14d] At the higher temperature in Figure 12b, the ratio of primary to secondary radicals is greatly increased. This is because at higher temperatures the β-scission decomposition processes predominate, and scheme 2 shows that β scission of both primary and secondary alkyl radicals results in formation of primary radicals and alkenes. As can be seen in Figure 12b, PES allows the detection of not only the nascent and rearranged radical intermediates, but also many of the stable alkene products such as ethylene and propylene. The bands due to primary and secondary radicals in Figure 12 may be due to a mixture of primary and secondary radicals formed by n,m-H shift isomerization and β-scission, so that

Scheme 1. The decomposition pathway for cyclopentyl radicals as determined by photoelectron spectroscopy. Ref. 14c.

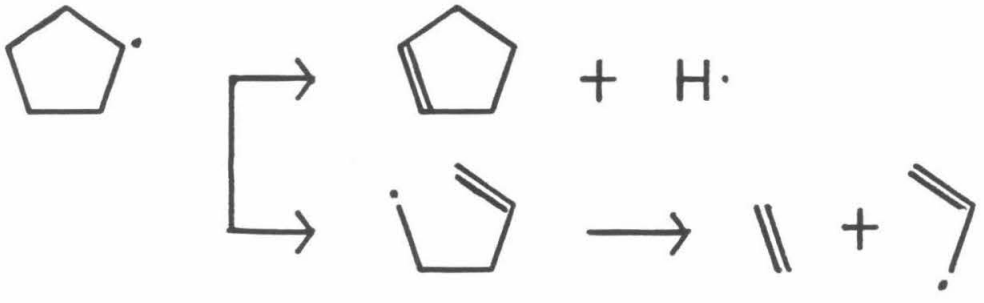
+ H·
+

Figure 12. Thermal decomposition and hydrogen shift isomerization of the 1-heptyl radical. (a) Inset showing pyrolysis products at 350 °C. The nascent products observed at this temperature are large primary n-alkyl radicals, and secondary radicals due to H-atom shift isomerizations of the primary radicals. (b) Spectrum at 550 °C showing predominantly radical decomposition products. From ref. 14h.

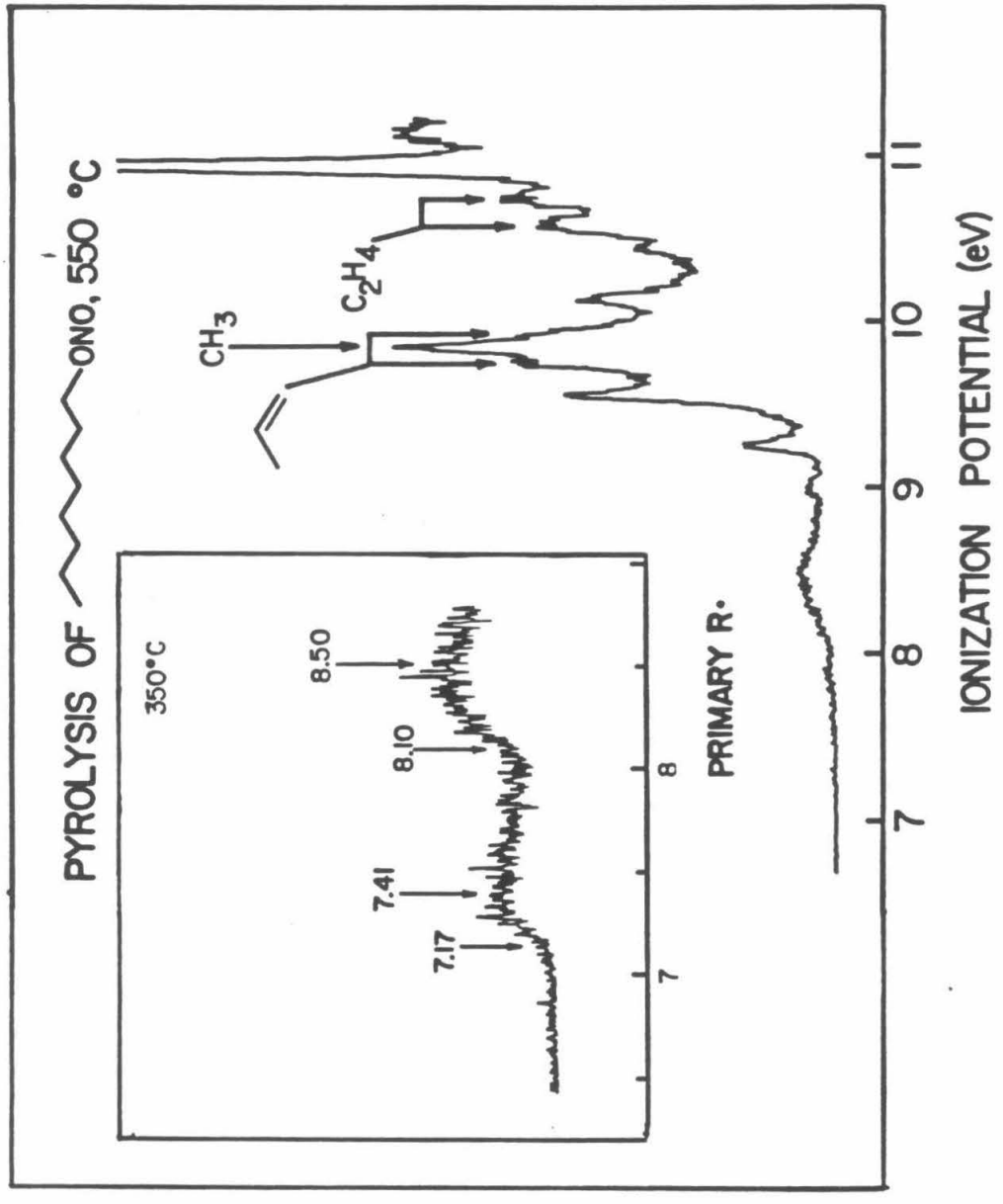
PYROLYSIS OF
ONO, 550 °C
CH_3
C_2H_4
350°C
8.50
8.10
7.41
7.17
7
8
PRIMARY R·
7
8
9
10
11
IONIZATION POTENTIAL (eV)

Scheme 2. The decomposition pathways for n-heptyl radicals, showing products due to β C-C bond cleavage, and n,m H-atom shifts. All of the free radical and stable alkene products shown in the scheme are observed in the photoelectron spectrum (Figure 12). Ref. 14h.

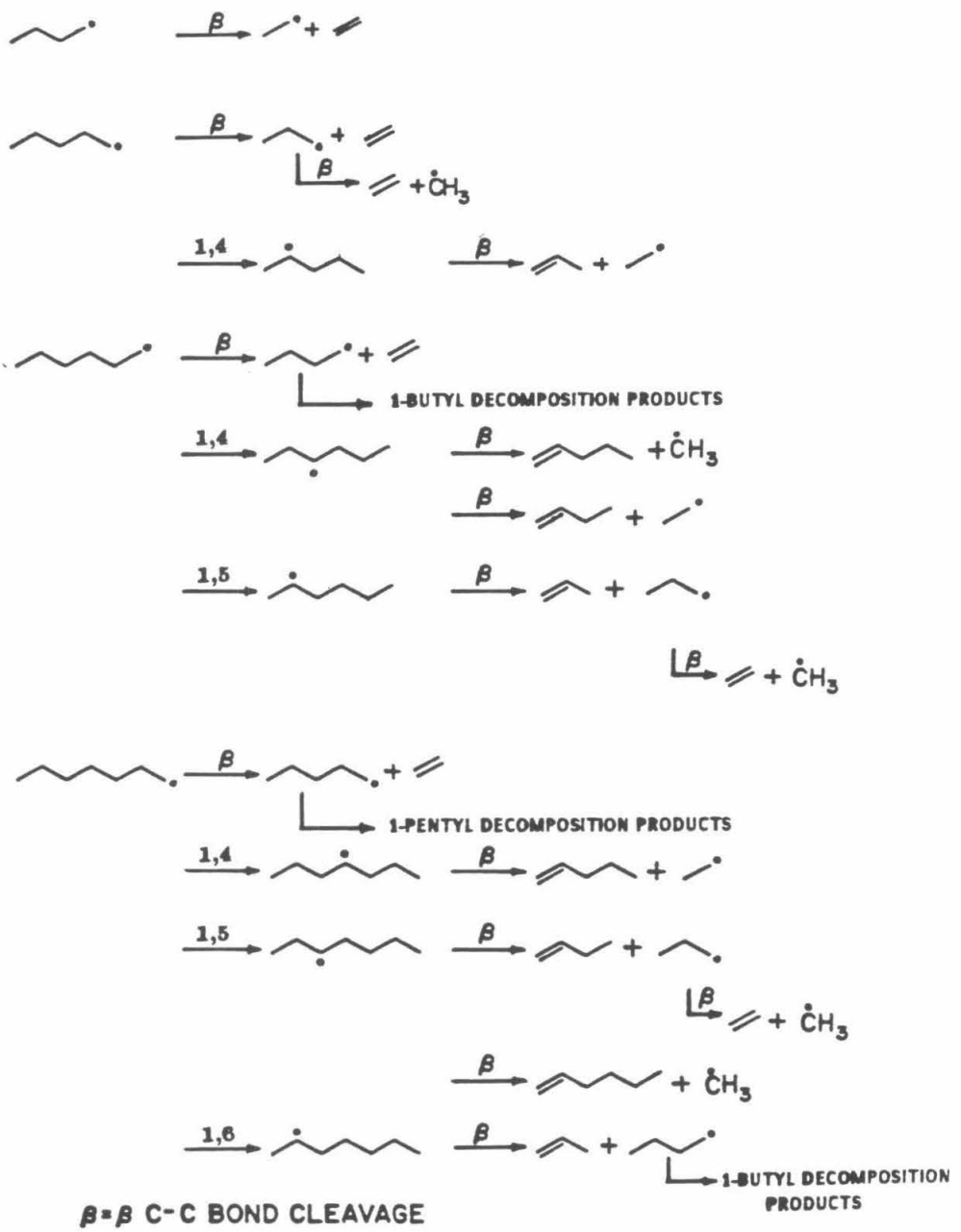

β=β C-C BOND CLEAVAGE

n,m=n,m H SHIFT

the adiabatic and vertical ionization potentials given for these species in Table 1 must be regarded as approximate.

Intermediates in Heterogeneous Catalysis. The first demonstration of the use of PES to observe hydrocarbon radicals formed in heterogeneous gas-solid reactions involved the generation of methylallyl radicals over a bismuth oxide (Bi_2O_3) catalyst.[13] Bismuth oxide is important as a component of bismuth molybdate catalysts used commercially for the oxidation of propylene to acrolein. Lunsford and co-workers[41] have previously shown the production of gas phase allyl radicals over heated bismuth oxide using matrix isolation ESR spectroscopy. In the PES experiments mixtures of propylene or isobutene with oxygen at a 1:5 ratio and total pressure of about 10^{-2} torr were passed over bismuth oxide chips packed into the pyrolysis region described above. The optimum temperature for the production of allylic radicals proved to be 750 °C. Radical production was independent of the alkene/O_2 ratio except at very low O_2 concentrations. Even with no O_2 in the flow radical production was observed, but the catalyst became poisoned over a period of several hours, consistent with the hypothesis that Bi_2O_3 serves as an oxidant. With O_2 at low concentrations in the flow the lattice oxygens in Bi_2O_3 are replenished, regenerating the active site for hydrogen abstraction. CO_2 and H_2O were the only stable products observed in the reaction.

CONCLUSION

Photoelectron spectroscopy has been shown to be a useful and illuminating technique for the study of the structure, energetics and unimolecular reactions of alkyl free radicals. Initial studies also show that PES can be a useful technique for the detection of reactive intermediates in heterogeneous gas phase catalysis. A number of important challenges remain. Several important and

highly reactive radicals such as the cyclopropenyl, cyclopentadienyl and phenyl radical have not been observed by PES to date, although a band tentatively assigned to cyclpentadienyl radical has been observed in an experiment to obtain the spectrum of the phenoxy radical.[42] The observation of excited states of both the radicals and ions is of great interest. In addition, much work remains to be done to fully develop PES as a technique for the detection of radicals in gas-surface reactions. In particular, it would be of great value to study gas phase species produced over catalysts at pressures of 1 atm or more, as this would be closer to conditions that the catalysts are actually used under. The solution to many of these problems may lie in the use of supersonic molecular beams as a sample source for PES. A catalyst could be placed in a high pressure reactor, with sampling through a supersonic nozzle, allowing the reactive intermediates to be sampled downstream at the intersection of the PES HeI photon beam with the molecular beam. Also, methods exist for the production of reactive species in the nozzle of a beam expansion, and highly reactive radicals such as phenyl could be produced and cooled in the beam allowing their detection by PES.[43] Laser or electron beams can interact with the molecular beam, producing excited radical states that can be observed in the PES. Another benefit of using molecular beams in PES is the resultant cooling of the radicals in the beam, combined with recent developments in high resolution spectrometers (with resolution of < 5 meV)[44] perhaps making it possible to resolve vibrational structure in the larger alkyl radicals. Analysis of such vibrational structure would make it possible to determine the structural relationships between alkyl radicals and their corresponding carbonium ions to the same degree that has been obtained with methyl radical. With systems of this type, PES can continue to make important contributions to the detection and investigation of reactive intermediates.

1. (a) Kochi, J. K., Editor, *Free Radicals*; Wiley-Interscience: New York, 1973. (b) Olah, G. A., Schleyer, P. v. R., Eds.; *Carbonium Ions*; Wiley: New York, 1973.

2. Houle , F. A.; Beauchamp, J. L. *J. Am. Chem. Soc.* **1978**, *100*, 3290.

3. (a) Turner, D. W.; Baker, C.; Baker, A. D.; Brundle, C. R. *Molecular Photoelectron Spectroscopy*; Wiley: London, 1970. (b) Eland, J. H. D.; *Photoelectron Spectroscopy*; Butterworths: London, 1984. (c) Berkowitz, J. *Photoabsorption, Photoionization, and Photoelectron Spectroscopy*; Academic Press: New York, 1979.

4. (a) Koenig, T.; Balle, T.; Snell, W. *J. Am. Chem. Soc.* **1975**, *97*, 662. (b) Koenig, T.; Balle, T.; Chang, J. C. *Spec. Lett.* **1976**, *9*, 755.

5. See the discussion in reference 4, and references 15-20 for a complete discussion of the methyl radical geometry.

6. Houle, F. A.; Beauchamp, J. L. *J. Am. Chem. Soc.* **1979**, *101*, 4067.

7. See the discussion in reference 6, and the additional references given in the section on radical geometries, references 24-26.

8. Schultz, J. C.; Houle, F. A.; Beauchamp, J. L. *J. Am. Chem. Soc.* **1984**, *106*, 3917.

9. Hehre, W. H.; Radom, L.; Schleyer, P. v. R.; Pople, J. A. *Ab Initio Molecular Orbital Theory*; Wiley-Interscience: New York, 1986; pp 383-396 and references contained therein.

10. Rosenstock, H. M.; Draxl, K.; Steiner, B. W.; Herron, J. T. *J Phys. Chem. Ref. Data, Suppl. 1* **1977**, *6*.

11. (a) Solomon, J. J.; Field, F. H. *J. Am. Chem. Soc.* **1975**, *97*, 2625. (b) Solomon, J. J.; Field, F. H. *Ibid.* **1976**, *98*, 1567. (c) Meot-Ner, M.; Solomon, J. J.; Field, F. H. *Ibid.* **1976**, *98*, 1025. (d) Sharma, R. B.; Sen Sharma, D. K.; Hiraoka, K.; Kebarle, P. *Ibid.* **1985**, *107*, 3747.

12. See chapter 8 in reference 1a. See also: Benson, S. W.; O'Neal, E. H. *Natl. Stand. Ref. Data Ser., Natl. Bur. Stand.* **1970**, No. 21, p. 565-616, and references contained therein for a discussion of free radical decompositions and experimental techniques.

13. Schultz, J. C.; Beauchamp, J. L. *J. Phys. Chem.* **1983**, *87*, 3587.

14. The radicals in Table 1 are from the following references. (a) Ref. 2. (b) Ref. 6. (c) Houle, F. A.; Beauchamp, J. L. *J. Phys. Chem.* **1981**, *85*, 3456. (d) Schultz, J. C.; Houle, F. A.; Beauchamp, J. L. *J. Am. Chem. Soc.* **1984**, *106*, 3917. (e) Schultz, J. C.; Houle, F. A.; Beauchamp, J. L. *Ibid.* **1984**, *106*, 7336. (f) Kruppa, G. K.; Beauchamp, J. L. *Ibid.* **1986**, *108*, 2162. (g) Hayashibara, K.; Kruppa, G. H.; Beauchamp, J. L. *Ibid.* **1986**, *108*, 5441. (h) Dearden, D. V.; Beauchamp, J. L. *J. Phys. Chem.* **1985**, *89*, 5359. (i) Kruppa, G. H.; Beauchamp, J. L. Results to be published.

15. Golob, L.; Jonathan, N.; Morris, A.; Okuda, M.; Ross, K. *J. Electron Spectrosc. Relat. Phenomena* **1973**, *1*, 65.

16. (a) Dyke, J.; Jonathan, N.; Lee, E.; Morris, A. *J. Chem. Soc. Far. Trans. II* **1976**, *72*, 1385. (b) Reference 4. (c) Reference 6.

17. Herzberg, G. *The Spectra and Structures of Simple Free Radicals*; Cornell University Press: Ithaca, New York, 1971.

18 Milligan, D. E.; Jacox, M. E. *J. Chem. Phys.* **1967**, *47*, 5146. Jacox, M. E. *J. Mol. Spectrosc.* **1977**, *66*, 272. Pacanasky, J.; Bargon, J. *J. Am. Chem. Soc.* **1975**, *97*, 6896.

19. Ellison, G. B.; Engelking, P. C.; Lineberger, W. C. *J. Am. Chem. Soc.* **1978**, *100*, 2556.

20. Marynick, J. M.; Dixon, D. A. *Proc. Natl. Acad. Sci.* **1977**, *74*, 410. Surratt, G. T.; Goddard, W. A. III *Chem. Phys.* **1977**, *23*, 39.

21. Kochi, J. K.; Krusic, P. J. *J. Am. Chem. Soc.* **1968**, *90*, 7157. Fessenden, R. W.; Schuler, R. H. *J. Chem. Phys.* **1963**, *30*, 2147. Carrington, A.; Smith, I. C. P. *Mol. Phys.* **1965**, *9*, 137. Fischer, H. *Z. Naturforsch A.* **1965**, *20*, 488.

22. Pacansky, J.; Dupuis, M. *J. Chem. Phys.* **1978**, *68*, 4276.

23. Kochi, J. K. *Adv. Free-Radical Chem.* **1975**, *5*, 189.

24. Yoshimine, M.; Pacansky, J. *J. Chem. Phys.* **1981**, *74*, 5168.

25. Wood, D. E.; Williams, L. F.; Sprecher, R. F.; Lathan, W. A. *J. Am. Chem. Soc.* **1972**, *94*, 6241.

26. Dyke, J.; Jonathan, N.; Lee, E.; Morris, A.; Winter, M. *Physica Scripta* **1977**, *16*, 197.

27. Fessenden, R. W.; *J. Chim. Phys.* **1964**, *61*, 1570. Hehre, W. J. *J. Am. Chem. Soc.* **1973**, *95*, 2643.

28. (a) Zhidomirov, G. M.; Abronin, I. A.; Micheikin, I. D.; Chuvylkin, N. D. *J. Magn. Res.* **1975**, *17*, 161. See also the discussion in reference 23.

29. Krusic, P. J.; Rettig, R. A.; Schleyer, P. v. R. *J. Am. Chem. Soc.* **1972**, *94*, 995. Mishra, S. P.; Symons, M. C. *Tetrahedron Lett.* **1983**, *25*, 2267.

30. Lomas, S. J. *J. Org. Chem.* **1985**, *50*, 4291. Lomas, S. J.; Dubois, J-E. *Tetrahedron Lett.* **1983**, *24*, 1161. Golzke, V.; Groeger, F.; Boerlineer, A.; Ruchardt, C. *Nouv. J. Chim.* **1978**, *2*, 169. Fort, R. C.; Franklin, R. E. *J. Am. Chem. Soc.* **1968**, *90*, 5266. Lorand, J. P.; Chodroff, S. D.; Wallace, R. W. *Ibid.* **1968**, *90*, 5266. Humphrey, C. B.; Hodgson, B.; Pincock, R. E. *Can. J. Chem.* **1968**, 3099.

31. Engel, P. S.; Chae, W. K.; Baughman, S. A.; Marschke, G. E.; Lewis, E. S.; Timberlake, J. W.; Luedtke, A. E. *J. Am. Chem. Soc.* **1983**, *105*, 5030.

32. For a review of bond energies and radical heats of formation determined by kinetic methods see: McMillen, D. F.; Golden, D. M. *Ann. Rev. Phys. Chem.* **1982**, *33*, 493.

33. Rosenstock, H. M.; Buff, R.; Ferreira, M. A. A.; Lias, S. G.; Parr, A. C.; Stockbauer, R. L.; Holmes, J. L. *J. Am. Chem. Soc.* **1982**, *104*, 2337.

34. (a) Baer, T. *J. Am. Chem. Soc.* **1980**, *102*, 2482, and references therein. (b) Ref. 33.

35. Tsang, W. *J. Am. Chem. Soc.* **1985**, *107*, 2872.

36. Neutral halocarbon and hydrocarbon heats of formation are from: Cox, S. C.; Pilcher, G. *Thermochemistry of Organic and Organometallic Compounds*; Academic Press: New York, 1970.

37. Brouard, M.; Lightfoot, P. D.; Pilling, M. J. *J. Phys. Chem.* **1986**, *90*, 445. Cao, J-R.; Back, M. H. *Int. J. Chem. Kinet.* **1984**, *16*, 961.

38. Dyke, J. M.; Ellis, A. R.; Keddar, N.; Morris, A. *J. Phys. Chem.* **1984**, *88*, 2565.

39. See the discussion and references in the references given in footnote 12.

40. Kossiakoff, A.; Rice, F. O. *J. Am. Chem. Soc.* **1943**, 65, 590.

41. Driscoll, D. J.; Lunsford, J. H. *J. Phys. Chem.* **1985**, *89*, 4415.

42. Dewar, M. J. S.; David, D. E. *J. Am. Chem. Soc.* **1980**, *102*, 7387.

43. Chen, P.; Colson, S. D.; Chupka, W. A.; Berson, J. A. *J. Phys. Chem.* **1986**, *90*, *2319.*

44. Morris, A.; Jonathan, N.; Dyke, J. M.; Francis, P. D.; Keddar, N.; Mills, J. D. *Rev. Sci. Instrum.* **1984**, *55*, 172. Feigerle, C. S. *PhD. Thesis*, Univ. Colorado, Boulder CO, 1983. Pollard, D. J.; Lee, Y. T.; Shirley, D. A. *Rev. Sci. Instrum.* **1981**, *12*, 1837.

CHAPTER 2

Energetics and Structure of the 1- and 2-Adamantyl Radicals and Their Corresponding Carbonium Ions by Photoelectron Spectroscopy.

G. H. Kruppa and J. L. Beauchamp

Reprinted from the Journal of the American Chemical Society, 1986, *108*, 2162.

Energetics and Structure of the 1- and 2-Adamantyl Radicals and Their Corresponding Carbonium Ions by Photoelectron Spectroscopy

Gary H. Kruppa and J. L. Beauchamp*

Contributon No. 7190 from the Arthur Amos Noyes Laboratory of Chemical Physics, California Institute of Technology, Pasadena, California 91125. *Received October 28, 1985*

Abstract: The first photoelectron bands of the 1- and 2-adamantyl radicals, formed by flash vacuum photolysis of 1- and 2-adamantylmethyl nitrite, have been obtained. The adiabatic (IP_a) and vertical (IP_v) ionization potentials of the 1-adamantyl radical are 6.21 ± 0.03 and 6.36 ± 0.05 eV, respectively. IP_a and IP_v for the 2-adamantyl radical are 6.73 ± 0.03 and 6.99 ± 0.05 eV, respectively. The difference in hydride affinities between the 1-adamantyl and *tert*-butyl cations (Sharma, R. B.; Sen Sharma, D. K.; Hiraoka, K.; Kebarle, P. *J. Am. Chem. Soc.* **1985**, *107*, 3747) combined with the difference in IP_a between the *tert*-butyl and 1-adamantyl radicals (0.49 ± 0.06 eV) yield a value of 99 kcal/mol for the tertiary C–H bond energy in adamantane, 3.7 ± 1.2 kcal/mol greater than the tertiary C–H bond energy in isobutane (assumed to be 95 kcal/mol). The effects of the geometrical constraints imposed by the adamantyl cage on the homolytic and heterolytic C–H bond cleavage energies are discussed for the 1- and 2-adamantyl cases. The width of the Franck–Condon envelope obtained is related to the geometry changes that occur upon ionization. The surprisingly broad envelope observed for the planar 2-adamantyl radical indicates that the Franck–Condon envelope for the 1-admantyl radical should not be interpreted as exclusively due to changes at the bridgehead position. Thermal decomposition products of the 1- and 2-adamantyl radicals are observed, and the pathways for thermal decompositions of the radicals are discussed. To confirm expected trends in ionization potentials and band shapes of tertiary radicals, the first photoelectron band of the 2-methyl-2-butyl radical has been obtained. The IP_a of the 2-metyl-2-butyl radical is 6.65 ± 0.04 eV with IP_v = 6.91 ± 0.05 eV.

Compared to acyclic hydrocarbons, the unique geometry of adamantane imposes constraints on the energetics of forming four of the possible reactive intermediates (I–IV) that can be generated by homolytic and heterolytic carbon–hydrogen bond cleavage.[1]

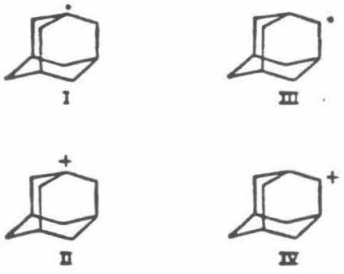

Starting from the tetrahedral configuration, the reactive centers in I–IV will relax in the direction of a planar configuration, subject to the geometric constraints imposed by the adamantyl cage. The effects of the constrained geometry on the rates of reactions that are believed to involve species I–IV as intermediates are of particular interest.[2] The thermodynamic stablities of I and II relative to the *tert*-butyl radical and cation are also of interest since II has been predicted to be unusually stable in the gas phase.[3]

As the reactive centers in I–IV attempt to adopt the preferred configuration, the strain energy increases as a result of distortion in the rigid tetrahedral ring system to accomodate the planar center. The change in strain energy on going from the parent hydrocarbon to the reactive intermediate will be referred to as Δ (strain energy). Studies of the thermal decomposition rates of azoalkanes,[4] peresters,[5] and rates of other reactions that are believed to reflect radical stabilities[6] indicate that the Δ(strain energy) for the formation of I from adamantane is substantially greater than the Δ(strain energy) for the formation of *tert*-butyl radicals. Recent thermolysis studies of compounds V[7] and VI[8]

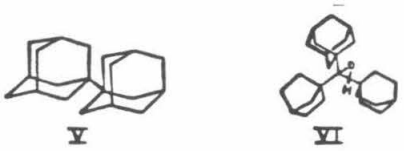

have been interpreted as showing that the formation of I has a greater Δ(strain energy) than *tert*-butyl radical by 0 and 2.2 kcal/mol, respectively. An empirical-force field calculation has yielded a value of 1.4 kcal/mol for this difference.[8] These studies provide qualitative estimates of the Δ(strain energy) for the formation of I that cover a range of values that may in part be due to phenomena such as polar and steric effects,[9] rather than incipient radical stability, that may influence reaction rates.

Information on the geometry of I is available from ESR experiments,[10] which indicate that the bridgehead radical site is only slightly flattened from tetrahedral geometry. An ESR study of the 2-adamantyl radical indicates that the radical site in III is planar.[11]

There have been a number of previous gas-phase studies of the stability, geometry, and Δ(strain energy) of II. The gas-phase

(1) (a) Fort, R. C.; Schleyer, P. v. R. *Adv. Alicyclic Chem.* **1966**, *1*, 283. (b) Ruchardt, C. *Angew. Chem., Int. Ed. Engl.* **1970**, *9*, 830.
(2) (a) Engel, P. S. *Chem. Rev.* **1980**, *80*, 99. (b) Bingham, R. C.; Schleyer, P. v. R. *Tetrahedron Lett.* **1971**, 23.
(3) (a) Houriet, R.; Schwarz, H. *Angew. Chem., Int. Ed. Engl.* **1979**, *18*, 951. (b) Staley, R. H.; Wieting, R. D.; Beauchamp, J. L. *J. Am. Chem. Soc.* **1977**, *99*, 5964.
(4) Golzke, V.; Groeger, F.; Boerlinner, A.; Ruchardt, C. *Nouv. J. Chim.* **1978**, *2*, 169.
(5) Fort, R. C.; Franklin, R. E. *J. Am. Chem. Soc.* **1968**, *90*, 5267. Lorand, J. P.; Chodroff, S. D.; Wallace, R. w. *Ibid.* **1968**, *90*, 5266. Humphrey, C. B.; Hodgson, B.; Pincock, R. E. *Can. J. Chem.* **1968**, 3099.
(6) See ref 2a for a summary of experiments completed before mid-1979.
(7) Beckhaus, H. D.; Flamm, M. A.; Ruchardt, C. *Tetrahedron Lett.* **1982**, *23*, 1805.
(8) Lomas, S. J.; Dubois, J. E. *Tetrahedron Lett.* **1983**, *24*, 1161.
(9) See ref 1b, 2a, and references contained therein for a more complete discussion of factors, other than incipient radical stabilities, that can influence pyrolysis rates.
(10) (a) Krusic, P. J.; Rettig, R. A.; Schleyer, P. v. R. *J. Am. Chem. Soc.* **1972**, *94*, 995. (b) Mishra, S. P.; Symons, M. C. . *Tetrahedron Lett.* **1983**, *25*, 2267.
(11) Kira, M.; Watanabe, M.; Ichinose, M.; Sakurai, H. *J. Am. Chem. Soc.* **1982**, *104*, 3762.

Table I. Gas-Phase Studies Relating to Ion Stability

reaction[a]	$\Delta G°$, kcal/mol	$\Delta H°$,[b] kcal/mol	$\Delta S°$, eu
$t\text{-}C_4H_9^+ + C_{10}H_{16} \rightarrow i\text{-}C_4H_{10} + C_{10}H_{15}^+$	−8.24	−7.62 ± 0.1	−2.06
$t\text{-}C_4H_9^+ + C_{10}H_{15}Cl \rightarrow i\text{-}C_4H_{10}Cl + C_{10}H_{15}^+$[c]		−6.3 ± 0.1	
$t\text{-}C_4H_9^+ + C_{10}H_{15}Br \rightarrow i\text{-}C_4H_{10}Br + C_{10}H_{15}^+$[d]		−10.8 ± 10	
$t\text{-}C_4H_9^+ + C_{10}H_{15}Br \rightarrow i\text{-}C_4H_{10}Br + C_{10}H_{15}^+$[e]		≤4.0	
$t\text{-}C_4H_9^+ + C_{10}H_{16} \rightarrow i\text{-}C_4H_{10} + C_{10}H_{15}^+$[f]		−4.1	
$t\text{-}C_4H_9^+ + i\text{-}C_5H_{12} \rightarrow i\text{-}C_4H_{10} + t\text{-}C_5H_{11}^+$[g]	−2.5	−3.3 ± 0.2	−2.7

[a] $C_{10}H_{16}$ refers to adamantane, $C_{10}H_{15}X$ (X = Cl and Br) refers to the 1-halo-adamantane, and $C_{10}H_{15}^+$ is assumed to be the 1-adamantyl ion. [b] $\Delta H°$ in this column yields the differences in hydride or halide affinities of the carbonium ions. [c] High-pressure mass spectrometry results, ref 12. [d] ICR equilibrium study, ref 3b. [e] ICR equilibrium study, ref 3a. [f] Calculated, ref 13. [g] High-pressure mass spectrometry, ref 34.

stability of II relative to $(CH_3)_3C^+$ has been determined by equilibrium studies using high-pressure mass spectrometry. For reaction 1, these measurements yielded $\Delta H° = -7.62 \pm 0.1$

(1)

kcal/mol and $\Delta S° = 2.1$ eu.[12] This result is in good agreement with previous gas-phase equilibrium results from ICR mass spectrometry[3b] and calculations,[13] which are summarized in Table I. Theoretical calculations have shown that there is a substantial difference in geometry between the minimum energy structure for adamantane and the minimum energy structure for II.[13] The formation of II from adamantane has been shown to have a Δ(strain energy) of 12 kcal/mol by an empirical force field (EFF) calculation.[14]

Photoelectron spectroscopy (PES) of free radicals offers an opportunity to interrelate directly the structure and energetics of a radical and its corresponding carbonium ion. In the general ionization process 2 the spectrum of electron kinetic energies

$$R\cdot + h\nu \rightarrow R^+ + e^- \qquad (2)$$

corresponding to ionization to the ground electronic state of R^+ contains information about the changes in geometry and force constants that occur in forming R^+ from R·. Since the ionization potentials of radicals are lower than those of stable species, the first band of the radical spectrum is at higher electron kinetic energies than the first band of stable species. Low concentrations of radicals (~0.1–0.01%) can easily be detected because the background signal in the high kinetic energy region is small. For systems with minor geometry differences between R· and R^+ (e.g., methyl,[15] allyl,[16] and benzyl[16]) the first band of the photoelectron spectrum is sharp with $IP_a = IP_v$. For other systems, where there is a large difference in geometry between R· and R^+, a broad Franck–Condon envelope for the first photoelectron band is observed, with a large difference between IP_a and IP_v (e.g., *tert*-butyl, where $IP_v - IP_a = 0.22$ eV[17]). In the present work, an investigation of the first photoelectron bands of I and III is presented. In these cases the rigid adamantyl ring system introduces a substantial increase in strain energy when the radicals or ion centers attempt to achieve a planar configuration.[14] The constraints of the ring system should be reflected in the observed Franck–Condon envelopes and the differences between IP_a and IP_v for I and III. Useful thermochemical information can also be derived from the photoelectron spectrum. The difference in

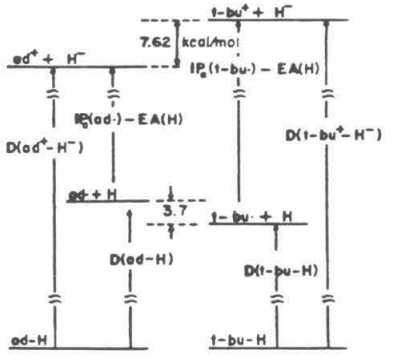

Figure 1. Thermochemical cycle showing the quantities relating the relative hydride affinities and relative homolytic bond dissociation energies for the tertiary bonds in adamantane and isobutane.

IP_a between I and *tert*-butyl radical can be used with the difference in hydride affinities between II and $(CH_3)_3C^+$ to obtain the difference in tertiary C–H bond energies (see Figure 1 for the factors relating these quantities). The differences in bond energies can be used to discuss the changes in strain energies for the formation of I and *tert*-butyl radical without some of the effects that may complicate the interpretation of the pyrolysis experiments mentioned above.

Only one other tertiary hydrocarbon radical, the *tert*-butyl radical, has previously been studied by PES.[15c,17] To confirm expected trends in ionization potentials and band shapes, the first photoelectron band of the 2-methyl-2-butyl radical has been obtained in this work.

Photoelectron bands that correspond to thermal decomposition products of the 1- and 2-adamantyl radicals are observed in this work, and the pathway for thermal decomposition of the two radicals are discussed.

Experimental Section

The apparatus used in these experiments is a photoelectron spectrometer specifically designed to study the products of pyrolysis reactions. It has been described in detail elsewhere.[16]

The radicals studied in this work were produced by the pyrolysis of the appropriate alkyl nitrites, reactions 3 and 4. The pyrolyzer used in

$$RCH_2ONO \rightarrow RCH_2O + NO \qquad (3)$$

$$RCH_2O \rightarrow R + CH_2O \qquad (4)$$

this study was 2 cm in length, corresponding to the "long" pyrolyzer used in an earlier study.[18] 2,2-Dimethyl-1-butyl nitrite was prepared from 2,2-dimethyl-1-butanol, obtained from Overlook Industries, Inc., by a standard method.[19] 1-Adamantylmethyl nitrite was prepared from 1-adamantanemethanol, obtained from Aldrich, using the same standard method with slight modifications. $NaNO_2$ (2.3 g, 33.3 mmol) and 1-adamantanemethanol (5.00 g, 32.1 mmol) were dissolved in 100 mL of 20% aqueous THF. This was stirred in an ice bath, and 16 mL of 2 M

(12) Sharma, R. B.; Sen Sharma, D. K.; Hiraoka, K.; Kebarle, P. *J. Am. Chem. Soc.* **1985**, *10m*, 3747.
(13) Sunko, D. E.; Hirsl-Starcevic, S.; Pollack, S. K.; Hehre, W. J. *J. Am. Chem. Soc.* **1979**, *101*, 6163.
(14) Bingham, R. C.; Schleyer, P. v. R. *J. Am. Chem. Soc.* **1971**, *93*, 3189.
(15) (a) Dyke, J.; Jonathan, N.; Lee, E.; Morris, A. *J. Chem. Soc., Faraday Trans. 2* **1976**, *72*, 1385. (b) Koenig, T.; Balle, T.; Snell, W. *J. Am. Chem. Soc.* **1975**, *97*, 662. (c) Koenig, T.; Balle, T.; Chang, J. C. *Spectrosc. Lett.* **1976**, *9*, 755.
(16) Houle, F. A.; Beauchamp, J. L. *J. Am. Chem. Soc.* **1978**, *100*, 3290.
(17) (a) Houle, F. A.; Beauchamp, J. L. *J. Am. Chem. Soc.* **1979**, *101*, 4067. (b) Dyke, J.; Jonathan, N.; Lee, E.; Morris, A.; Winter, M. *Phys. Soc.* **1977**, *16*, 197.
(18) Schultz, J. C.; Houle, F. A.; Beauchamp, J. L. *J. Am. Chem. Soc.* **1984**, *106*, 3917.
(19) Levin, N.; Hartung, W. *Organic Syntheses*; Wiley: New York, 1955; Collect. Vol. III, p 192.

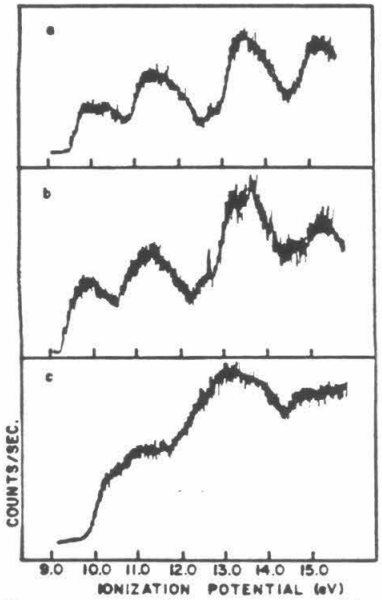

Figure 2. Room temperature photoelectron spectra of the nitrite precursors to the radicals used in this study: (a) 1-adamantylmethyl nitrite; (b) 2-adamantylmethyl nitrite; (c) 2,2-dimethyl-1-butyl nitrite.

H_2SO_4 was added over 1 h. The solution was stirred for 1 h and warmed to room temperature. $CHCl_3$ (10 mL) was added, the organic layer was separated, and the volume was reduced on a rotary evaporator. The purity of the clear yellow liquid obtained in approximately 80% yield was checked by NMR spectroscopy. 2-adamantylmethyl nitrite was prepared from 2-adamantanone obtained from Aldrich. The 2-adamantanone was first converted to 2-methyleneadamantane via a Wittig reaction[20] followed by hydroboration to obtain 2-adamantanemethanol.[21] The 2-adamantanemethanol obtained (in about 50% yield from the 2-adamantanone) was converted to 2-adamantylmethyl nitrite by the method for 1-adamantylmethyl nitrite described above. For the 2-adamantanemethanol case, the conversion to nitrite went only 50% to completion, but it was found to be unnecessary to separate the alcohol and nitrite since the alcohol had insufficient vapor pressure at room temperature to interfere with the spectrum of the nitrite.

The pyrolysis spectra were obtained with both HeI and NeI radiation. The band shapes obtained with the HeI and NeI radiation sources were the same within experimental error. The pyrolysis spectra were obtained at temperatures from 350 to 500 °C. The energy scale was calibrated with the He Iα and He Iβ bands of CH_3I, CH_2O, Xe, and Ar. The resolution for these experiments is 30–40 mV as determined from the full width at half-maximum of Ar $^2P_{3/2}$ band. 1-1'-azoadamantane was also tried as a source of 1-adamantyl radicals, but a sufficient vapor pressure of the azo compound could not be obtained in the pyrolyzer due to the sample handling system, which cannot be uniformly heated.

Results

The HeI photoelectron spectrum of the nitrite precursors to I are shown in Figure 2. The adiabatic IP's of the first bands are 9.56, 9.25, and 9.92 eV for 1-adamantylmethyl nitrite, 2-adamantylmethyl nitrite, and 2,2-dimethyl-1-butyl nitrite, respectively, where the errors are ±0.05 eV and the energy scale was calibrated with the He Iα bands of Ar. Spectra from 5.9 to 7.5 eV of the pyrolysis products of the 1-adamantylmethyl nitrite are shown in Figure 3. Figure 3a shows the spectrum at 355 °C, where about 25% of the precursor decomposes (the amount of decomposition is estimated from the relative intensities of the pyrolysis product bands, the CH_2O band, and the nitrite bands). Figure 3bv shows the spectrum at 430 °C, where 50% of the precursor decomposes. Finally, Figure 3c shows the spectrum at 470 °C, where pyrolysis is 60–80% complete. The observed band shapes were reproduced at a given temperature over several days. Over longer periods of time the quartz pyrolyzer surface became coated with carbon deposits, and the temperature at which a particular band shape was observed shifted to lower temperature. A spectrum of the pyrolysis products of 2-adamantylmethyl nitrite at 480 °C is shown in Figure 4. The spectrum of the pyrolysis products of 2,2-dimethyl-1-butyl nitrite from ~6.5 to 7.4 eV is shown in Figure 5. The observed band shapes did not change with temperature.

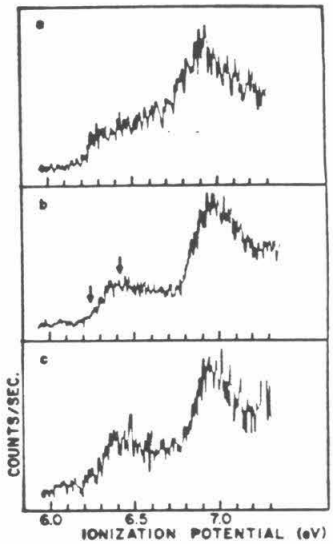

Figure 3. Photoelectron spectra of the pyrolysis product of 1-adamantylmethyl nitrite (1-adamantyl radical) in the energy range 6.0–7.4 eV at (a) 355 °C; (b) 430 °C; (c) 470 °C. Estimated adiabatic and vertical ionization potentials are indicated by arrows in (b).

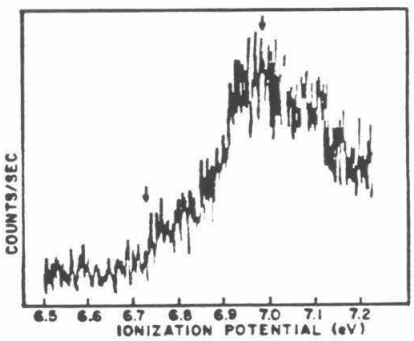

Figure 4. Spectrum of the pyrolysis product of 2-adamantylmethyl nitrite (2-adamantyl radical) at 480 °C.

The first point to be made about the photoelectron bands presented in Figure 3 is that the bands are due to He Iα ionization of alkyl radicals, produced by pyrolysis, and not He Iβ or He Iγ ionization of the nitrite precursor. Since the first adiabatic IP of the precursor is at about 9.45 eV (see Figure 2), a weak band due to ionization of the nitrite by He Iγ radiation (which is <1% of the total intensity of the He UV lamp output) would appear about 7.0 eV. Bands due to He Iβ ionization (which is a stronger impurity line, about 2% of the total HeI lamp output) would not appear below 7.58 eV. This is confirmed by room temperature spectra of the region 5.9–8.0 eV, taken with collection times similar to those used to produce the spectra in Figures 3, which show no

(20) Wittig, G.; Schoelkopf, U. *Org. Syn.* **1960**, *40*, 66.
(21) Brown, H. C. *Organic Syntheses via Boranes*; Wiley: New York, 1975; pp 23–24.

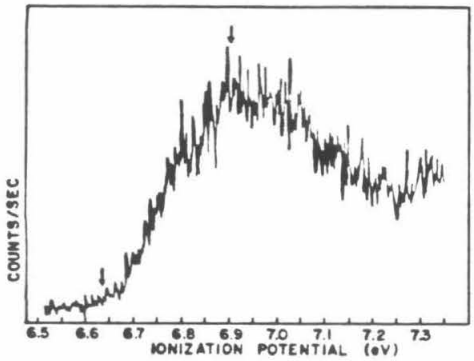

Figure 5. Spectrum of the pyrolysis product of 2,2-dimethyl-1-butyl nitrite (2-methyl-2-butyl radical) at 400 °C.

peaks below 7.0 eV. In addition, a spectrum was taken of the pyrolysis products at 430 °C using NeI radiation, and the band shape observed was close to that in Figure 3b.

Discussion

Identification of Radicals. An important feature of the spectra in Figure 3 is the change in band shapes and relative intensities with temperature, especially in going from 355 to 430 °C. The IP_a of the first band remains constant with temperature and was determined to be 6.21 ± 0.03 eV. No low-lying excited electronic states are expected in the 1-adamantylcarbonium ion. Hence the data in Figure 3 indicate the presence of at least two radicals and possibly a third. The additional radicals result from the thermal decomposition of 1-adamantyl radicals prior to ionization. Lossing[22] has previously noted this difficulty in attempts to measure the ionization potentials of the 1- and 2-norbornyl and 1-bicyclo[2.2.2]octyl radicals formed by pyrolysis of the corresponding alkyl nitrites, using monoenergetic electron impact ionization and mass spectrometry detection. Only rearrangement products of the desired norbornyl and bicyclooctyl radicals were observed in the mass spectrometer. An RRKM calculation was performed in order to determine the feasibility of observing adamantyl radicals as the product of reactions 3 and 4 in the photoelectron spectrometer. Typical activation energies for reactions 3 and 4 are 37 and 12 kcal/mol, respectively,[23] and the residence time in the pyrolyzer is about 1 ms. A reasonable value of the activation energy for subsequent decomposition of the 1-adamantyl radical is 25 kcal/mol.[24] The RRKM calculation shows that even under conditions where the rate constants for the reactions 3 and 4 are large enough so that most of the nitrite decomposes to adamantyl radicals, the resulting adamantyl radicals have internal energies of ~10 kcal/mol. This is well below the 25 kcal/mol required for decomposition or rearrangement. Hence, any decomposition or rearrangement products observed are the result of adamantyl radicals undergoing further energizing collisions with the hot pyrolyzer wall after they have been produced from the nitrite. Since residence times in the pyrolyzer are short, some of the adamantyl radicals should escape from the pyrolyzer to be detected.

Ionization potentials of alkyl radicals generally decrease in the order primary > secondary > tertiary. There is also a qualitative correlation between ionization potentials and the number of carbons in a primary, secondary, or tertiary radical as shown in Figure 6.[25] Based on these correlations, the band in Figure 3 with the adiabatic IP of 6.21 ± 0.03 eV can be confidently assigned to ionization of I. Inspection of Figure 6 and general trends in ionization potentials of alkyl radicals show that only a large tertiary radical such as I would be expected to have an IP as low as 6.21 eV. From inspection of a number of spectra with the best signal-to-noise ratios, IP_v(I) is estimated to be 6.36 ± 0.05 eV. The second band in Figure 3 in the region 6.5–7.0 eV is probably due to thermal decomposition products of I and will be discussed further below.

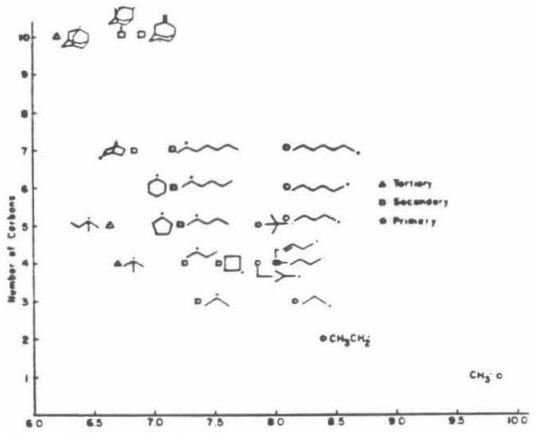

Figure 6. Correlation of the IP_a of primary, secondary, and tertiary alkyl radicals with the number of carbon atoms. Ionization potentials are from ref 25.

The band shown in Figure 4 is assigned to ionization of the 2-adamantyl radical. The IP_a of 6.73 eV for this radical fits well on Figure 6. The IP_v is 6.99 ± 0.05 eV.

The band in Figure 5 is assigned to ionization of the 2-methyl-2-butyl radical. The IP_a of the 2-methyl-2-butyl radical obtained in this work is 6.64 ± 0.04 eV and the IP_v is 6.91 ± 0.05 eV. This value is in reasonable agreement with an earlier determination by nitrite pyrolysis followed by monoenergetic electron impact ionization, which gave a value of 6.85 eV for IP_a of the 2-methyl-2-butyl radical.[26] Also, the IP_a determined in this work for the 2,2-dimethyl-1-butyl radical fits well on Figure 6.

Thermal Decomposition of 1- and 2-Adamantyl Radicals. Previous studies have shown that photoelectron spectroscopy is a useful tool for elucidating the thermal decomposition pathways of alkyl radicals,[27] and in this section a discussion of the thermal decomposition pathways of the 1- and 2-adamantyl radicals is presented. Alkyl radicals may decompose by β-CC and β-CH cleavages as well as more complex skeletal rearrangements.[28] The thermal decomposition of 1-adamantyl radicals has been studied by gas chromatographic analysis of the products of pyrolysis of 1-nitroadamantane.[29] Orbital overlap considerations suggest that

(22) McAllister, J.; Dolesek, Z.; Lossing, F. P.; Gleiter, B.; Schleyer, P. v. R. *J. Am. Chem. Soc.* **1967**, *89*, 5982.

(23) Benson, S. W. *Thermochemical Kinetics*; Wiley: New York, 1968; pp 464 ff.

(24) Reference 23, pp 567 ff. No direct experimental data are available on the activation energy for the decomposition of I, but this reference contains data for other simple alkyl radicals. The value of 25 kcal/mol was chosen because it is at the lower end of the range of values observed for other radicals, which might be expected for I since the orbitals are favorably oriented for decomposition. See also the discussion in ref 22.

(25) The ionization potentials plotted in Figure 6 are from this work and the following references: (a) ref 16; (b) ref 17a; (c) ref 18; (d) Schultz, J. C.; Houle, F. A.; Beauchamp, J. L. *J. Am. Chem. Soc.* **1984**, *106*, 7336; (e) Houle, F. A. Ph.D. Thesis, California Institute of Technology, Pasadena, CA, 1979. (f) Dearden, D. V.; Beauchamp, J. L. *J. Am. Chem. Soc.* **1985**, *89*, 5359.

(26) Lossing, F. P.; Maccoll, A. *Can. J. Chem.* **1976**, *54*, 990. Lossing also obtained a higher value for the IP_a of the *tert*-butyl radical than the value from this laboratory (ref 17). The difference between 2-methyl-2-butyl radical and the *tert*-butyl radical IP_a from PES measurements is 0.06 eV, which is close to the difference obtained by Lossing, 0.08 eV. Hence, it appears that Lossing's measurements do not measure the true adiabatic IP of alkyl radicals. Interestingly, the IP's obtained by Lossing are close to the vertical IP's measured by PES.

(27) Houle, F. A.; Beauchamp, J. L. *J. Phys. Chem.* **1981**, *85*, 3456.

(28) Pryor, W. A. *Free Radicals*; Wiley-Interscience: New York, 1973; Vol. 1. Kossiakoff, A.; Rice, F. O. *J. Am. Chem. Soc.* **1943**, *65*, 590.

(29) Fields, E. K.; Meyerson, S. *Adv. Free Radical Chem.* **1975**, *5*, 178.

Scheme I

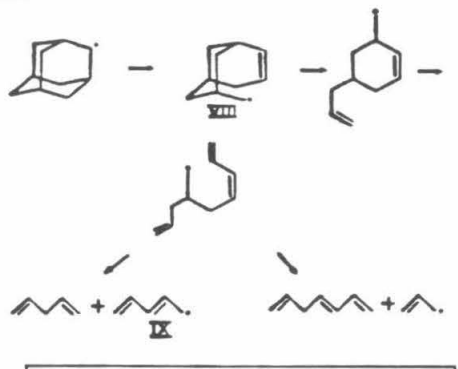

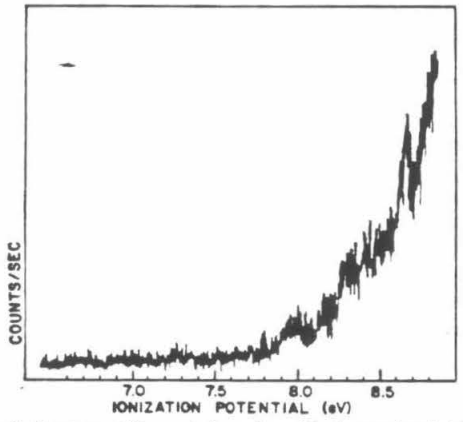

Figure 7. Spectrum of the pyrolysis product of 2-adamantylmethylnitrite at 550 °C. Note that this temperature is sufficiently high that all of the 2-adamantyl radical decomposes before entering the source chamber of the photoelectron spectrometer.

the 1-adamantyl radical would most likely undergo β-CC cleavage to yield the radical VII. Inspection of the trends in Figure 6 shows

VII

that a large secondary radical such as VII would be expected to have an IP_a in the range 6.5–7.0 eV. This possibility is confirmed by the spectrum of 2-adamantyl radical in Figure 4 with an IP_a of 6.73 eV, which shows that a large secondary radical such as VII could have an IP_a low enough to be responsible for the second band in Figure 3. Further decomposition of radical VII by successive β-CC or β-CH cleavages leads to a series of secondary radicals and stable alkenes. The topology of the 1-adamantyl radical is such that it can open to a series of secondary radicals but it can never come apart to give primary radicals by β-CC cleavage.

The 2-adamantyl radical can open to a series of primary radicals by β-CC cleavage and can cleave to smaller radicals (see Scheme I). The initial radicals resemble isobutyl radical in that the radical site is α to a tertiary carbon. Figure 7 shows the pyrolysis products of 2-adamantylmethyl nitrite at 550 °C, a temperature sufficiently high that all of the 2-adamantyl radical produced decomposes before being detected. Although it is not very distinctive, the band at 7.84 eV in Figure 7 has an IP_a just below that of isobutyl (IP_a = 7.93 eV[25d]) and may be due to radical VIII. Further decomposition of the radical VIII by successive β-cleavages, Scheme I, leads to a series of primary radicals and finally the allyl radical

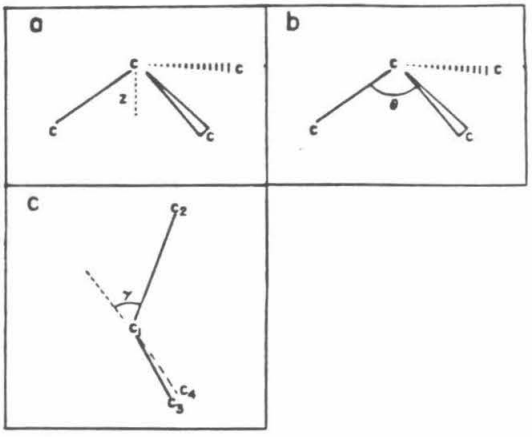

Figure 8. Three commonly used measures of nonplanarity at a carbon center: (a) out-of-plane distance, z; (b) C–C–C bond angle θ; (c) out-of-plane angle, γ. These parameters are discussed further in the text.

Table II. Comparison of Out-of-Plane Angles γ^a for the *tert*-Butyl and 1-Adamantyl Radicals and Ions

	adamantyl	*tert*-butyl
γ (radical)	43.4°[b]	22.1°[c]
γ (ion)	29.6°[c]	0°
difference	13.8°	22.1°
$IP_v - IP_a$	0.15 eV[d]	0.22 eV[g]

[a] See text for the definition of γ. [b] Reference 10. [c] Reference 13. [d] This work. [e] Reference 31. [f] The difference between the vertical and adiabatic IP's of the radical. [g] Reference 17a.

and radical IX. There is no obvious evidence for the allyl radical (IP_a = 8.17 eV) or IX ($IP_a \simeq$ 7.25 eV)[30] in Figure 7, but the decomposition pathway is complicated by the possibility of intramolecular hydrogen abstractions in the intermediates leading to these species.[28] The complexities arising from the possibility of hydrogen abstractions and β-CH cleavages make it difficult to assign all of the products in the region 8.1–9.0 eV in Figure 7. While PES cannot be used to identify all of the products of hydrocarbon pyrolysis, it is a unique method that can be used to directly observe the reactive intermediates that can only be inferred in mechanisms derived from gas chromatographic product studies. For this reason, PES studies of hydrocarbon pyrolysis are a useful complement to GC product studies.[18,25b,25d,27]

Geometries of the Carbonium Ions and Radicals. Several measures of nonplanarity at a radical or ion center have been used previously in the literature, and these are illustrated in Figure 8. Figure 8a shows the distance z, defined as the perpendicular distance from the spin-bearing or positive carbon to the plane containing the three α carbons. The angle θ is defined simply as the C–C–C bond angle (Figure 8b). Figure 8c shows the angle γ, which is defined as the angle between the bond formed by C_1 and C_2 and the plane formed by C_1 and the remaining carbons, C_3 and C_4. ESR data for I indicate that the distance z is 0.4 Å, a flattening of only 0.1 Å from tetrahedral geometry.[10] Yoshimine and Pacansky[31] have performed ab initio SCF calculations to determine the optimum geometries of isobutane and the *tert*-butyl radical. The calculations show that the angle γ (Figure 8c) is 22.1° for the *tert*-butyl radical. Hehre[13] and co-workers have calculated the optimum geometry for II and found the C–C bonds α to the carbocation center shortened by 0.043 Å from the length in adamantane, β–γ C–C bonds lengthened by 0.050 Å, and the C–C–C bond angle at the carbocation center opened to 117.5°. The *tert*-butyl cation is known to be planar. These geometrical

(30) Lossing, F. P.; Holmes, J. *Int. J. Mass Spectrom. Ion Phys.* **1976**, *19*, 9.

(31) Yoshimine, M.; Pacansky, J. *J. Chem. Phys.* **1981**, *74*, 5168.

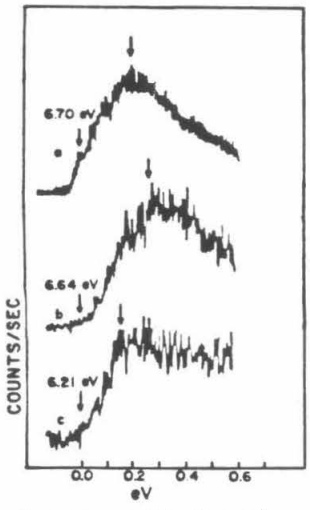

Figure 9. Photoelectron spectra of the three tertiary radicals that have been studied to date: (a) *tert*-butyl radical (from ref 17a); (b) 2-methyl-2-butyl radical from this work; (c) 1-adamantyl radical from this work. The spectra are shown so that the adiabatic ionization potentials coincide on the x axis, and the scale is in electron volts above the adiabatic ionization potential.

results are summarized in Table II, where they have all been converted to the out-of-plane angle γ for purposes of comparison. The substantial geometry difference between I and II predicted by the ESR data and the calculation is supported by the broad Franck–Condon envelope for the first photoelectron band of I with a 0.15-eV difference between IP_a and IP_v observed in this study. Table II also shows that the difference between IP_a and IP_v correlates well with the differences in geometries between the radical and cation. Figure 9 shows the photoelectron spectra of the two tertiary radicals measured in this study along with the spectrum of the *tert*-butyl radical. Interference in the 1-adamantyl radical spectrum from the spectrum of thermal decomposition products makes it difficult to compare the band for 1-adamantyl radical to the others in Figure 9. However, it is clear that the 1-adamantyl radical has a sharper onset and greater slope in the rising portion of the band than *tert*-butyl radical. The geometry changes that occur upon ionization of the 2-methyl-2-butyl radical are not known quantitatively, but the added methylene group would be expected to allow a greater geometrical change to stabilize the ion than is seen for the *tert*-butyl radical. As can be seen from Figure 9, 2-methyl-2-butyl radical has the broadest photoelectron band, with the least slope in the rising portion of the band. Hence the band widths, the difference between IP_a and IP_v, and the slopes in the rising portions of the bands all correlate well with the extent of geometrical reorganization expected upon ionization of these radicals.

The 2-adamantyl radical has been studied previously by ESR,[11] and the ESR data indicate that the radical center is planar. Since carbonium ions are also known to prefer planarity, a sharp first photoelectron band might be expected for the 2-adamantyl radical, as is the case for methyl radical, where both the cation and radical are known to be planar.[15] In Figure 10 the first band of 2-adamantyl radical is plotted on the same scale as 2-propyl radical for comparison. Figure 10 shows that the first band of 2-adamantyl is sharper than a typical secondary radical, but it is not as sharp as would be expected for a planar alkyl radical (e.g., methyl, allyl). Either the 2-adamantyl radical is not planar or the possibility of other factors leading to a broad Franck–Condon envelope must be considered. One such factor is that while the radical may be planar, as the ESR data indicate, it is unlikely that the C–C–C bond angle at the radical center is 120° due to the constraints of the adamantyl cage. This bond angle in the

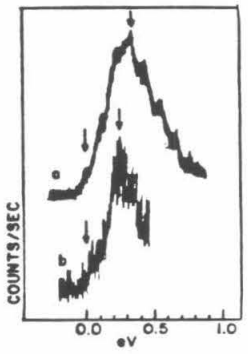

Figure 10. Photoelectron spectra of (a) 2-propyl radical (from ref 17a), and (b) 2-adamantyl radical. The spectra are plotted so that the adiabatic ionization potentials coincide on the x axis, and the scale is in electron volts above the adiabatic ionization potential.

parent hydrocarbon is 108.8° ± 1°.[32] For comparison (from Table II), the C–C–C angle in I is 112° at the bridgehead position. Carbonium ions strongly prefer a planar sp^2 geometry with C–C–C bond angles of 120°, so that the width of the 2-adamantyl band may be due to the bond angles in the radical distorting toward 120° upon ionization. Structural relaxation at the sites β and γ to the ion center, which is known to occur in the formation of the 1-adamantyl cation,[13] may also be contributing to the width of the Franck–Condon envelope.

Radical and Ion Thermochemistry. From the data for the hydride transfer reaction 1 and the difference in IP_a between I and *tert*-butyl radical,[17] adamantane is found to have a tertiary C–H bond dissociation energy 3.7 ± 1.2 kcal/mol greater than isobutane (see Figure 1 for the factor relating these quantities). The absolute value for the tertiary C–H bond dissociation energy in adamantane is 98.5 ± 1.5 kcal/mol, assuming a tertiary bond dissociation energy of 95 ± 1 kcal/mol in isobutane. The thermochemical data used in these calculations and the errors associated with them are discussed in the Appendix. In a condensed-phase study, 1-adamantyl radicals were found to abstract hydrogen from solvents such as cyclohexane,[33] implying that the tertiary C–H bond in adamantane is stronger than a typical secondary C–H bond and supporting the high tertiary bond energy found for adamantane in this study.

Similar data can be derived for the 2-methyl-2-butyl radical using the reported value of $\Delta H°$ for reaction 5 (−3.37 ± 0.20

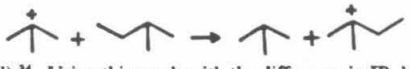

(5)

kcal/mol).[34] Using this result with the difference in IP_a between *tert*-butyl[15] and 2-methyl-2-butyl radicals (0.06 eV) gives a tertiary bond energy for isopentane 2.0 ± 1.7 kcal/mol lower than the tertiary bond energy in isobutane. As expected, the added methylene has a slightly stabilizing effect in the radical and a greater stabilizing effect in the 2-methyl-2-butyl cation.

No data on the relative hydride affinity of the 2-adamantyl cation are available from high-pressure mass spectrometry equilibrium studies or other techniques. Assuming a typical secondary C–H bond dissociation energy of 96 kcal/mol in adamantane gives a heat of formation for the 2-adamantyl radical of 12.3 kcal/mol. Combining this with the IP determined in this work (6.73 eV) gives ΔH_f[2-adamantyl cation] = 167 kcal/mol and a hydride affinity of 233.5 kcal/mol.

Strain and Stabilization Energies. The thermodynamic data discussed above and summarized in Table III show that while the

(32) Hargittai, I. *Chem. Commun.* **1971**, 1499.
(33) Engel, P. S.; Chae, W. K.; Baughman, A. S.; Marschke, E. G.; Lewis, E. S.; Timberlake, J. W.; Leudtke, A. E. *J. Am. Chem. Soc.* **1983**, *105*, 5030.
(34) Solomon, J. J.; Field, F. H. *J. Am. Chem. Soc.* **1974**, *97*, 2625.
(35) Gleicher, G. J.; Schleyer, P. v. R. *J. Am. Chem. Soc.* **1967**, *89*, 582.

Table III. Thermochemical Data for the Radicals and Ions[a]

R	$IP_a(R\cdot)$	$\Delta H_f°[R\cdot]$	$\Delta H_f°[R^+]$	$D[R-H]$	$D[R^+-H^-]$
1-adamantyl	(6.21)[†]	14.8	158.0	98.5	(224.3)[f]
2-adamantyl	(6.73)[†]	12.3	167.5	(96.0)[c]	233.8
2-methyl-2-butyl	(6.65)[†]	3.7	156.8	92.6	(228.2)[g]
tert-butyl	(6.70)[b]	(10.3)[c]	164.8	94.8	231.9

[a] All quantities except the IP_a are in kilocalories per mole. The IP_a data are in electron volts. Numbers in parenthesis are either measured or assumed. Numbers with daggers are from this work. The remaining numbers in each row are derived from these values using thermochemical cycles analogous to those shown in Figure 1. Error limits on the derived values are ±1.5 kcal/mol assuming that the assigned values for $\Delta H_f°[(CH_3)_3C\cdot]$ and D[2-adamantyl–H] are correct. Isobutane and isopentane heats of formation are from ref 46; adamantane heat of formation is from the text. [b] Reference 17a. [c] See the Appendix and ref 50. All of the values in this table are referenced to this value for $\Delta H_f°[(CH_3)_3C\cdot]$. [d] See ref 50 for the conventions used in calculating ionic heats of formation and hydride affinities. [e] Assumed value, see text. [f] Derived from the hydride affinity of *tert*-butyl carbonium ion and the relative hydride affinities measured in ref 12. [g] Derived from the relative hydride affinities from ref 34 and the hydride affinity of *tert*-butyl carbonium ion.

1-adamantyl radical is 3.7 ± 1.2 kcal/mol less stable than the *tert*-butyl radical, the 1-adamantyl cation is 7.62 ± 0.1 kcal/mol[12] *more* stable than the *tert*-butyl cation from the differences in bond energies and hydride affinities between adamantane and isobutane. This is surprising since empirical force field (EFF) calculations indicate that II would have a strain energy 12 kcal/mol greater than the strain energy in adamantane,[14] while the corresponding energy difference between the *tert*-butyl cation and isobutane calculated by the same method is only 2.85 kcal/mol.[14] Formation of II has a Δ(strain energy) 9.15 kcal/mol[14] greater than the Δ(strain energy) for formation of the *tert*-butyl cation, yet II is 7.62 kcal/mol more stable[12] than *tert*-butyl cation in the gas phase, implying that II has a total of 16.8 kcal/mol more stabilization than the *tert*-butyl cation. Carbonium ions are known to be more effectively stabilized by hyperconjugative effects than are radicals,[36] and the large stabilization energy in II can be explained on the basis of these effects.[13] Experimental evidence for the presence of C–C hyperconjugation, eq 6, has been found in the

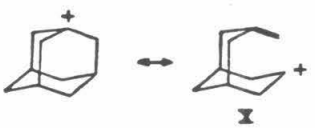

(6)

X

^{1}H NMR spectrum of II in superacid media,[37] which shows the γ protons (δ 5.21) to be more deshileded than the β protons (δ 4.19). In another study, γ-deuterium isotope effects were observed in the solvolysis of 1-adamantyl tosylates and bromides.[13] No β-deuterium isotope effect was observed. Calculations reported with the solvolysis study indicated that the C–C bonds α to the carbocation center shortened by 0.043 Å and β–γ C–C bonds lengthened by 0.050 Å.[13] Such geometry changes could reflect the importance of hyperconjugative resonance forms such as X in stabilizing II. These effects can explain the large stabilization in II since there are three carbons α to the carbocation center with orbitals ideally oriented for homohyperconjugation and C–C hyperconjugation, which are held rigidly in place by the adamantyl cage.

The difference in tertiary C–H bond energies between adamantane and isobutane shows that I is 3.7 ± 1.2 kcal/mol less stable than the *tert*-butyl radical, implying that the Δ(strain energy) for the formation of I is 3.7 kcal/mol greater than the Δ(strain energy) for the formation of *tert*-butyl radical. This result supports the results of studies on the thermal decomposition of azoalkanes,[4] peresters,[5] and other compounds,[6] which suggest the presence of substantial bridgehead strain in I. It does not agree with a more recent study on the thermal decomposition of V, which found no difference between the Δ(strain energy) for the formation of I and the *tert*-butyl radical.[7] Another recent study[8] gave a value of 2.2 kcal/mol for the difference in Δ(strain energy) between I and *tert*-butyl radical, but no error limits were given.

Table IV.[a] Determinations of the Heat of Formation of Adamantane

$H_c°(C)$[b]	ΔH_{sub}	$\Delta H_f°(g)$
−1439.89 ± 0.17[c]	14.18 ± 0.04[c]	−32.96 ± 0.19[c]
−1441.95 ± 0.68[d]	14.45 ± 0.30[d]	−30.65 ± 0.98[d]
−1442.01 ± 0.48[e]	14.23 ± 0.20[e]	−30.57 ± 0.90[e]
−1441.01 ± 0.09[f]	14.26 ± 0.20[f]	−32.51 ± 0.32[f]

[a] From Table IV of reference 43. [b] The crystalline heat of combustion. [c] Data from ref 4a. [d] Data from ref 41. [e] Data from ref 42. [f] Data from ref 43. [g] Data from ref 40b.

The hydride affinity of the 2-adamantyl cation (233 kcal/mol) shows that it is a highly stabilized carbonium ion compared to typical secondary cations such as isopropyl cation (hydride affinity = 249 kcal/mol) or 2-butyl cation (246 kcal/mol).[18] Hence, the adamantyl cage effectively stabilizes carbonium ions at both possible sites. It is also of interest to note that the norbornyl cation, a secondary C_7 ion, has a hydride affinity of 232 kcal/mol, lower than that of 2-adamantyl cation, a secondary C_{10} species. The low hydride affinity of the 2-norbornyl cation is another example of its unusual stability, which is difficult to explain without invoking nonclassical effects.

In solvolysis the 1- and 2-adamantyl cation systems have been regarded as standards for limiting S_N1 solvolytic behavior. The solvolysis rate of the 1-adamantyl tosylate exceeds that of the 2-isomer by 10^5, corresponding to an energy difference of 7 kcal/mol.[39] The smaller differences in solution than in the gas phase, 9 kcal/mol, suggests a slight preferential solvation of the 2-adamantyl cation relative to the 1-isomer. As discussed elsewhere,[3,39] studies of ion energetics in solution as well as solvolysis studies indicate that the 1-adamantyl cation is itself poorly solvated relative to species such as the *tert*-butyl cation.

Conclusion

The geometry changes that occur upon forming four of the possible reactive intermediates, I, II, III, and IV from adamantane have been shown to correlate well with the Franck–Condon envelopes observed in the first bands of the photoelectron spectra for I and III. Thermochemical data related to I, II, III, and IV that agree well with previous experimental and theoretical work have been derived from the adiabatic ionization potentials determined in this work. Unusually large stabilization of the 1- and 2-adamantyl carbonium ions, by mechanisms that have been previously determined,[13] is reflected in the hydride affinities determined in this work and the previous high-pressure mass spectrometry equilibrium measurements.[12] The difference in tertiary C–H bond energies between adamantane and isobutane determined in this work shows that there is more strain energy in I than some recent studies have determined and that alkyl radicals have a stronger preference for planarity than some of these recent studies have suggested.[7,8]

Acknowledgment. We thank J. A. Martinho Simoes and Jocelyn Schultz for helpful conversations.

Appendix

Thermochemistry. In this section the selection of appropriate values for thermochemical data relevant to this study is discussed, along with the errors associated with these data. The heat of formation of adamantane has been obtained by many groups,[40–43]

(36) See ref 14 and references contained therein.
(37) Olah, G. A.; Surya Prakash, G. K.; Shih, J. G.; Krishnamurthy, V. V.; Mateescu, G. D.; Liang, G.; Sipos, G.; Buss, V.; Gund, M. T.; Schleyer, P. v. R. *J. Am. Chem. Soc.* **1985**, *107*, 2764.
(38) Lossing, F. P.; Holmes, J. L. *J. Am. Chem. Soc.* **1984**, *106*, 6917.
(39) Schleyer, P. v. R.; Nicholas, R. D. *J. Am. Chem. Soc.* **1961**, *83*, 2700.
(40) (a) Manssen, M.; Rapport, N.; Westrum, E. F., Jr. *J. Am. Chem. Soc.* **1970**, *92*, 7296. (b) Unpublished results by Dr. M. Manssen. See Table I and ref 12 in: Schulman, J. M.; Disch, R. L. *J. Am. Chem. Soc.* **1984**, *106*, 1202.
(41) Boyd, R. H.; Sanwal, S. N.; Shury-Tehrany, S.; McNally, D. *J. Phys. Chem.* **1971**, *75*, 1264.

and the 1-adamantyl carbonium ion heat of formation has been estimated by several methods.[44,45]

McKervey and Mackle et al.[43] have determined the heats of formation of nine bridged-ring hydrocarbons and critically compared the values they obtained to previous measurements and EFF calculations. The values that they present are summarized in Table IV. From the data in Table IV, it seems most reasonable to choose $\Delta H_f°$[adamantane] = −31.6 ± 0.6 kcal/mol.

Of the published values for $\Delta H_f°$[II], one[44] requires the estimation of $\Delta H_f°$[1-adamantyl bromide] and another[45] requires the estimation of both $\Delta H_f°$[1-adamantyl bromide] and $\Delta H_f°$[1-adamantyl chloride] by group methods. Benson's group method fails for adamantane, giving $\Delta H_f°$[adamantane] = −36.52 kcal/mol.[46] This is not surprising since a substantial amount of strain energy in the adamantane ring system is predicted by EFF calculations.[14] On this basis, there is no reason to expect that the group method can be applied successfully to calculations of the heats of formation of 1-chloro- and 1-bromo-adamantane. Hence, estimates of $\Delta H_f°$[II] calculated from estimated heats of formation of the 1-halo-adamantanes must be regarded with suspicion.

A reliable estimate of $\Delta H_f°$[II] can be derived from a photoionization appearance potential measurement of II from adamantane.[47] The appearance potential obtained, 10.6 eV, yields $\Delta H_f°$[II] = 160 kcal/mol. This value should be a good estimate since 1,2-hydride shifts are not allowed in II,[48] and Schwarz[49] has shown that loss of hydrogen occurs exclusively at the bridgehead sites in electron impact ionization of adamantane, so that II should be the only ion formed by the loss of hydrogen from the parent adamantyl radical ion. Comparison of this absolute value for $\Delta H_f°$[II] to the values for the relative hydride affinity of II from the gas-phase equilibrium studies presented in Table X is made difficult by uncertainty in the value for $\Delta H_f°[(CH_3)_3C\cdot]$,[50] which leads to uncertainty in the value for $\Delta H_f°[(CH_3)_3C^+]$. Choosing $\Delta H_f°[(CH_3)_3C\cdot]$ = 10.3 ± kcal/mol gives $\Delta H_f°[(CH_3)_3C^+]$ = 165 kcal/mol.[51] Then, from Kebarle and Sharma's measurement of ΔH for reaction 1, with $\Delta H_f°$[adamantane] and $\Delta H_f°$[isobutane], $\Delta H_f°$[II] is calculated to be 158 ± 3 kcal/mol, in good agreement with the value calculated from the ionization potential measurement mentioned above.

Clearly, the measurement of $\Delta H°$ for reaction 1 by high-pressure mass spectrometry equilibrium experients is the most precise, and it is this value that was used to calculate the difference in tertiary bond energies between adamantane and isobutane. It should be stressed that this difference is known to a precision of ±1 kcal/mol, but the final assignment of absolute bond energies must await agreement on a value for $\Delta H_f°[(CH_3)_3C\cdot]$.

(42) Butler, R. S.; Carson, A. S.; Laye, P. G.; Steele, W. V. *J. Chem. Thermodyn.* **1971**, *3*, 277.

(43) Clark, T.; Mc O. Knox, T.; McKervey, M. A.; Mackle, H.; Rooney, J. J. *J. Am. Chem. Soc.* **1979**, *101*, 2404.

(44) Fort, R. C. In *Carbonium Ions*; Olah, G. A., Schleyer, P. v. R., Eds.; Wiley: New York, 1973, Vol. IV, p 1783 ff.

(45) Allison, J.; Ridge, D. P. *J. Am. Chem. Soc.* **1979**, *101*, 4998.

(46) Group values from: Cox, S. C.; Pilcher, G. *Thermochemistry of Organic and Organometallic Compounds*; Academic: New York, 1970.

(47) Federova, M. S.; Potapov, V. K.; Denisor, Yu. V.; Sorokin, v. V.; Erlasheva, T. I. *Zh. Fiz. Khim.* **1974**, *48*, 1828; *Russ. J. Phys. Chem. Engl. Transl.* **1974**, *48*, 1078.

(48) Schleyer, P. v. R.; Lam, L. K. M.; Raber, D. F.; Fry, J.L.; McKervey, M. A.; Alford, J. R.; Cuddy, B. D.; Keizer, V. G.; Celuk, H. W.; Schlatmann, J. L. M. A. *J. Am. Chem. Soc.* **1970**, *92*, 5246.

(49) Wesdemiotis, C.; Schilling, M.; Schwarz, H. *Angew. Chem., Int. Ed. Engl.* 1979, *18*, 950; *Angew. Chem.* **1979**, *91*, 1017.

(50) (a) Doering, W. v. E. *Proc. Natl. Acad. Sci. U.S.A.* **1981**, *78*, 5279. $\Delta H_f[(CH_3)_3^+]$ = 165 kcal/mol was calculated from $\Delta H_f[(CH_3)_3\cdot]$ = 10.3 kcal/mol from ref 50a and the IP_a of $(CH_3)_3\cdot$ from ref 17a. The ionic heat of formation was calculated by using the convention that the heat of formation of an electron at rest is zero at all temperatures.[51] Therefore, $\Delta H_f[H^-]$ = 34.7 kcal/mol.[51] Some recent results that support a high value for $\Delta H_f[(CH_3)_3C\cdot]$ were reported by Tsang (ref 50b), who obtained $\Delta H_f[(CH_3)_3C\cdot]$ = 12.3 kcal/mol. (b) Tsang, W. *J. Am. Chem. Soc.* **1985**, *107*, 2872.

(51) Rosenstock, H. M; Draxl, K.; Steiner, B. W.; Herron, J. T. *J. Phys. Chem. Ref. Data, Suppl.* **1977**, 6.

CHAPTER 3

Photoelectron Spectroscopy of the *o*-, *m*- and *p*-Methylbenzyl Radicals. Implications for the Thermochemistry of the Radicals and Ions.

K. Hayashibara, G. H. Kruppa and J. L. Beauchamp

Reprinted from the Journal of the American Chemical Society, 1986, 108, 5441.

Photoelectron Spectroscopy of the *o*-, *m*-, and *p*-Methylbenzyl Radicals. Implications for the Thermochemistry of the Radicals and Ions

K. Hayashibara, G. H. Kruppa, and J. L. Beauchamp*

Contribution No. 7331 from the Arthur Amos Noyes Laboratory of Chemical Physics, California Institute of Technology, Pasadena, California 91125. *Received March 3, 1986*

Abstract: The first photoelectron bands of *o*-, *m*-, and *p*-methylbenzyl radicals have been obtained by studying the products from the flash vacuum pyrolysis of the appropriate alkyl nitrites. The photoelectron spectra all show vibrational structure, and the vertical and adiabatic ionization potentials coincide in all cases. The ionization potentials are 7.07 ± 0.02, 7.12 ± 0.02, and 6.96 ± 0.02 eV for the *o*-, *m*-, and *p*-methylbenzyl radicals, respectively. These values are all lower than the adiabatic ionization potential of the benzyl radical (7.20 ± 0.02 eV). These results, when combined with relative heterolytic bond energy data, give accurate relative homolytic bond-dissociation energies. The homolytic benzylic C–H bond-dissociation energies in *o*-, *m*-, and *p*-xylene were found to be 0.91 ± 0.5, 0.36 ± 0.5, and 0.58 ± 0.5 kcal mol^{-1} lower than the benzyl C–H bond energy in toluene, respectively. The implications of these ionization potentials and relative bond energies for the absolute values of the heterolytic and homolytic benzyl C–H bonds in toluene and the tertiary C–H bond in isobutane are discussed.

Homolytic bond-dissociation energies have previously been measured by kinetic techniques such as bromination[1] and iodination[2] kinetics and very low pressure pyrolysis (VLPP).[3] These techniques all measure individual absolute homolytic bond energies and are subject to moderate uncertainty. Difficulties also arise from complications such as chain and wall reactions.[2] As an alternative to these experiments we have recently explored the combination of relative heterolytic bond-dissociation energies, i.e., relative hydride and chloride affinities from high-pressure mass spectrometry, with ionization potentials of radicals from photoelectron spectroscopy to provide highly precise *relative* homolytic bond-dissociation energies.[4] The relationships between relative heterolytic bond-dissociation energies, ionization potentials, and relative homolytic bond-dissociation energies are shown in the thermochemical cycle in Figure 1, where X = H or Cl. The difference in the adiabatic ionization potentials for two radicals, $\Delta H°$ for reaction 1, can be combined with the difference in heterolytic bond energies for the corresponding carbonium ions, $\Delta H°$ for reaction 2, to yield the difference in homolytic bond-dissociation energies, $\Delta H°$ for reaction 3. Errors associated with

$$R_1^+ + R_2^\cdot \rightarrow R_2^+ + R_1^\cdot \quad (1)$$

$$R_1X + R_2^+ \rightarrow R_2X + R_1^+ \quad (2)$$

$$R_1X + R_2^\cdot \rightarrow R_2X + R_1^\cdot \quad (3)$$

the ionization potential measurements are about 0.4 kcal mol^{-1}, and the relative heterolytic bond dissociation energy measurements have errors of about 0.2–0.4 kcal mol^{-1}.[5] Hence relative homolytic bond energies can be determined to within an accuracy of about 0.4–1.0 kcal/mol^{-1} with this method, which approaches the accuracy of the best kinetic methods.[2] The precise relative homolytic bond energies obtained in this way can be used to check the consistency of the bond energies obtained by kinetic methods and to extend bond energy measurements to include values that have not been previously determined by kinetic methods.

In this study the first photoelectron bands and adiabatic ionization potentials of the *o*-, *m*-, and *p*-methylbenzyl radicals have been obtained. The first photoelectron band of the unsubstituted benzyl radical is available from a previous study from this laboratory.[6] The methyl-substituted benzyl radicals make an excellent test case for this method of determining bond energies. The effect of substituents on the benzyl bond energies and reactivity of substituted toluenes has been the subject of extensive study.[7] Several recent studies have shown the importance of benzyl C–H bond energy changes caused by substitution in determining H atom abstraction rates from substituted toluenes.[8] The benzyl C–H bond energy in toluene is used as a reference for other homolytic bond energy determinations, and there is a need for further experimental work to confirm and refine the kinetic values for this bond energy.[9]

The earliest measurements of the benzylic C–H bond energies in toluene and substituted toluenes were made by Szwarc and co-workers, who studied the kinetics of C–H bond fission in toluene and the three xylenes.[10] They determined benzylic C–H bond energies of 77.5 kcal mol^{-1} for toluene and 74.0, 77.5, and 75 kcal mol^{-1} for *o*-, *m*-, and *p*-xylene, respectively. A subsequent study of gas-phase free radical bromination kinetics yielded a value of 89.6 kcal mol^{-1} for the benzyl C–H bond energy in toluene.[1] Benson critically reviewed much of the early kinetic work on toluene and the xylenes and recommended 88.3 kcal mol^{-1} for the benzyl C–H bond energy in toluene.[11] Zavitsas recommended a value of 88.1 kcal mol^{-1},[12] and Golden gave a value of 88.0 ± 1 kcal mol^{-1} in a recent review.[9] Further support for $DH°(C_6H_5CH_2–H)$ = 88 ± 1 kcal mol^{-1} comes from a recent proton affinity study by Meot-Ner which yielded a value of 88.9 kcal mol^{-1}.[13] A recent VLPP study of benzyl C–C bond strengths in substituted ethylbenzenes yielded 74.1 ± 0.6 kcal mol^{-1} for the benzylic C–C bond in ethylbenzene.[3] The same study yielded values of 72.9 ± 0.6, 73.8 ± 0.5, and 73.7 ± 0.5 kcal mol^{-1} for the benzylic C–C bond energies in *o*-, *m*-, and *p*-methylethylbenzene, respectively, thus suggesting that methyl substitution has a very small effect on the benzyl bond energy in toluene.

* To whom correspondence should be addressed.

(1) Anderson, H. R.; Scheraga, H. A.; Van Artsdalen, E. R. *J. Chem. Phys.* **1953**, *21*, 1258.
(2) Golden, D. M.; Benson, S. W. *Chem. Rev.* **1969**, *69*, 125.
(3) Barton, B. D.; Stein, S. E. *J. Phys. Chem.* **1980**, *84*, 2141.
(4) Kruppa, G. H.; Beauchamp, J. L. *J. Am. Chem. Soc.*, submitted.
(5) Sharma, R. B.; Sen Sharma, D. K.; Hiroaka, K.; Kebarle, P. *J. Am. Chem. Soc.* **1985**, *107*, 3747.
(6) Houle, F. A.; Beauchamp, J. L. *J. Am. Chem. Soc.* **1978**, *100*, 3290.
(7) (a) Pryor, W. A. *Free Radicals*; McGraw-Hill: New York, NY; p 170. (b) Pryor, W. A.; Church, D. F.; Tang, F. Y.; Tang, R. H. *Frontiers in Free Radical Chemistry*; Pryor, W. A., Ed., Academic Press: New York, 1980; p 355. (c) Afanas'ev, I. B. *Int. J. Chem. Kinet.* **1981**, *13*, 173. (d) Patnaik, L. N.; Mallick, N.; Rout, M. K.; Rout, P. S. *Can. J. Chem.* **1980**, *58*, 2754. (e) Zavitsas, A. A.; Pinto, J. A. *J. Am. Chem. Soc.* **1972**, *94*, 7390. (f) Gilliom, R. D.; Ward, F. W., Jr. *J. Am. Chem. Soc.* **1965**, *87*, 3944.
(8) (a) Zavitsas, A. A.; Fogel, G.; Halwagi, K. E.; Legotte, P. A. D. *J. Am. Chem. Soc.* **1983**, *105*, 6960. (b) Pryor, W. A.; Tang, F. Y.; Tang, R. H.; Church, D. F. *J. Am. Chem. Soc.* **1982**, *104*, 2885.
(9) McMillen, D. F.; Golden, D. M. *Annu. Rev. Phys. Chem.* **1982**, *33*, 514–515.
(10) Szwarc, M. *J. Chem. Phys.* **1948**, *16*, 128.
(11) Benson, S. W.; O'Neal, H. E. *Natl. Stand. Ref. Data Ser. (U.S. Natl Bur. Stand.)* **1970**, *No. 21*, 394–396.
(12) Zavitsas, A. A.; Melikian, A. A. *J. Am. Chem. Soc.* **1975**, *97*, 2757.
(13) Meot-Ner, M. *J. Am. Chem. Soc.* **1982**, *104*, 5.

0002-7863/86/1508-5441$01.50/0

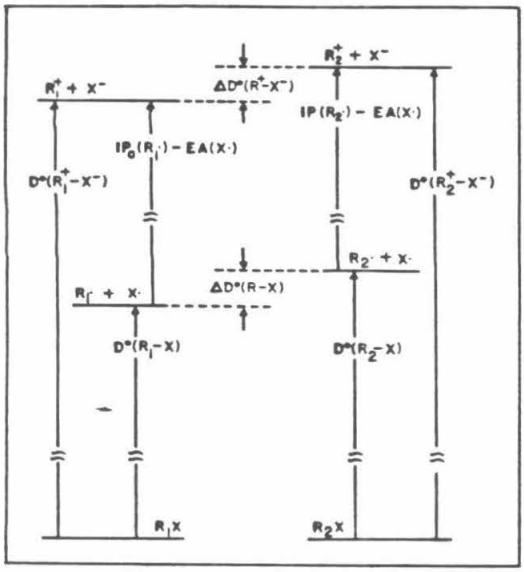

Figure 1. Thermochemical scheme showing the relationships between relative homolytic bond energies, $\Delta D^\circ(R-X)$, relative heterolytic bond energies, $\Delta D^\circ(R^+-X^-)$, and free radical adiabatic ionization potentials, IP ($R^\cdot$). For comparison of the two species R_1X and R_2X, heats of formation of the parent molecules are used to define the zero of the energy scales.

Experimental Section

The radicals studied in this work were produced by pyrolysis of the appropriate alkyl nitrites, (reactions 4 and 5). The nitrites were synthesized from *o*-, *m*-, and *p*-methylphenethyl alcohol obtained from Aldrich, using a standard method.[14] In each case the purity of the nitrite product was checked by NMR spectroscopy.

$$RCH_2ONO \rightarrow RCH_2O^\cdot + NO \quad (4)$$

$$RCH_2O^\cdot \rightarrow R^\cdot + CH_2O \quad (5)$$

The photoelectron spectrometer used in these experiments was an instrument of standard design that has been modified to study the products of flash vacuum pyrolyses. A description of the instrument can be found in a previous publication.[6] The pyrolyzer used in this study was 2 cm in length, corresponding to the "long" pyrolyzer used in an earlier study.[15]

Photoelectron spectra of the pyrolysis products were obtained with He I radiation, at temperatures from 450 to 650 °C. The energy scales for the pyrolysis product spectra were calibrated with He Iα bands of CH_3I and CH_2O and the He Iβ bands of CH_3I. The room temperature spectra of the nitrites were calibrated with the He Iα bands of Ar and CH_3I. The typical instrumental resolution for these experments was 30–35 mV, as determined from the fwhm of the $Ar^2P_{3/2}$ band. The instrumental resolution is the full-width at half-maximum of an atomic line. Peak maxima can easily and reproducibly be determined to within 0.02 eV with careful calibration in cases where the peak is sharp. Error limits of 0.03–0.05 eV are assigned for cases where the peak maxima are difficult to locate or calibrate accurately.

Results

The He I photoelectron spectra of the *o*-, *m*-, and *p*-methylphenethyl nitrites are similar to the spectrum of the 2-phenylethyl nitrite obtained in a previous study,[6] and the spectra are not reproduced here. The vertical ionization potentials of the first photoelectron bands of *o*-, *m*-, and *p*-methylphenethyl nitrite are 8.88 ± 0.05, 8.92 ± 0.05, and 8.58 ± 0.05 eV, respectively. The spectra of the first photoelectron bands of *o*-, *m*-, and *p*-methylbenzyl radicals are shown in Figure 2 along with the spectrum of benzyl radical from the previous study.[6] The spectra shown in Figure 2 were recorded at a pyrolyzer temperature of 570 °C, which was sufficient to decompose all of the nitrite. The spectra shown in Figure 2 appeared at pyrolysis temperatures above 380 °C and were independent of temperature over the range studied, to 650 °C.

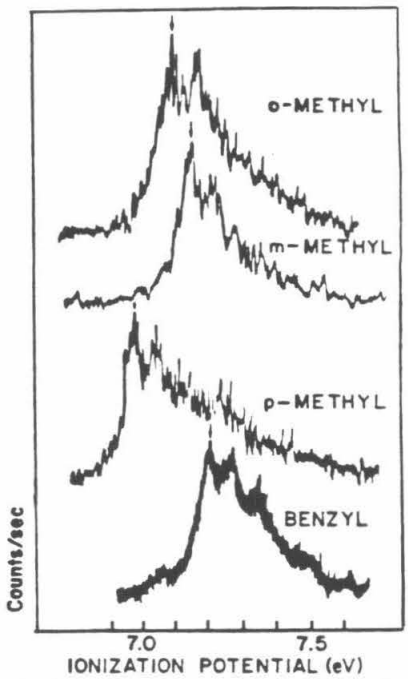

Figure 2. The He I photoelectron spectra of benzyl radical (ref 6) and the methyl-substituted benzyl radicals (this work). The radicals were produced by pyrolysis of the appropriate alkyl nitrites at 570 °C. The adiabatic ionization potentials are indicated by the arrow on each spectrum.

As is the case for the benzyl radical, all of the methylbenzyl radicals show evidence for vibrational structure in the first band of their photoelectron spectra. The spectra are all similar, and the adiabatic and vertical ionization potentials coincide in all cases. From the spectra in Figure 2 the adiabatic ionization potentials are 7.07 ± 0.02 eV, 7.12 ± 0.02 eV, and 6.96 ± 0.02 eV for the *o*-, *m*-, and *p*-methylbenzyl radicals, respectively. The vibrational structure in the methylbenzyl radicals is less well resolved than in the benzyl radical, and the vibrational spacings can only be determined within an error of 80 cm^{-1}. The vibrational frequencies observed are 480, 490, and 400 cm^{-1} for the *o*-, *m*-, and *p*-methylbenzyl radicals, respectively. The vibrational frequency observed in the first band of the benzyl radical photoelectron spectrum is 560 cm^{-1}.[6]

Discussion

The band shapes and vibrational envelopes of the first photoelectron bands of the *o*-, *m*-, and *p*-methylbenzyl radicals are all similar to each other and to the benzyl radical.[6] However, the radicals have significantly different ionization potentials, which suggests that photoelectron spectroscopy could be used as a technique to distinguish the isomeric xylyl radicals.

The ionization potentials of benzyl[6] and *m*- and *p*-methybenzyl radicals obtained by PES are considerably lower than those reported by Lossing in an earlier electron-impact study.[16] His

(14) Levin, N.; Hartung, W. *Organic Synthesis*; Wiley: New York, 1955; Collect. Vol. III, p 192.
(15) Schultz, J. C.; Houle, F. A.; Beauchamp, J. L. *J. Am. Chem. Soc.* **1984**, *106*, 3917.
(16) Lossing, F. P.; Ingold, K. U.; Henderson, I. H. S.; *J. Chem. Phys.* **1954**, *22*, 621.

Table I. Heterolytic and Homolytic Bond Energies for Isobutane, Toluene, and the Isomeric Xylenes[a]

R	IP	$\Delta H_f°[R^+]$	$DH°[R-H]$	$D°[R^+-H^-]$	$\Delta H_f°[R^\cdot]$
tert-butyl	(6.70)[b]	(166.5)[c]	96.5	233.7	12.0
$C_6H_5CH_2$	(7.20)[d]	214.1[e]	88.2	236.9	48.1
o-$CH_3C_6H_4CH_2$	(7.07)[f]	202.8[g]	87.3	233.0	39.8
m-CH_3-$C_6H_4CH_2$	(7.12)[f]	204.0[g]	87.8	234.7	39.8
p-$CH_3C_6H_4CH_2$	(6.96)[f]	200.3[g]	87.6	230.8	39.8

[a] All values are in kcal mol^{-1} except the IP which are given in eV. Values in parentheses are numbers measureed in this work or other studies. *All* other values are derived from the numbers in parentheses and relative hydride and chloride affinities from ref 5. Errors on all quantities are estimated to be ±1 kcal mol^{-1}, but relative bond energies and hydride affinities are known to ±0.5 kcal mol^{-1} for toluene and the xylyl radicals (see text). All calculations use the convention that the heat of formation of an electron at rest is zero at all temperatures.[24] [b] Reference 20. [c] Recommended value, see ref 19. [d] Reference 6. [e] Derived by using the relative chloride affinity between $(CH_3)_3C^+$ and $C_6H_5CH_2^+$ from ref 5. $\Delta H_f°[(CH_3)_3CCl]$ and $\Delta H_f°[C_6H_5CH_2Cl]$ from ref 22, $\Delta H_f°[Cl^\cdot]$ from ref 23, the IP of $C_6H_5CH_2$ from column 1, and $\Delta H_f°[(CH_3)_3C^+]$ from column 2, row 1. [f] This work. [g] From $D°[R^+-H^-]$, $\Delta H_f°[H^-] = 34.8$ kcal mol^{-1}, ref 19b, and the hydrocarbon heats of formation, ref 22.

measurements yielded adiabatic ionization potentials of 7.73 ± 0.08, 7.65 ± 0.03, and 7.46 ± 0.03 eV for benzyl radical and *m*- and *p*-methylbenzyl radicals, respectively. In a later electron impact study of the benzyl radical Lossing obtained a vertical ionization potential of 7.27 ± 0.03 eV,[17] which is in better agreement with the PES result of 7.20 ± 0.02 eV.[7] Lossing attributed the difference between the two electron-impact results to an underestimation of the onset of the ionization efficiency curve in the earlier study. This may also explain the difference between the electron impact and PES results for the *m*- and *p*-methylbenzyl radicals.

Relative Bond Energies and Reactivities. The bond-dissociation energies of the benzyl C–H bonds, relative to the benzyl C–H bond in toluene ($\Delta H°$ for reaction 3), were calculated from measured enthalpy changes for reactions 1 and 2 as described in the introduction. Kebarle and co-workers determined the relative chloride affinities of the benzyl and the *o*-, *m*-, and *p*-methylbenzyl cations in a high-pressure mass spectrometry equilibrium study which provided values with error limits of 0.2 kcal mol^{-1} and good internal consistency.[5] The heats of formation of the parent xylyl chlorides have not been determined, so it is not possible to convert the relative chloride affinities to relative hydride affinities. Equality of the relative chloride and hydride affinities of two cations, R_1^+ and R_2^+, requires that eq 6 be satisfied. For similar compounds like benzyl chloride and the xylyl chlorides, this

$$\Delta H_f°(R_1H) - \Delta H_f°(R_2H) = \Delta H_f°(R_1Cl) - \Delta H_f°(R_2Cl) \quad (6)$$

condition would be expected to be met, and the chloride and hydride affinities would be expected to be nearly equal.[5] Evidence to support the equality of the hydride and chloride affinities in this case comes from a theoretical calculation of the hydride affinities,[18] which gave values for the relative hydride affinities of *p*-, and *m*-methylbenzyl cations that are very close to the relative chloride affinities determined by Kebarle and co-workers.[5] With the assumption that the relative hydride and chloride affinities are equal, the homolytic benzyl C–H bond-dissociation energy of the ortho species was found to be 0.9 ± 0.5 kcal mol^{-1} lower than that for toluene, while the bond energies for the meta and para species were 0.36 ± 0.5 kcal mol^{-1} and 0.59 ± 0.5 kcal mol^{-1} lower, respectively, than that for toluene. These results agree qualitatively with the earlier work by Szwarc,[10] who found that the bond energies in *o*-, *m*-, and *p*-xylene were 3.5, 0.0, and 0.5 kcal mol^{-1} lower than the C–H bond energy in toluene. Our results show better quantitative agreement with a more recent VLPP study on the benzylic C–C bond energies in substituted ethylbenzenes,[3] which showed that the benzylic C–C bond energies in *o*-, *m*-, and *p*-methylethylbenzene are 1.20, 0.31, and 0.41 kcal mol^{-1} less than the benzylic C–C bond energy in ethylbenzene. Benson has reexamined the early work of Szwarc and others and concluded that many of the experiments suffer from errors due to chain reactions and wall reactions.[11] The results from our laboratory and the VLPP results suggest that methyl substitution at the meta and para positions has only a small effect on the benzyl bond energy in toluene. The larger effect of methyl substitution at the ortho position is probably due to steric considerations, as has been suggested by Barton and Stein.[3] The small but significant effect on benzylic C–H bond energies caused by methyl substitution at the meta and para positions in toluene could be partly responsible for the different rates observed for H atom abstractions from *m*- and *p*-xylene.[7]

Absolute Bond Energies. In order to assign absolute bond energy values to the xylenes studied in this work, it is necessary to choose a reference absolute bond energy or hydride affinity. The most recent recommended value for $\Delta H_f°[(CH_3)_3C^+]$ is 166.5 kcal mol^{-1},[19] from which the hydride affinity of the *tert*-butylcarbonium ion can easily be derived. Using this value for the heat of formation of the *tert*-butylcarbonium ion with the adiabatic ionization potential of the *tert*-butyl radical from an earlier PES study from this laboratory[20] (6.70 ± 0.03 eV) gives 12.0 ± 0.5 kcal mol^{-1} for the heat of formation of the *tert*-butyl radical, in excellent agreement with the value of 12.5 kcal mol^{-1} recently recommended by Tsang.[21] Combining these absolute values with the adiabatic ionization potential of the benzyl radical,[6] the relative chloride affinity between *tert*-butyl- and benzylcarbonium ions,[5] the heats of formation of the parent chlorocarbons,[22] and $\Delta H_f°(Cl^\cdot)$[23] leads to a value of 88.2 ± 1.0 kcal mol^{-1} for the benzylic C–H bond energy in toluene, in excellent agreement with the value of 88 ± 1.0 kcal mol^{-1} recommended by Golden and others.[9,11-13] The heats of formation, bond energies, and hydride affinities resulting from the choice of $\Delta H_f°[(CH_3)_3C^+] = 166.5$ kcal mol^{-1} are summarized in Table I. The consistency of these data lends strong support to Tsang's recommended value of 12.5 kcal mol^{-1} for the heat of formation of *tert*-butyl radical and suggests that the value preferred by Golden[9] in a recent review may be too low. Most important, Golden's recommended values for the heats of formation of the *tert*-butyl and benzyl radicals are not consistent with current ion-thermochemistry data. If the heat of formation of *tert*-butyl radical is indeed lower than 12.5 kcal mol^{-1}, then the heat of formation of the benzyl radical must be lower by the same amount.

Acknowledgment. We are grateful for the support of the National Science Foundation under Grant CHE-840857.

Registry No. *t*-BuH, 75-28-5; *t*-Bu$^\cdot$, 1605-73-8; *t*-Bu$^+$, 14804-25-2; $PhCH_3$, 108-88-3; $PhCH_2^\cdot$, 2154-56-5; $PhCH_2^+$, 6711-19-9; *o*-$CH_3C_6H_4CH_3$, 95-47-6; *o*-$CH_3C_6H_4CH_2^\cdot$, 2348-48-3; *o*-$CH_3C_6H_4CH_2^+$, 63246-55-9; *m*-$CH_3C_6H_4CH_3$, 108-38-3; *m*-$CH_3C_6H_4CH_2^\cdot$, 2348-47-2; *m*-$CH_3C_6H_4CH_2^+$, 60154-94-1; *p*-$CH_3C_6H_4CH_3$, 106-42-3; *p*-$CH_3C_6H_4CH_2^\cdot$, 2348-52-9; *p*-$CH_3C_6H_4CH_2^+$, 57669-14-4.

(17) Lossing, F. P. *Can. J. Chem.* **1971**, *49*, 357.
(18) Hehre, W. J.; Taagepera, M.; Taft, R. S.; Topson, R. D. *J. Am. Chem. Soc.* **1981**, *103*, 1344.
(19) (a) Reference 5. (b) Lias, S. G.; Liebman, K. J. F.; Levin, R. D. J. *J. Phys. Chem. Ref. Data* **1977**, *6*, Suppl. 1. (c) Baer, T. J. *J. Am. Chem. Soc.* **1980**, *102*, 2482.
(20) Houle, F. A.; Beauchamp, J. L. *J. Am. Chem. Soc.* **1978**, *100*, 4067.
(21) Tsang, W. *J. Am. Chem. Soc.* **1985**, *107*, 2872.
(22) All neutral hydrocarbon heats of formation are from the following: Cox, S. C.; Pilcher, G. *Thermochemistry of Organic and Organometallic Compounds*; Academic Press: New York, 1970.
(23) Darwent, B. deB. *Natl. Stand. Ref. Data. Ser. (U.S. Natl. Bur. Stand.)* **1970**, *No. 31*, 25.
(24) Rosenstock, H. M.; Draxl, J.; Steiner, B. W.; Herron, J. T.; *J. Phys. Chem. Ref. Data Suppl.* **1977**, *6*.

CHAPTER 4

Studies of the Gas Phase Reactive Intermediates Formed by Heterogeneous Processes in Chemical Vapor Deposition using Photoelectron Spectroscopy and Mass Spectrometry.

G. H. Kruppa, S. K. Shin and J. L. Beauchamp

INTRODUCTION

The chlorosilanes, SiH_xCl_{4-x}, have commonly been used for the deposition of thin silicon films.[1] A wide variety of conditions have been employed for the chemical vapor deposition of silicon films, with pressures ranging from 0.1 torr (Low Pressure CVD, LPCVD) to 760 torr (Atomospheric Pressure CVD, APCVD), and surface temperatures ranging from 900-1100 °C. The importance of CVD to the electronics industry has led to a number of attempts to measure the concentrations and identities of the species present in CVD systems. The techniques employed to date include thermodynamic equilibrium calculations,[2] gas chromatography,[3] mass spectrometry,[4] optical studies[5] and laser induced fluorescence.[6] The remainder of this paper will be confined to discussion of CVD systems using dichlorosilane and trichlorsilane as source gases. In spite of the extensive studies performed on chlorosilane CVD systems some controversy remains as to the identities and concentrations of the reactive intermediates present in these systems.

Sedgwick *et al.* used fluorescence scattering to profile the concentration of $SiCl_2$ in an APCVD reactor using $SiCl_4$ and SiH_2Cl_2 as input gases.[5] $SiCl_2$ was found to be the major intermediate present, and the concentration profiles best fit a model where $SiCl_2$ is formed *homogeneously* in the gas phase above the hot susceptor. This result agrees with thermodynamic calculations which indicate that $SiCl_2$ is the dominant silicon containing species in the vapor phase under CVD conditions between 1000 and 1200 °C.[2] $SiCl_2$ has also been detected by mass spectrometric sampling of the hot gases in a reactor designed to simulate CVD conditions, with a variety of Si-Cl-H compounds and mixtures used as input gases.[4] However, in a more recent study, Ho and Breiland detected the laser induced fluorescence spectrum of SiHCl in a CVD reactor under both APCVD

and LPCVD conditions.[6] Ho and Breiland also asserted that the fluorescence observed by Sedgwick *et al.* was due to SiHCl and not $SiCl_2$. Finally, a recent study by Sausa and Ronn on the IR multiphoton dissociation of SiH_2Cl_2 showed that $SiCl_2$ and H_2 were the only products observed in the homogeneous gas phase decomposition of dichlorosilane.[7] Further studies are clearly needed to determine the relative importance of intermediates such as $SiCl_2$ and SiHCl in CVD systems using the chlorosilanes as source gases.

In this report results on the mechanism of the flash vacuum pyrolysis of dichlorosilane and trichlorosilane obtained using a combination of Photoelectron Spectroscopy (PES) and mass spectrometry are presented. The flash vacuum pyrolysis conditions employed in this study were 1-10 millitorr of the chlorosilane gas over a quartz pyrolyzer surface at 600-1100 °C (see experimental section for further details). While the conditions used in this study involve pressures considerably lower than typical CVD conditions,[1] the formation of a thin silicon film was observed on the pyrolyzer surface, showing that CVD does take place at these low pressures. In addition, under flash vacuum pyrolysis conditions thermal activation takes place primarily by contact with the hot pyrolyzer walls, so that processes observed in this study are the result of heterogeneous reactions. This is in contrast to many studies of CVD reactions where both heterogeneous and homogeneous reactions must be considered.[1] Hence, although the results in this study were not obtained under typical CVD conditions, they do have important implications for the mechanism of surface processes in CVD systems.

PES has previously been shown in our laboratory,[8] and by others,[9] to be a useful technique for studying reactive intermediates in gas-solid heterogeneous reactions. Bock *et al.* have previously measured the photoelectron spectrum of $SiCl_2$ produced by $SiCl_4$ thermal decomposition on solid silicon.[10] Unlike laser

Figure 1. Diagram of the instrument used in this work. (a) Cutaway view of the instrument showing the pyrolyzer, scattering chamber, electron energy analyzer, and mass spectrometer ionizer. (b) Detail of the flash vacuum pyrolyzer.

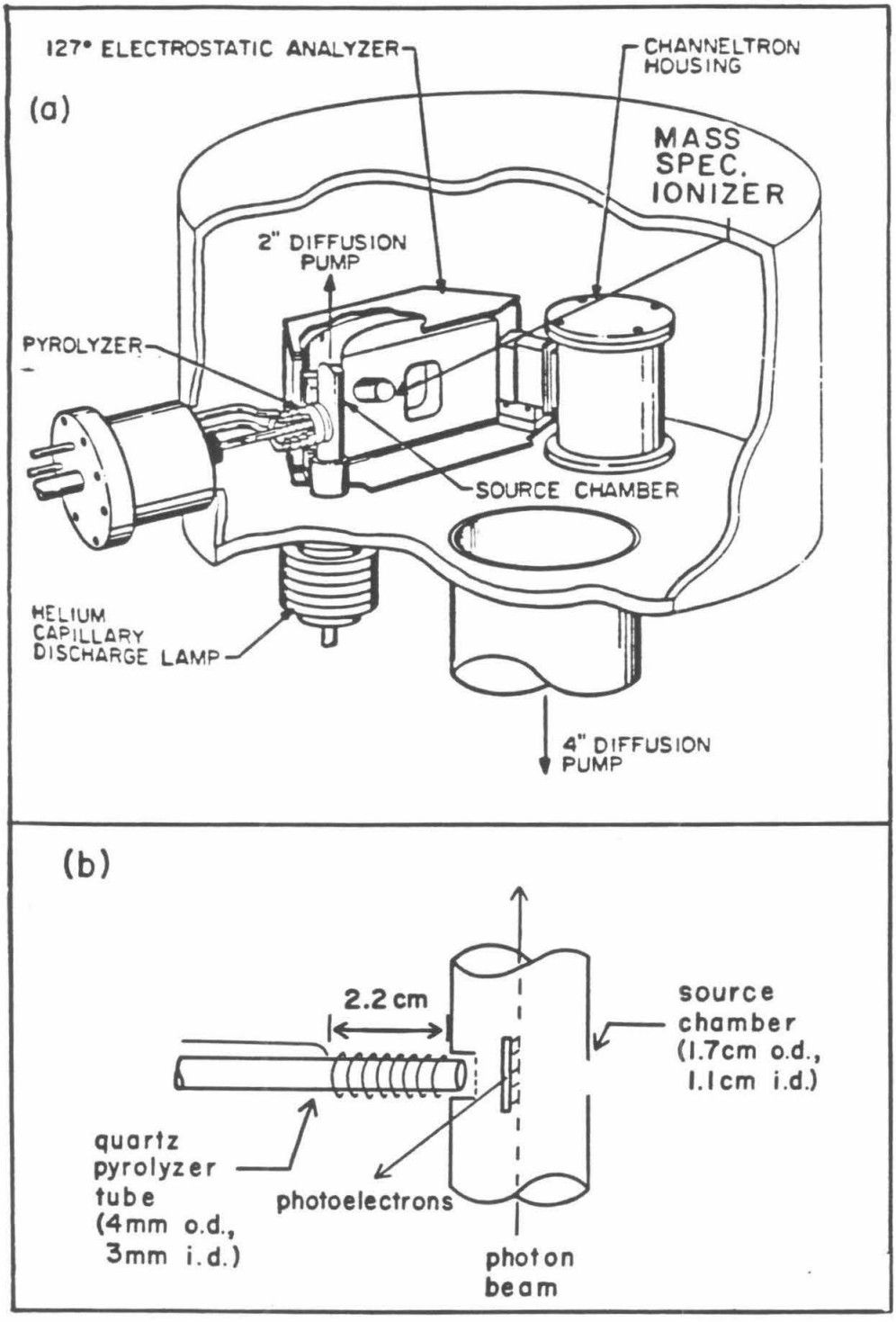
127° ELECTROSTATIC ANALYZER
CHANNELTRON HOUSING
(a)
MASS SPEC. IONIZER
2" DIFFUSION PUMP
PYROLYZER
SOURCE CHAMBER
HELIUM CAPILLARY DISCHARGE LAMP
4" DIFFUSION PUMP
(b)
2.2 cm
source chamber (1.7cm o.d., 1.1cm i.d.)
quartz pyrolyzer tube (4mm o.d., 3mm i.d.)
photoelectrons
photon beam

induced fluorescence, where species of interest are selectively induced by a laser, PES detects all species present in a gas mixture simultaneously. Hence qualitative estimates of relative concentrations of the reactive intermediates and stable species in a gas mixture can be made, which is difficult to accomplish by laser induced fluorescence. Quantitative measurements of relative concentrations are hindered because the relative photoionization cross sections of the species of interest must be known and often are unavailable. Mass spectrometric measurements on pyrolysis mixtures are often complicated by fragmentation of the ions formed by electron impact. The fragment ions produced often have the same masses as reactive intermediate species that are of interest. As will be shown in the results below, PES is a complimentary technique to mass spectrometry which allows the unambiguous detection of reactive intermediates and the determination of relative product concentrations in the heterogeneous decomposition of SiH_2Cl_2 and $SiHCl_3$ on a hot silicon surface.

EXPERIMENTAL SECTION

Figure 1a shows the photoelectron spectrometer used in these studies which has been specially modified to detect the reactive intermediate products of flash vacuum pyrolyses and has been described in detail previously.[11] Only details of the pyrolyzer will be discussed here, and a detail drawing of the pyrolzyer is shown in Figure 1b. The pyrolysis takes place within a quartz tube with an inner diameter of 3 mm. The pyrolyzer is heated by double stranded heating wire wound over a 2 cm length of the quartz tube, and temperatures up to 1100 ^{o}C may be obtained. The HeI photon beam intersects the sample about 0.5 cm downstream from the end of the pyrolysis region. Since the pyrolysis is done at low pressures (about 10^{-2} torr) the residence time in the pyrolyzer is kept

to about 1 msec, and thermal activation results mainly from collisions with the walls. Because the distance from the end of the pyrolyzer to the detection region is short, all reactive intermediates that escape the surface should be detected.

As shown in Figure 1, a quadrupole mass spectrometer has recently been added to the apparatus used in these studies to help confirm the identification of reactive intermediates. The gases exiting the pyrolysis region traverse the scattering chamber (diameter = 1.7 cm, pressure about 10^{-3} torr) and exit the scattering chamber through a 4 mm aperture in the chamber directly opposite the pyrolysis tube. The ionizer region of the quadrupole mass spectrometer is 3 cm from the scattering chamber exit and the pressure in this region is in the 10^{-6} torr range. Hence, while the gases exiting the pyrolyzer must traverse nearly 5 cm to the quadrupole ionizer, the pressures in this region are quite low, so recombination rates are slow, and reactive intermediates can easily be seen in the mass spectra.

The chlorosilane gases were obtained from Petrarch. HCl contamination due to reactions of the chlorosilanes with residual water and air in the sample handling system was a common problem. All samples were carefully put through several freeze-pump-thaw cycles to remove residual gases, and vacuum distillation at low temperatures was carried out to remove HCl when necessary. Room temperature spectra were recorded before and after all experiments to insure that the results obtained were not complicated by HCl contamination of the sample.

For temperature measurements a thermocouple was inserted between the heater coil and outside of the quartz tube. The temperature of the inner pyrolyzer surface was not measured directly, and the temperatures given in the spectra discussed below are probably somewhat higher than the true surface

temperature. While the material used for the pyrolyzer tube was quartz, visual inspection of the pyrolysis region after operation at high temperature for one or more hours showed the deposition of a thin silicon film. The deposition of silicon films on SiO_2 surfaces by the chlorosilanes has previously been shown to occur.[12] Also, the same results were obtained in one experiment using a graphite tube. Hence both surfaces rapidly became coated with a silicon film similar to that observed under LPCVD conditions, and our results should have direct implications for surface processes that take place in CVD using the chlorosilanes as source gases.

RESULTS

The photoelectron spectra of the pyrolysis products of dichlorosilane at temperatures from room temperature to 780 °C are shown in Figure 2. The krypton present in all the spectra is used to calibrate the electron energy scale, and is admitted to the spectrometer at room temperature through an inlet system separate from the pyrolyzer. The first obvious change in the spectra with increasing temperature is the appearance of HCl peaks at 610 °C. At 780 °C a new peak appears at an ionization potential of 10.3 eV. Figure 3 shows a spectrum at 850 °C plotted with a spectrum of $SiCl_2$, obtained previously by Bock *et al.*, produced by $SiCl_4$ thermal decomposition over solid silicon.[10] Comparison of the spectra, allowing for the presence of HCl, some undecomposed SiH_2Cl_2 and Kr in the spectra from this work, shows that the band with an IP of 10.2 eV is due to $SiCl_2$. No H_2 or SiHCl is observed in the photoelectron spectra at any temperature. The ionization potentials and photoelectron band shapes for the species that have been detected in previous CVD studies are given in Table 1. Also apparent in the spectrum at 850 °C is that the spectrometer resolution is degraded (the vibrational progression in the second HCl peak is no longer

Table 1. Photoelectron Spectrum Features for Species Expected in CVD Systems

Species	IP (eV)	Band Shape
$SiCl_2$[a]	10.35	Broad unstructured first band with several bands at higher IP. See Figure 3.
SiH_2	9.02	No reference spectrum is available for this species, but the IP is known from photoionization appearance potential measurements.[b]
SiHCl	9.6	No reference spectrum is available for this species. See text for estimation of IP.
HCl[c]	12.75 16.28	Sharp doublet Sharp vibrational progression beginning at 16.25 eV.
H_2[c]	15.98	Sharp vibrational progression beginning at 15.45 eV.

a. Ref. 10. b. Ref. 15. c. Kimura, K.; Katsumata, S.; Achiba, Y.; Yamazaki, T.; Iwata, S. *Handbook of HeI Photoelectron Spectra of Fundamental Organic Molecules*, Halsted Press: New York, 1981. Turner, D. W.; Baker, C.; Baker, A. D. ; Brundle, C. R. *Molecular Photoelectron Spectroscopy*, Wiley Interscience: New York, 1970.

Figure 2. Photoelectron spectra of SiH_2Cl_2 at under flash vacuum pyrolysis conditions at three different temperatures. (a) Room temperature. (b) 720 °C. (c) 780 °C.

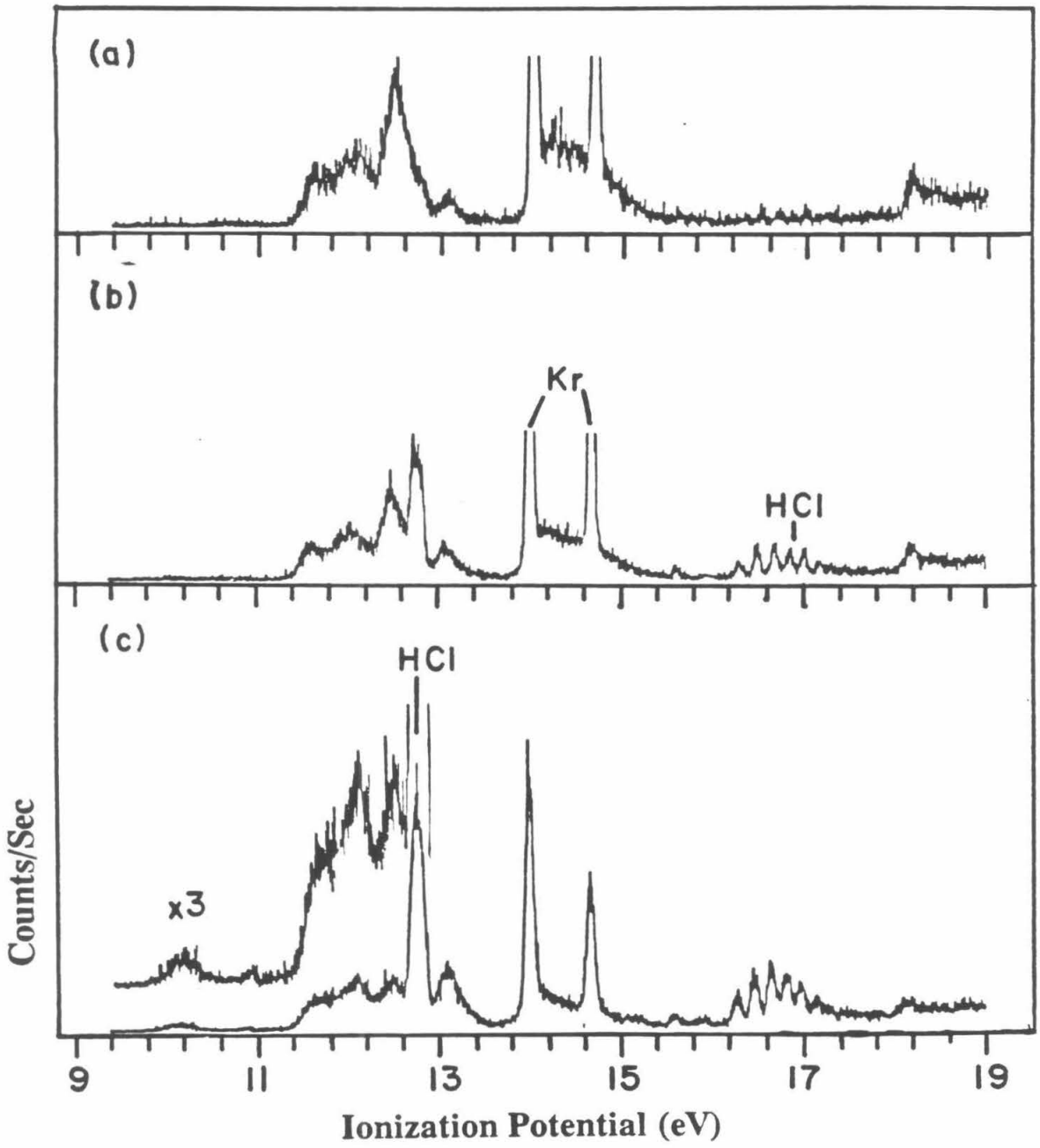
(a)
(b)
Kr
HCl
(c)
HCl
x3
Counts/Sec
9
11
13
15
17
19
Ionization Potential (eV)

Figure 3. Comparison of the photoelectron spectrum of $SiCl_2$, (a), obtained from the pyrolysis of $SiCl_4$ over solid Si (reference 10), with the photoelectron spectrum of SiH_2Cl_2 pyrolyzed at 850 °C (b). Kr and HCl are also present in the SiH_2Cl_2 pyrolyis products spectrum, but $SiCl_2$ is clearly a major component of the product mixture.

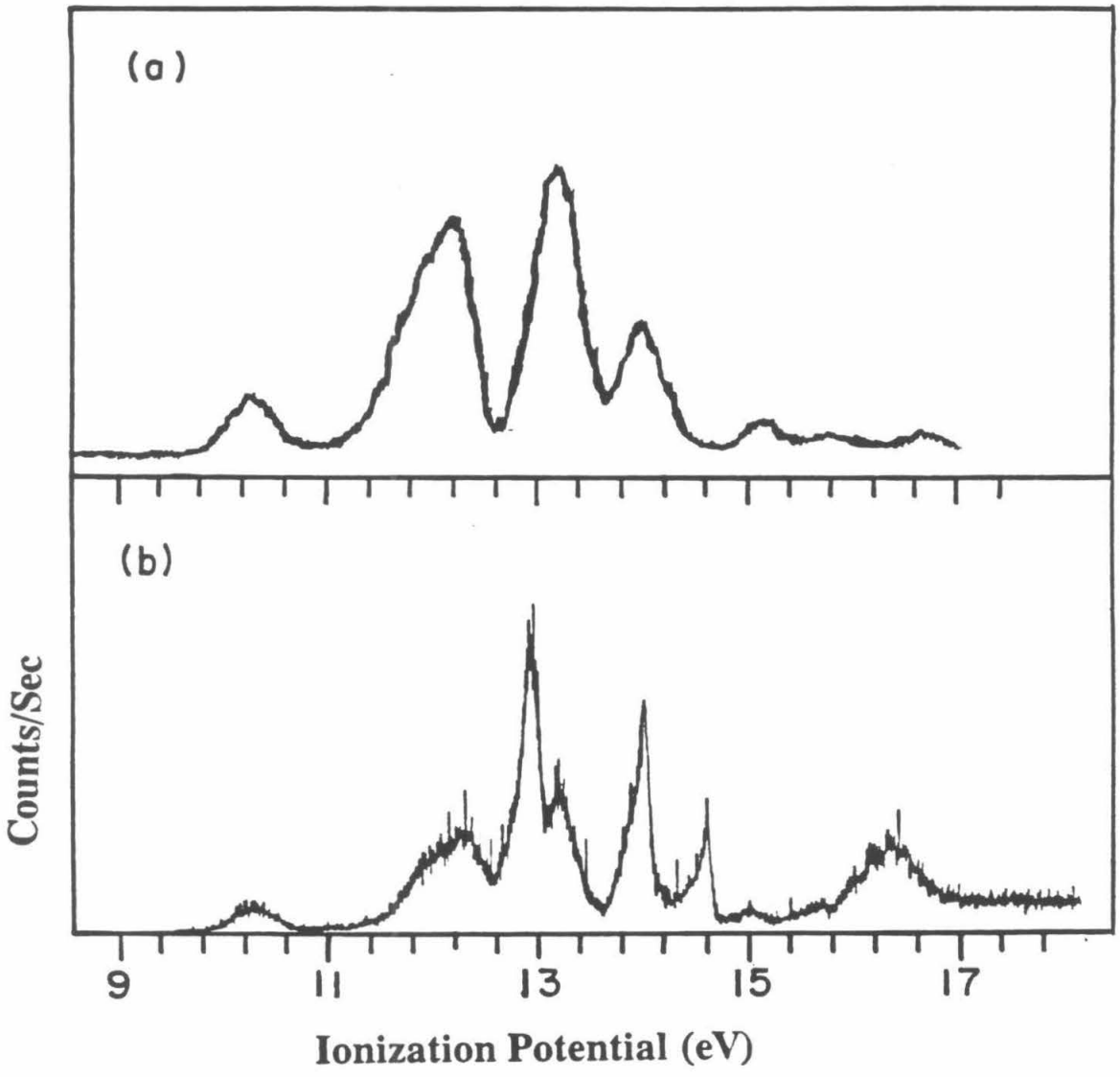
(a)
(b)
Counts/Sec
9
11
13
15
17
Ionization Potential (eV)

resolved). The degradation in spectrometer performance is due to $SiCl_2$ polymerizing on the electron energy analyzer surfaces, and photoelectron spectra could not be obtained above 850 °C. Mass spectra could be obtained up to the maximum temperature of the pyrolyzer, 1100 °C.

Mass spectra of the pyrolysis products of dichlorosilane at three different temperatures are shown in Figure 4. The electron impact source electron energy was reduced to 20 eV in all of the spectra presented in this paper, to reduce complications due to fragmentation. The results agree well with the photoelectron spectra, showing the appearance of HCl^+ at 600 °C. At 1000 °C the parent dichlorosilane is completely decomposed, and only $SiCl_2^+$, HCl^+ and $SiCl^+$ (from loss of $Cl^\cdot$ from $SiCl_2^+$ after electron impact ionization) are observed in the mass spectrum. The room temperature and high temperature mass spectra reported here also agree reasonably well with mass spectra reported previously for SiH_2Cl_2, $SiHCl_3$ and $SiCl_2$.[4] The small amount of Kr^+ present in the spectra was used to calibrate the mass scale. The water observed in the spectra is due to background water in the main vacuum chamber and not in the inlet system or sample. The sodium and potassium ions observed at the highest pyrolyzer temperature are due to thermal desorption of sodium and potassium from the sodium silicate ceramic cement used in construction of the pyrolyzer. Hence the combination of the mass spectra and photoelectron spectra shows unambiguously that the only products of the heterogeneous thermal decomposition of dichlorosilane are HCl and $SiCl_2$.

Trichlorosilane decomposed at higher temperatures than dichlorosilane, consistent with previous determinations that the activation energy for silicon deposition is higher for $SiHCl_3$ than for SiH_2Cl_2.[1] At temperatures above 900 °C emission of sodium and potassium from the pyrolyzer ceramic insulation made it

Figure 4. Mass spectra of the pyrolysis products of SiH_2Cl_2 at three temperatures. (a) Room temperature. (b) 600 °C. (c) 900 °C.

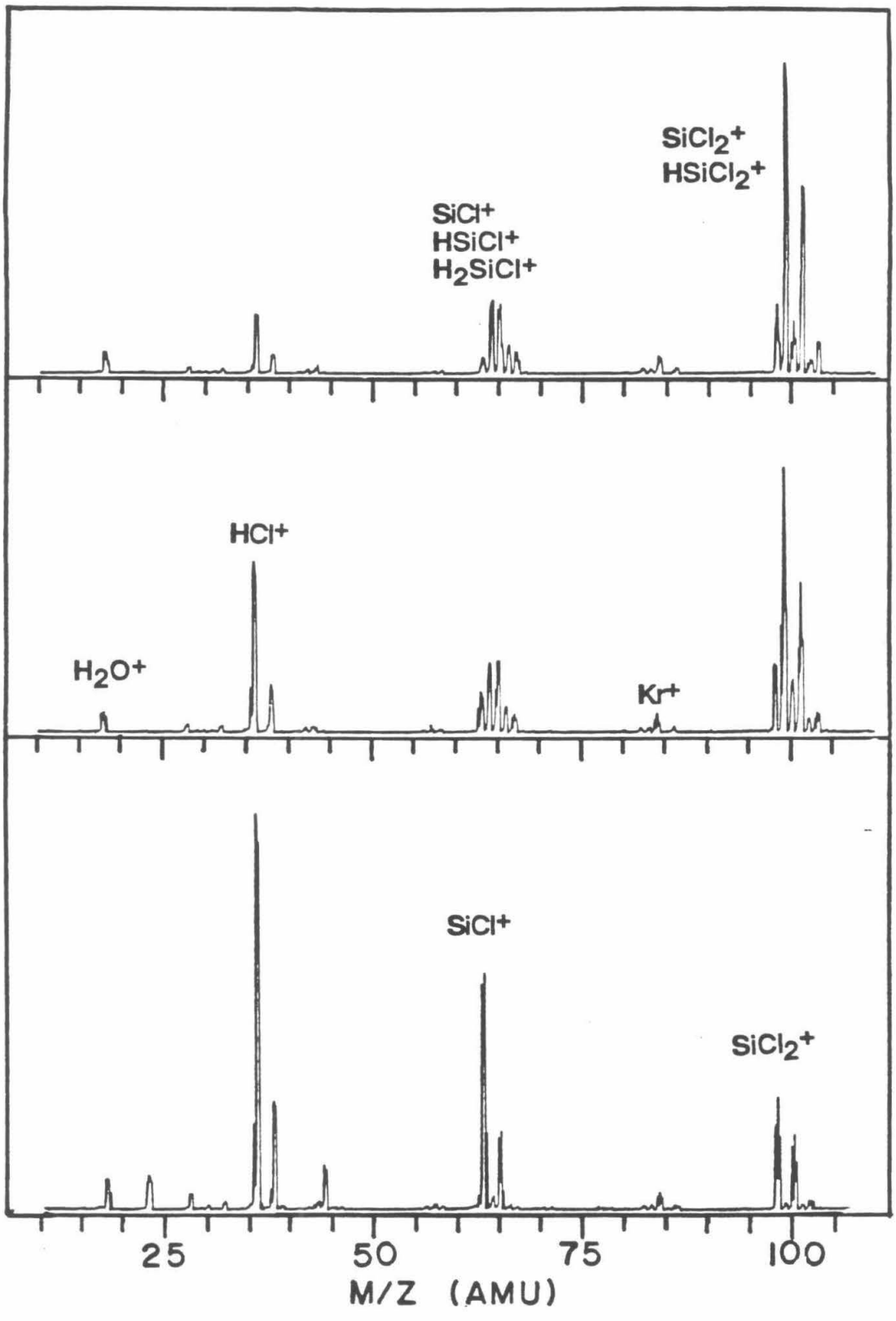
SiCl2+
HSiCl2+
SiCl+
HSiCl+
H2SiCl+
HCl+
H2O+
Kr+
SiCl+
SiCl2+
25
50
75
100
M/Z (AMU)

Figure 5. Mass spectra of the pyrolysis products of $SiHCl_3$ at three temperature. (a) Room temperature (b) 850 ^{o}C. (c) 1100 ^{o}C.

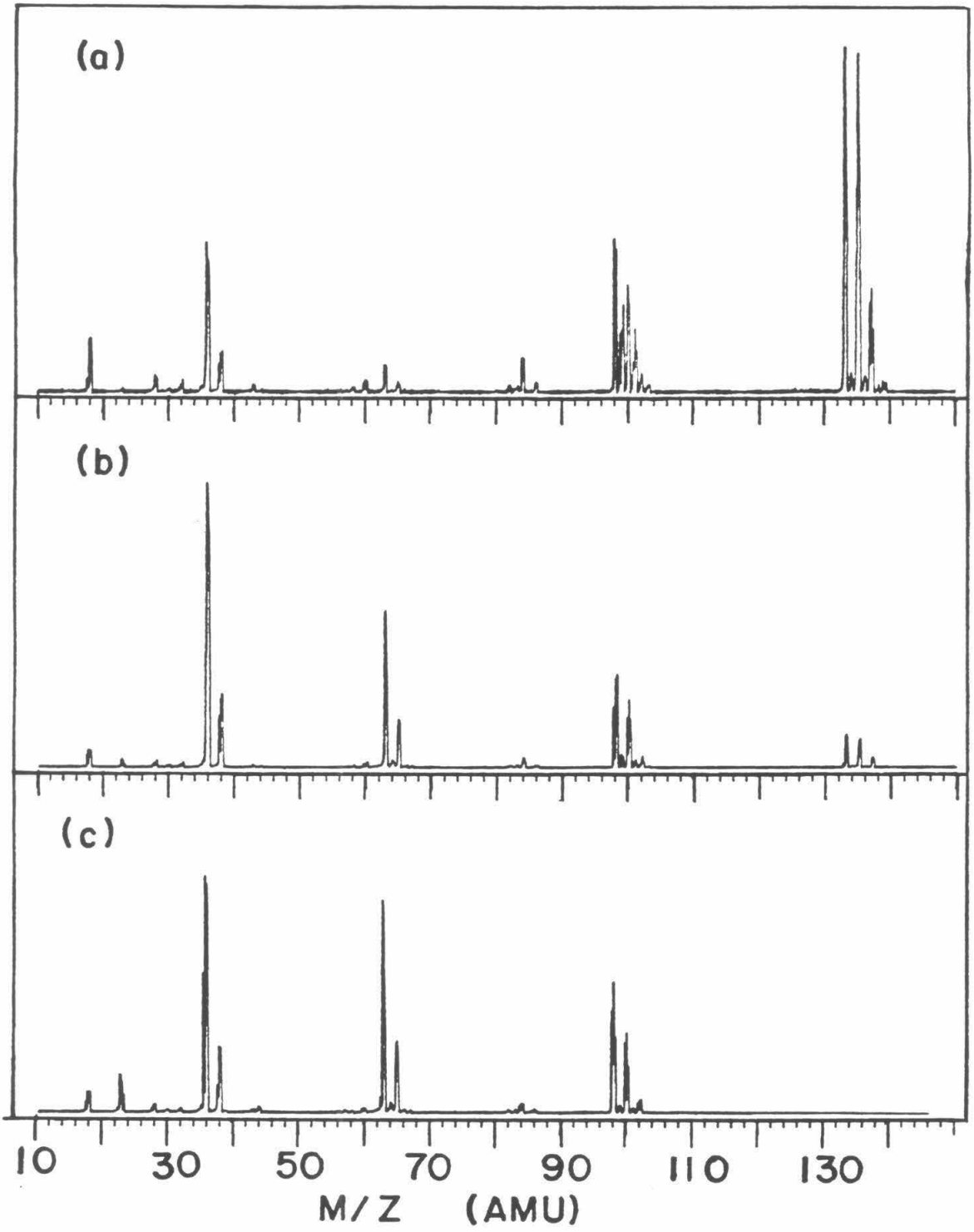
(a)
(b)
(c)
10
30
50
70
90
110
130
M/Z (AMU)

impossible to obtain photoelectron spectra. Mass spectra could be obtained however, and these are shown in Figure 5. Comparison of these spectra with those for dichlorosilane shows the same general trend, disappearance of the parent molecule and appearance of HCl and $SiCl_2$ as the only pyrolysis products with increasing temperature.

Discussion

The possible decomposition pathways for dichlorosilane along with the heat of reaction and estimated activation energy for each pathway are given in Table 2. $SiCl_2$ is the thermodynamically favored product by stepwise or one step molecular elimination decomposition of dichlorosilane. Sausa and Ronn observed $SiCl_2$ and H_2 as the only products of the homogeneous gas phase IR multiphoton dissociation of dichlorosilane,[7] which is not surprising since IR multiphoton dissociation is expected to yield the product resulting from the process with the lowest activation energy. This result is an interesting contrast to the results presented by Ho and Breiland and the results presented in this study, which clearly indicate that the mechanisms for heterogeneous and homogeneous decomposition of $SiCl_2$ are different. Ho and Breiland observed laser induced fluorescence due to HSiCl and suggested that HSiCl is formed by homogeneous decomposition above the hot silicon surface.[6] The results from this study show that in the heterogeneous decomposition of dichlorosilane $SiCl_2$ and HCl are the only pyrolysis products.

Given the results of Sausa and Ronn showing that $SiCl_2$ is the major silicon containing reactive intermediate in the homogeneous decomposition of dichlorosilane, and the results presented here which show that $SiCl_2$ is the major silicon containing intermediate formed in the heterogeneous decomposition, it is hard to explain the observation of SiHCl by Ho and Breiland. One possible

Table 2. Heats of Reaction and Activation Energies for the Decomposition Pathways of Dichlorosilane.

Reaction				ΔH_{298} [a] (Kcal mol^{-1})	E_a [b] (Kcal mol^{-1})
Stepwise Processes					
SiH_2Cl_2	SiH_2Cl	+	Cl	111.3	~111.3
SiH_2Cl_2	$SiCl_2H$	+	H	92.3	~92.3
$SiCl_2H$	$SiCl_2$	+	H	48.8	~48.8
$SiCl_2H$	SiClH	+	Cl	80.3	~80.3
Molecular Elimination					
SiH_2Cl_2	SiH_2	+	Cl_2	143.5	~143.5
SiH_2Cl_2	SiHCl	+	HCl	69.5	~81.5
SiH_2Cl_2	$SiCl_2$	+	H_2	36.9	~71.9

(a) Heats of reaction were calculated from heats of formation in: Ho, P.; Coltrin, M. E.; Binkley, J. S.; Melius, C. F. *J. Phys. Chem.* **1985**, *89*, 4647.
(b) Reference 13.

explanation lies in the relative sensitivities of the detection methods in the two studies, the different experimental conditions and the activation energies for the decomposition pathways yielding the two intermediates. Although $SiCl_2$ is the thermodynamically favored product by 32.5 kcal mol^{-1}, the activation energy for the elimination of HCl from dichlorosilane is estimated from theoretical considerations to be only 9.6 kcal mol^{-1} higher than for the elimination of H_2.[13] At 1000 °C, a difference of 5 kcal mol^{-1} yields a ratio of reaction rates of 0.008. Hence small concentrations of SiHCl may be formed at high temperatures in a homogeneous system. The laser induced fluorescence technique is capable of detecting concentrations of species approximately 10^3 lower in concentration than the PES technique used in this study. Also, laser induced fluorescence is a highly specific technique allowing the detection of one species at a time and Ho and Breiland were unable to comment on the relative concentration of SiHCl to $SiCl_2$, H_2 or HCl in their study. (SiHCl fluorescence was detected at wavelengths from 445-490 nm, while $SiCl_2$ fluorescence is observed between 310 nm and 350 nm.[14]). As shown in Table 1, SiH_2 has an ionization potential of 9.02 eV[15] and $SiCl_2$ has an ionization potential of 10.35 eV.[10] SiHCl would be expected to have an ionization potential intermediate between $SiCl_2$ and SiH_2, and if it were present in the experiments presented in this study at a concentration more than 5% of the $SiCl_2$ concentration, it would have been observed as another band below 10 eV in the photoelectron spectrum. Based on the studies discussed above, it appears that $SiCl_2$ is the major reactive intermediate in CVD systems using SiH_2Cl_2 as a source gas, formed both by homogeneous and heterogeneous decomposition of SiH_2Cl_2, while SiHCl is present as a minor species.

It is interesting to note from the mass spectra in Figures 4 and 5 that at temperatures where the precursor chlorosilane is completely decomposed, the

relative concentrations of HCl and $SiCl_2$ are nearly the same for dichlorosilane and trichlorosilane. The ratio of $SiCl_2$/HCl is higher in the trichlorosilane case, presumably because there is more chlorine carried to the surface by this feed gas. This is in agreement with previous optical and mass spectrometric studies which showed that the gas phase species present in CVD systems were independent of the chlorosilane source gas.[4,5] Gilbert and Ban,[4] using mass spectrometry, showed that the gas phase species found in CVD reactions were independent of the feed gas, and that their relative concentrations depended only on the temperature and Cl/H ratio of the feed gas. The IR multiphoton dissociation results of Sausa and Ronn showed that only H_2 and $SiCl_2$, and not HCl, are produced by the homogeneous gas phase decomposition of dichlorosilane.[7] The results in this study show that the HCl observed in previous studies of CVD systems using chlorosilanes as source gases is probably generated by heterogeneous surface decomposition of the chlorosilanes, followed by surface reactions.

Conclusions

The results presented in this study show that $SiCl_2$ and HCl are formed in the heterogeneous decomposition of SiH_2Cl_2 and $SiHCl_3$ on silicon surfaces above 600 °C and 800 °C respectively. $SiCl_2$ and HCl desorb from the surface at these temperatures, and these species are likely to be important in the removal of excess chlorine and hydrogen from the growing polycrystalline thin silicon film. Under heterogeneous conditions, where the dichlorosilane decomposes on the surface and not above it, species I and II in Scheme 1 would be likely to form by dissociative adsorption on the surface. I and II can react further with the surface to form species such as III and IV. Because Si-Cl bonds are stronger than Si-H or Si-Si bonds (see Table 1 and the references to Table 1), and the Cl_2 bond is weak

Scheme 1 Scheme illustrating the species that may be formed on the hot silicon surface under heterogeneous conditions. Dissociative adsorption of SiH_2Cl_2 on the surface would produce species such as I and II. I and II can then react further with the surface to yield species such as III and IV. The loss of $SiCl_2$ is favored for III, while the loss of HCl is favored for IV (see text).

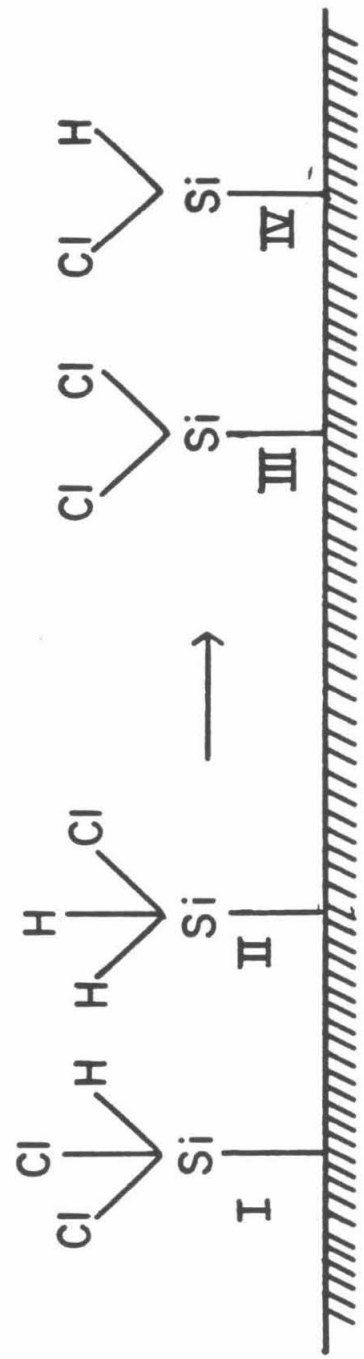
Cl
Cl
H
Si
I
H
H
Cl
Si
II
Cl
Cl
Si
III
Cl
H
Si
IV

(58.0 kcal mol^{-1} [16]), a surface moiety such as III is most likely to desorb $SiCl_2$, rather than Cl_2. The results in this study indicate that species such as IV are most likely to lose HCl rather than SiHCl. In this case breaking the SiCl bond (~110 kcal mol^{-1}, see Table 1) is in large part compensated by the formation of the H-Cl bond (103 kcal mol^{-1} [16]). The results presented here, when combined with results on the homogeneous IR multiphoton decomposition of dichlorosilane, indicate that SiHCl is not an abundant intermediate in CVD systems using dichlorosilane as a source gas. A relative concentration of SiHCl to $SiCl_2$ of more than a few percent would have been observed by the PES technique used in this study. Further work is needed to quantify the relative concentrations of $SiCl_2$ and SiHCl in CVD systems.

1. For recent reviews see: (a) Jasinski, J. M.; Meyerson, B. S.; Scott, B. A. *Ann. Rev. Phys. Chem.* **1987**, *38*, 109. (b) Bloem, J.; Giling, L. J. in Einspruch, N. G.; Huff, H. Eds. *VLSI Electronics Microstructure Science*; Academic Press: Orlando. V. 12, p. 89.

2. (a) Lever, R. F. *IBM J. Res. Dev.* **1964**, *8*, 460. (b) Hunt, L. P.; Sirtl, E. *J. Electrchem. Soc.* **1974**, *119*, 1741. (c) Sirtl, E.; Hunt, L. P.; Sawyer, D. H. *J. Electrochem. Soc.* **1974**, *121*, 919.

3. (a) Duchemin, J. P.; Bonnet, M.; Beuchet, G. *J. Vac. Sci. Technol.* **1979**, *16*, 76. (b) Couchet, G.; Mellottee, H.; Delbourgo, R. *J. Electrochem. Soc.* **1978**, *113*, 487.

4. Ban, V. S.; Gilbert, S. L. *J. Cryst. Growth* **1975**, *31*, 284. Ban, V. S.; Gilbert, S. L. *J. Electrochem. Soc.* **1975**, *122*, 1382.

5. (a) Sedgwick, T. O.; Smith, J. E. *Thin Solid Films* **1977**, *40*, 1. (b) Nishizawa, J. *J. Cryst. Growth* **1982**, *56*, 273, and references therein.

6. (a) Ho, P.; Breiland, W. G. *Appl. Phys. Lett.* **1983**, *43*, 125. (b) Breiland, W. G.; Ho, P.; Coltrin, M. E. *J. Appl. Phys.* **1986**, *60*, 1505.

7. Sausa, R. C.; Ronn, A. M. *Chem. Phys.* **1985**, *96*, 183.

8. Schultz, J. C.; Beauchamp, J. L. *J. Phys. Chem.* **1983**, *87*, 3587.

9. Bock, H.; Solouki, B. *Angew. Chem. Int. Ed. Engl.* **1984**, *20*, 427.

10. Bock, H.; Solouki, B.; Maier, G. *Angew. Chem. Int. Ed. Engl.* **1985**, *24*, 205.

11. Houle, F. A.; Beauchamp, J. L. *J. Am. Chem. Soc.* **1978**, *100*, 3290.

12. See the discussion in references 1 and 4 and also: Rosler, R. S.; *Solid State Technol.* **1977**, *20*, 63.

13. The recombination of radicals is generally assumed to occur without activation energy, so the reverse activation barriers for the stepwise decomposition processes should be near zero. Hence the activation energies for these processes are equal to the reaction endothermicities. SiH_2 is known to insert into H_2 with an activation energy of less than 1 kcal mol^{-1} (Gordon, M. S.; Gano, D. R.; Stephen, B.; Frisch, M. J. *J. Am. Chem. Soc.* **1986**, *108*, 2191. Jasinski, J. M. *J. Phys. Chem.* **1986**, *90*, *555.*) so by analogy the activation energy for the elimination of Cl_2 from dichlorosilane should approximately equal the endothermicity of the reaction. The order of reactivities for the insertion of SiXY into the Si-H bond is SiH_2 > SiHCl >> $SiCl_2$ (Jenkins, R. L.; Vanderwielen, A-J.; Ruis, S. P.; Gird, S. R.; Ring, M. A. *Inorg. Chem.* **1973**, *12*, 2968). The activation energies for the elimination of HCl and H_2 from dichlorosilane were calculated assuming that the difference in reactivity in the reverse insertion reaction is caused by a difference in activation energy due to the difference in single-triplet splittings in the series SiH_2, SiHCl, $SiCl_2$. Calculations at the MP2/6-31G** level show that the sinlet-triplet splitting in $SiCl_2$ is 39.1 kcal mol^{-1} greater than SiH_2 and SiHCl has a singlet-triplet splitting 15.1 kcal mol^{-1} greater than SiH_2 (Shin, S. K.; Beauchamp, J. L.; Goddard, W. A. III, results to be published). For SiHCl and $SiCl_2$ formation from dichlorosilane, the difference in singlet-triplet splitting between SiXY and SiH_2 was added to the reaction endothermicity to obtain the activation energy given in Table 1.

14. Suzuki, M.; Washida, N.; Inoue, G. *Chem. Phys. Lett.* **1986**, *131*, 24, and references therein.

15. Berkowitz, J.; Greene, J. P.; Cho, H.; Ruscic, B. *J. Chem. Phys.* **1987**, *86*, 1235.

16. Edwards, J. G.; Franklin, H. F.; Gilles, P. W. *J. Chem. Phys.* **1971**, *54*, 545. Kant, A. *Ibid.* **1968**, *49*, 5144.

CHAPTER 5

Homolytic and Heterolytic C-H Bond Energies in α- and β-Methylnaphthalene as Determined by Photoelectron Spectroscopy and Fourier Transform Mass Spectrometry.

G. H. Kruppa, C. H. Nelson and J. L. Beauchamp

INTRODUCTION

The α-methylnaphthyl and β-methylnaphthyl radicals, (I) and (II) (The α - and β- positions are also the 1- and 2- positions in the standard numbering of the naphthalene ring) respectively, have been the subject of a number of energetic and reactivity studies. These two radicals and their corresponding carbonium ions are important as prototypes for

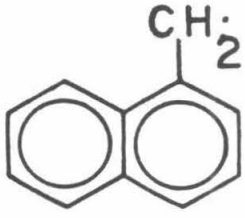

I

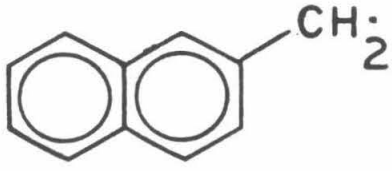

II

the larger α- and β-type polycyclic aromatic hydrocarbon (PAH) carbinyl radicals.[1] The methylnaphthalenes and higher molecular weight polycyclic aromatic hydrocarbons are abundant in crude petroleum, and radicals such as I and II and their corresponding carbonium ions are expected to be important intermediates in hydrocarbon flame chemistry, especially in soot formation.[2]

Studies of H-atom abstraction rates from α- and β-methylnaphthalene by trichloromethyl radicals showed that the reaction rate was a factor of 0.682 slower for β-methylnaphthalene than α-methylnaphthalene.[3] Since the transition state in this reaction has been shown to have a considerable amount of free radical character,[4] the observed reaction rates were taken as evidence that the α-methylnaphthyl radical is more stable than the β-methylnaphthyl radical.[3] A number of theoretical approaches have subsequently shown that the α-methylnaphthyl radical would be expected to be more stable than the β-methylnaphthyl radical.[5] However, the only available gas phase data on the two

radicals is a measurement of the ethyl C-C bond energy in α-ethylnaphthalene, which yielded ΔH_f[α-methylnaphthyl radical] = 59.6 kcal mol^{-1}.[6]

Similar results are available for the relative stabilities of the corresponding carbonium ions. In solvolysis reactions, where a high degree of carbonium ion character is expected in the transition state, α-methylnaphthyl tosylate hydrolyzes faster than the β- isomer, with an activation energy 1.25 kcal mol^{-1} lower than the β-isomer.[7] This value for the difference in activation energies is somewhat lower than the difference in carbonium ion stabilities predicted by SCF STO-3G calculations, which indicate that the α-methylnaphthyl carbonium ions is 2.05 kcal mol^{-1} more stable than the β-methylnaphthyl carbonium ion.[8] The ionization potentials of the α-methylnaphthyl and β-methylnaphthyl radicals have been measured by electron impact appearance potential measurements,[9] resulting in an estimated difference of 4.8 kcal mol^{-1} in the heat of formation of the two carbonium ions, with the α-methylnaphthyl carbonium ion favored. As will be shown below, however, the values reported by the electron impact technique are about 0.5 eV too high.

Given the importance of I and II as prototypical PAH carbinyl radicals, it would be of interest to obtain gas phase data on the relative stabilities of the radicals and their corresponding carbonium ions, for comparison with the solution phase reactivity data. Recent results from this laboratory have shown that adiabatic ionization potentials of free radicals obtained from photoelectron spectroscopy (PES) can be combined with relative heterolytic bond energies from mass spectrometric equilibrium experiments to obtain accurate relative C-H bond energies. The relative homolytic and heterolytic C-H bond energies obtained by the combination of these techniques can reveal subtle geometrical and substituent effects on radical and carbonium ion stabilities.[10] In previous

studies,[10] the thermochemical cycle summarized by reactions 1 - 3 was used to derive the relative homolytic bond energies for two species, R_1H and R_2H.

$$R_1^+ + R_2\cdot \rightarrow R_1\cdot + R_2^+ \quad (1)$$

$$R_1H + R_2^+ \rightarrow R_1^+ + R_2H \quad (2)$$

$$R_1H + R_2\cdot \rightarrow R_1\cdot + R_2H \quad (3)$$

ΔH for reaction 1 is the difference in ionization potentials for the two radicals, obtained from the photoelectron spectra. ΔH for reaction 2 is the relative heterolytic bond dissociation energy obtained from mass spectrometric equilibrium studies.[11] Adding ΔH for reactions 1 and 2 yields ΔH for reaction 3, which is the relative homolytic bond energy. ΔH for reaction 2 is not available from the literature for the case of α- and β-methylnaphthalene, and because the carbonium ions of interest have the same mass, could not be determined in this study. Meot-Ner has applied the proton affinity bracketing technique to measure the proton affinity and heat of formation of the benzyl radical,[12] and was able to measure C-H bond energy differences as small as 0.5 kcal mol^{-1} in a series of substituted toluenes. The success of the proton affinity technique with the benzyl radical suggests that this technique could be applied successfully to a study of the methylnaphthyl radicals. In this study we report measurements of the proton affinities, by Fourier transform mass spectrometry (FTMS), and ionization potentials, by PES, of the α- and β - methylnaphthyl radicals.

EXPERIMENTAL

Photoelectron Spectra. The radicals studied in this work were produced by the flash vacuum pyrolysis of the appropriate alkyl nitrite, reactions 4 and 5.

$$RCH_2ONO \rightarrow RCH_2O\cdot + NO \quad (4)$$

$$RCH_2O\cdot \rightarrow R\cdot + CH_2O \quad (5)$$

The nitrites were synthesized from 1- and 2-naphthaleneethanol, obtained from

Aldrich, *via* the reaction of the alcohols with NOCl in pyridine, as has been previously described.[13] NOCl was prepared from nitrosylsulfuric acid, obtained from Aldrich, and sodium chloride.[14] The 1-naphthaleneethylnitrite obtained was a liquid, while the 2-naphthaleneethylnitrite could be crystallized from pentane after refrigeration. The purity of the nitrites was checked by NMR spectroscopy.

The photoelectron spectrometer used in these experiments was an instrument of standard design that has been modified to study the products of flash vacuum pyrolyses. A description of the instrument can be found elsewhere.[15]

Photoelectron spectra of the pyrolysis products were obtained with HeI and NeI radiation, at pyrolysis temperatures from 450 to 650 °C. The band shapes using the two different sources of radiation were the same within experimental error. The energy scales for the pyrolysis spectra were calibrated with He Iα bands of CH_3I and CH_2O. The room temperature spectra of the nitrites were calibrated using the HeIα bands of Ar and CH_3I. The typical resolution for these experiments was 35-45 mV as determined from the fwhm of the $Ar^2P_{3/2}$ band. Peak maxima can easily be reproduced to within 0.02 eV with careful calibration in cases where the peaks are sharp. Error limits of 0.03-0.05 eV are assigned for cases where the peak maxima are difficult to locate or calibrate accurately.

Proton Affinity Measurements. Experimental techniques associated with ICR spectroscopy,[16] and in particular Fourier transform mass spectrometry,[17] have previously been described in detail. Experiments were performed with an Ion Spec-2000 Fourier transform mass spectrometer equipped with a 1-in. cubic trapping cell[18] built by Bio-Med Tech[19] situated between the poles of a Varian

15-in. electromagnet maintained at 1.8 T. Chemicals were obtained in high purity from Aldrich, and used as supplied except for multiple freeze-pump-thaw cycles to remove noncondensable gases. Pressures were measured with a Schulz-Phelps ion gauge[20] calibrated against an MKS baratron (Model 390 HA-0001) capacitance manometer. The principal errors in the rate constants (estimated to be ±20%) arise from uncertainties in pressure measurements.[21] Mixtures of α- or β-methylnaphthalene at 3 x 10^{-7} torr with bases at pressures from 5 x 10^{-7} to 5 x 10^{-6} torr were used. The rate constant for each base was measured at several different pressures, that varied by a factor of at least 2, to confirm pseudo-first order kinetics. Ionization was by electron impact at 12.5 eV. In some experiments NO^+(IP = 9.26 eV[22]) was used to ionize the methylnaphthalene (IP = 8.01 eV[22]), by charge transfer chemical ionization. In all cases, regardless of the electron energy used, the proper pseudo-first order exponential decays were observed. The rate constants calculated from the observed decays were the same, within experimental error, using NO^+ chemical ionization or electron impact ionization at 12.5 eV. Meot-Ner observed the same independence of rate constants and electron impact ionization energies in studies on benzyl ions.[12] It was therefore concluded that any excess internal energy of the methylnaphthyl ions does not affect the rate constants of the proton transfer reactions.

This study focused on the proton transfer reactions from methylnaphthalene radical cations to a series of neutral bases. Other products were often observed, but these were ignored, except to confirm by double resonance techniques that they did not interfere in the rate constant measurements for the proton transfer reactions. The methylnaphthalene radical parent cation is the only ion formed by low energy electron impact ionization (< 15 eV) or by charge transfer chemical ionization with NO^+ on the

methylnaphthalenes. In the chemical ionization experiments, NO^+, formed by electron impact ionization, was isolated in the FTMS cell by a series of ejection pulses,[23] followed by a reaction period during which the methylnaphthyl radical cations were formed. After this period the remaining NO^+ ions were ejected from the cell along with any other ions to isolate the methylnaphthyl cations. In the electron impact ionization experiments the methylnaphthalene radical cations were isolated by a series of eject pulses immediately following the electron beam pulse. After isolation of the methylnaphthalene radical cation the temporal variations of the reactant and product ions were recorded and used to calculate the rate constants directly. As an example, Figure 1 shows the temporal variations of the 1-methylnaphthyl cation, $C_{11}H_{10}^+$, (M/Z = 142) and the protonated product ion $C_6H_8N^+$ from the proton transfer reaction from the 1-methylnaphthalene radical cation to dipropargyl amine, $(HC{\equiv}C\text{-}CH_2)_2NH$.

RESULTS

Photoelectron Spectra. The photoelectron spectra of the α- and β-methylnaphthyl radicals are shown in Figure 2, along with a spectrum of the benzyl radical[15] for comparison. Immediately apparent from Figure 2 is that the signal-to-noise ration for the α-methylnaphthyl radical spectrum is higher than for the β - isomer. The conditions for the two spectra were nearly identical, and the relative intensities of NO and CH_2O (other products of the pyrolysis reaction that produces the radicals, see reactions 3 and 4) were comparable. The reason for the poor signal for the β - isomer has not been definitely assigned. The precursor nitrites to the radicals had low vapor pressures and it was necessary to heat the inlet system to 85 ^{o}C to obtain a sufficient vapor pressure of the α-naphthaleneethylnitrite for these experiments. The β - naphthyl radical precursor had a significantly lower vapor pressure, and the inlet was heated to

Figure 1. Timeplot showing the temporal variation of relative ion concentrations in a proton transfer rate constant measurement. The α-methylnaphthyl ion (m\z) = 142 (O) was isolated by a series of eject and sweepout pulses 110 msec after the ions were formed by the electron beam pulse. Dipropargylamine abstracts a proton from the α-methylnaphthalene radical cations forming a protonated amine ion of m\z = 95 (X), and the α-methylnaphthyl radical.

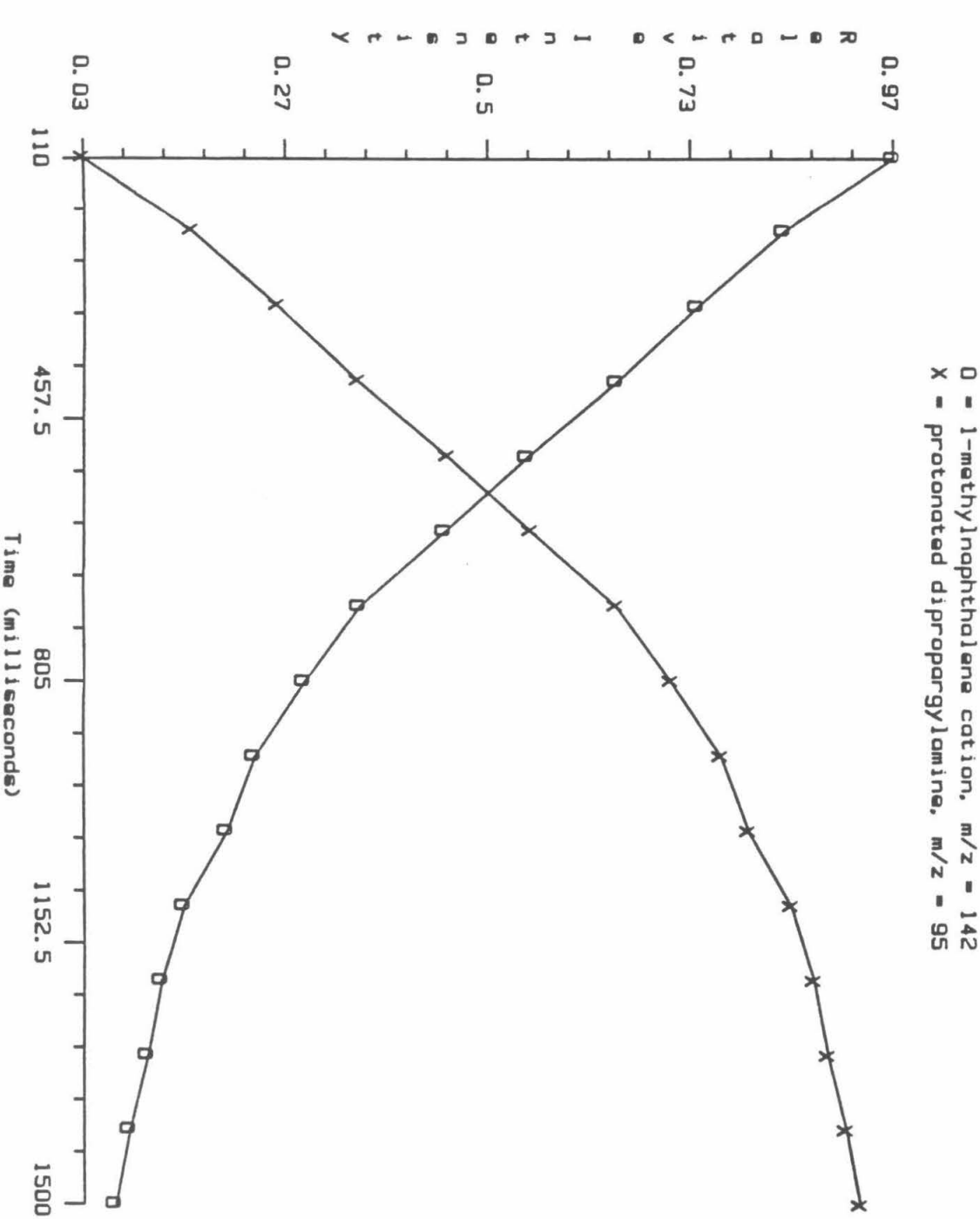
O = 1-methylnaphthalene cation, m/z = 142
X = protonated dipropargylamine, m/z = 95
Relative Intensity
0.97
0.73
0.5
0.27
0.03
110
457.5
805
1152.5
1500
Time (milliseconds)

120 °C to obtain spectra of this radical. Hence it is possible that more of the β-methylnaphthyl radical precursor decomposed before reaching the flash vacuum pyrolyzer, and was lost to the walls of the inlet system. However, from the spectra in Figure 2, ionization potentials can be assigned for both isomers.

While no vibrational structure is observed in the spectra in Figure 2, the bands are quite sharp, relative to other radical photoelectron spectra, with band shapes similar to that for the benzyl radical. Hence, as for benzyl radical, it can be concluded that the methylnaphthyl radicals are planar, with adiabatic and vertical ionization potentials coincident. The spectra shown in Figure 2 were reproduced a minimum of 5 times over several months and the ionization potentials assigned were IP[α-methylnaphthyl radical] = 6.88 $\pm$ 0.03 eV and IP[β - methylnaphthyl radical] = 6.93 $\pm$ 0.03 eV.

Proton Affinities. Table 1 lists the bases studied along with the base strengths,[24] rate constants, and reaction efficiencies for the proton transfer reactions. Charge transfer reactions were not a problem in these studies since the bases chosen for study all had ionization potentials at least 0.5 eV above the methylnaphthalenes.[22] In cases where the proton transfer product was observed, double resonance techniques[16-18] were used to show that other products were due to subsequent reactions of the protonated base with neutral base or methylnaphthalene. Hence for the bases in Table 1 the only process for decay of the parent methylnaphthalene radical cation signal was due to direct proton transfer. In all cases the presence or absence of direct proton transfer from the parent methylnaphthalene radical cation to the neutral base was confirmed by double resonance techniques.

The variation of the reaction efficiency (the ratio of the observed rate constant to the calculated collision rate) with base strength is plotted in Figure 3.

Figure 2. Photoelectron spectrum of the α- and β-methylnaphthyl radicals along with the benzyl radical for comparison. (a) Benzyl radical, ref. 15. (b) α-methylnaphthyl radical. (c) β-methylnaphthyl radical. See text for an explanation of the poor signal-to-noise ration for this spectrum. The vertical and adiabatic ionization potentials coincide in all three cases, and are indicated by arrows on the spectra.

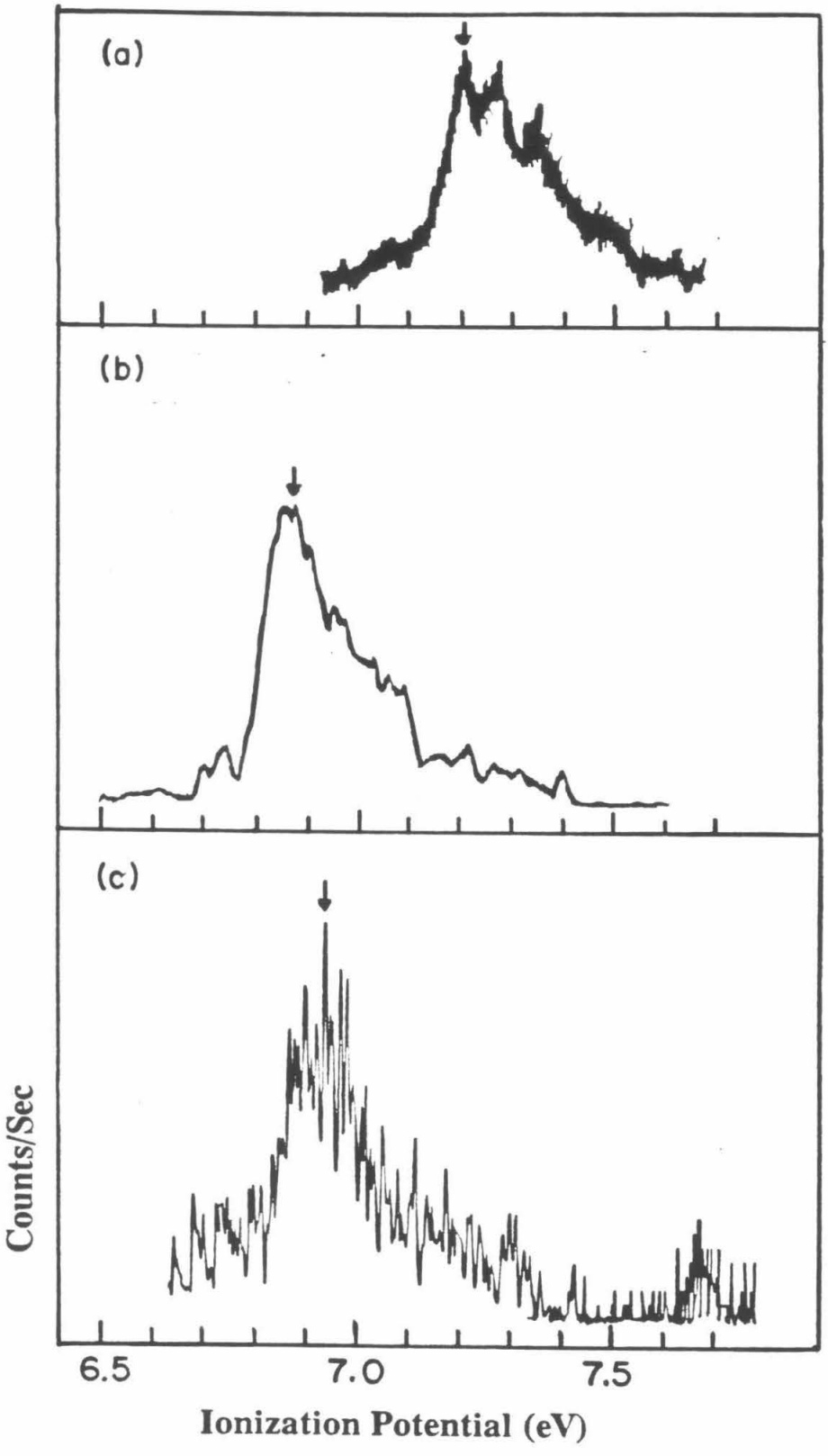
(a)
(b)
(c)
Counts/Sec
6.5
7.0
7.5
Ionization Potential (eV)

Table 1. Rate Constants for Proton Transfer Reactions: $RH^+ + B \rightarrow BH^+ + R\bullet$

Base	PA[a]	k[b]	k/k_{ado}[c]
	R = α-METHYLNAPHTHYL		
p-anisaldehyde	213.5	0	0
2-chloropyridine	214.4	0	0
3-chloropyridine	214.8	0	0
$CH_2=CHCH_2NH_2$	215.8	0	0
$(HC=C\text{-}CH_2)_2NH$	216.1	0.30	0.026
$CH_3CON(CH_3)_2$	216.8	0.62	0.055
$CH_3CH_2CH_2NH_2$	217.9	0.60	0.049
$(CH_3)_2NH$	220.6	2.2	0.22
	R = β-METHYLNAPHTHYL		
p-anisaldehyde	213.5	0	0
2-chloropyridine	214.4	0	0
3-chloropyridine	214.8	0	0
$CH_2=CHCH_2NH_2$	215.8	0	0
$(HC=C\text{-}CH_2)_2NH$	216.1	0.32	0.029
$CH_3CON(CH_3)_2$	216.8	0.45	0.040
$CH_3CH_2CH_2NH_2$	217.9	0.41	0.033
$(CH_3)_2NH$	220.6	2.1	0.18

a. All proton affinities from ref. 24. b. Rate constants for the proton transfer reaction in units of 10^{-10} cm^3 molecule $^{-1}sec^{-1}$. c. The proton transfer reaction efficiency. k_{ado} is the collision rate constant calculated by average dipole orientation theory: Su, T.; Bowers, M. T.; *Int. J. Mass Spectrom. Ion Phys. 1973*, **12**, 347.

Both the α- and β-isomers display similar reactivity with the series of bases studied. The reaction efficiencies are quite low, with a maximum efficiency of 0.2 for the reaction of α-methylnaphthyl radical with dimethylamine, a reaction which must be at least 4 kcal mol^{-1} exothermic. For comparison, Meot-Ner found a maximum reaction efficiency of about 0.5 for proton transfer from a series of substituted toluene cations when the reaction exothermicity was approximately 3 kcal mol^{-1}.[12] The reason for the small reaction efficiencies with the larger methylnaphthyl system is not clear, although ion molecule reactions generally show decreasing efficiencies as the reactant ions become larger and exothermicities decrease.[25] From Figure 3 the proton affinities, defined as $-\Delta H$ for reaction 6, for the α- and β-methylnaphthyl radical are both

$$R\cdot + H^+ \rightarrow RH^+ \qquad (6)$$

assigned to be 216.0 $\pm$ 2.0 kcal mol^{-1}. This assignment is based on the observation that only exothermic or thermoneutral reactions are observed by the FTMS technique.[16,17] The error in this measurement is due to a number of factors including the difficulty in locating the thermoneutral point for reactions that have such small reaction efficiencies, and the difficulties in assigning absolute values to the proton affinity scale.[24] If only the relative proton affinities are considered the errors due to assignment of absolute values to the proton affinity scale can be eliminated. Since the rate constants of the proton transfer reactions for the two isomers are so close, the relative proton affinities of the α- and β-methylnaphthyl isomers can be confidently assigned to be the same within 1 kcal mol^{-1}.

Figure 3. Plot of the proton affinity of the bases studied in this work vs. the reaction efficiency k/k_{ADO}. See Table 1.

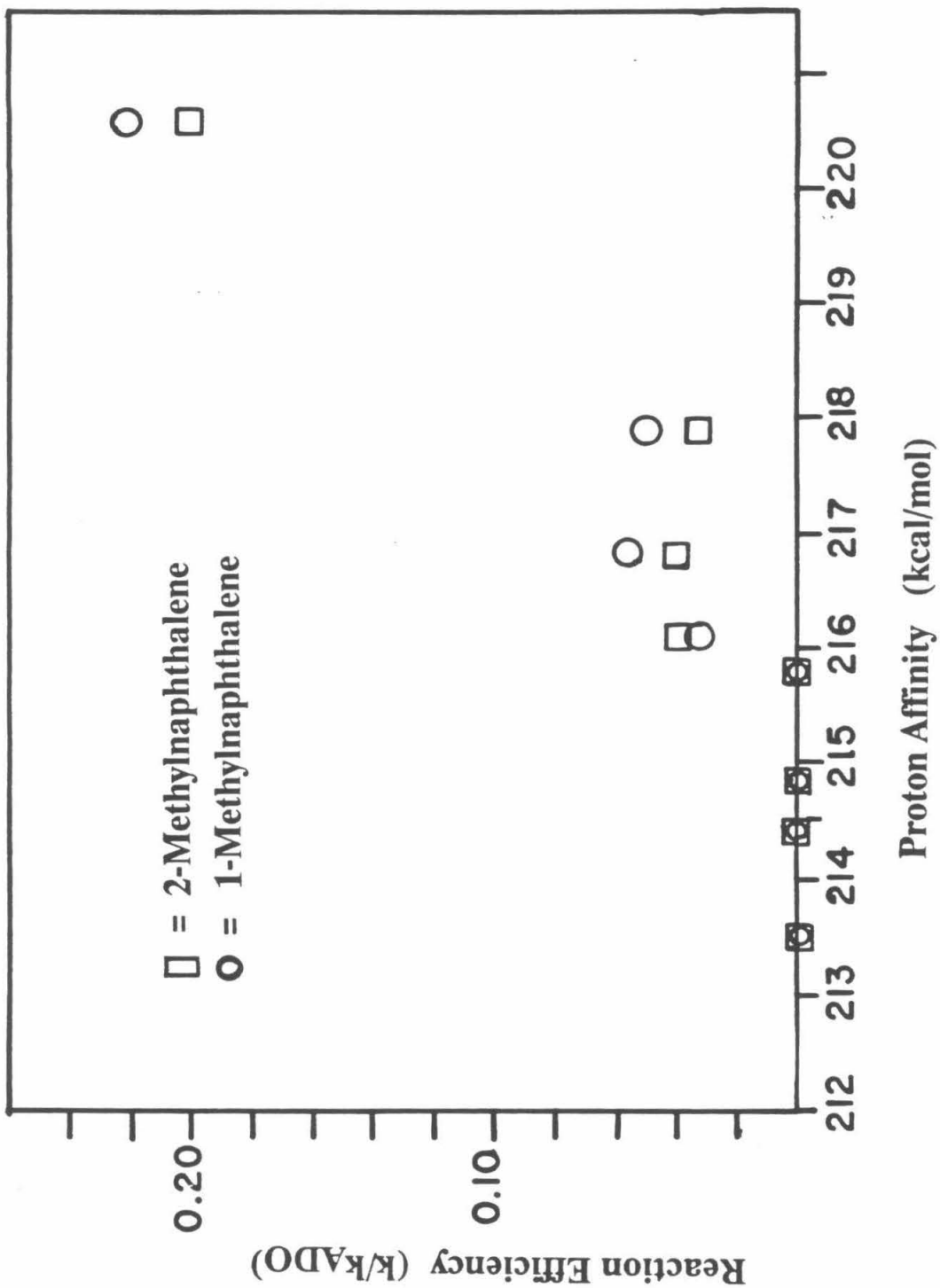
□ = 2-Methylnaphthalene
O = 1-Methylnaphthalene
0.20
0.10
Reaction Efficiency (k/kADO)
212
213
214
215
216
217
218
219
220
Proton Affinity (kcal/mol)

DISCUSSION

The ionization potentials of the α-methylnaphthyl and β-methylnaphthyl radicals obtained by PES are considerably lower than those reported by Lossing in an earlier electron-impact study.[9] His measurements yielded ionization potentials of 7.56 ± 0.05 eV, and 7.35 ± 0.1 eV for the α-methylnaphthyl and β-methylnaphthyl radicals respectively. In the same study an ionization potential for the benzyl radical was reported as 7.73 eV, which is also more than 0.50 eV above the PES value of 7.20 eV.[15] In a later study of the benzyl radical Lossing obtained a vertical ionization potential of 7.27 ± 0.03 eV,[26] in better agreement with the value from PES. The difference between the two electron-impact results was attributed to an underestimation of the onset of the ionization efficiency curve in the earlier study. This may also explain the difference between the electron impact and PES results for the α- and β - methylnaphthyl radicals.

Relative C-H Homolytic and Heterolytic Bond Dissociation Energies from Proton Affinities and Ionization Potentials. The thermochemical data that can be derived from the ionization potentials and proton affinities of the methylnaphthyl radicals presented above are summarized in Table 2. All of the data and assumptions needed for the calculation of the radical and carbonium ion heats of formation are also presented in Table 2. The data in Table 2 show that the α-methylnaphthyl and β-methylnaphthyl radicals have the same absolute heat of formation and C-H bond energies to within 2 kcal mol^{-1}. The absolute values in Table 2 require the use of the parent hydrocarbon heats of formation, the ionization potentials of the parent hydrocarbons, and the heat of formation of H^+, all of which add to the error estimate for the final result, to derive the heats of formation of the two radicals. The heat of formation of the α-methylnaphthyl radical calculated in this work, 62.9 ± 2.0 kcal mol^{-1}, does not

Table 2. Thermodynamic Data for the α-Methylnaphthyl and β-Methylnaphthyl Radicals and Carbonium Ions.[a]

R	$\Delta H_f^\circ{}_{298}[RH]g$[b]	IP[RH][c]	IP[R•][d]	PA[R•][e]	$\Delta H_f^\circ{}_{298}[R•]$[f]	$\Delta H_f^\circ{}_{298}[R+]$[g]	$D^\circ{}_{298}[R\text{-}H]$[h]	$D^\circ{}_{298}[R+\text{-}H\text{-}]$[i]
α-Methylnaphthyl	27.93±.64	8.01±.05eV	6.88±.03 eV	216.0	62.9	221.6	87.1	228.3
β-Methylnaphthyl	27.75±.62	8.01 .05 eV	6.93±.03 eV	216.0	62.8	222.6	87.1	229.5

a). All values in Table 2 were calculated using the stationary electron convention, which states that the heat of formation of an electron at rest is zero at all temperatures. This yields $\Delta H_f^\circ{}_{298}[H] = 52.1$ kcal mol^{-1} $\Delta H_f^\circ{}_{298}[H+] = 365.7$ Kcal mol^{-1} IP(H) = 13.598 eV. Unless otherwise noted all units are kcal mol^{-1}. Unless otherwise noted errors on the absolute values are estimated to be ± 2.0 kcal mol^{-1}, but relative values between the two isomers are known to ± 1.0 kcal mol^{-1}, see text. b). These values use estimated heats of vaporization of α- and β-Methylnaphthyl, ref. 27a. A more recently recommended value is available, but only for the β-isomer, ref. 27b and 27c. c). From ref. 28. d). This work, e). This work. Absolute values are ± 1.5 kcal, but the two isomers have the same proton affinity within 1 kcal mol^{-1}, see text. f). Derived from $D^\circ[R\text{-}H]$, equation 7, and $\Delta H_f^\circ{}_{298}[RH]$. g). Derived from $\Delta H_f^\circ{}_{298}[R•]$ and IP[R•], h). From equation 7. i). From $\Delta H_f^\circ{}_{298}[H-] = 34.7$ kcal mol^{-1} and $\Delta H_f^\circ{}_{298}[R+]$.

agree very well with an earlier determination of 59.6 ± 1.5 kcal mol^{-1} although the two numbers are within experimental error of each other. The reason for this discrepancy could be due to errors in the assignment of absolute values to the proton affinity scale,[24] and the choice of values for the heats of formation of the α-methylnaphthalene[27] in addition to incremental errors from the experimental values used in the calculations. Even though error limits of ± 2.0 kcal mol^{-1} have been assigned to the absolute values for the radical heats of formation, due to uncertainty in absolute values used to derive them the relative bond energies can be derived directly from the relative proton affinities. The proton affinity of a radical, defined as $-\Delta H$ for reaction 6 can also be written as shown in equation 7, where $D^{o}[R_1\text{-}H]$ is the homolytic C-H bond dissociation energy. Since the

$$-\Delta H_6 = D^{o}[R_1\text{-}H] + IP[H] - IP[R_1H] \qquad (7)$$

ionization potentials of the two methylnaphthalenes are equal[28] the difference in proton affinities between the α-methylnaphthyl and β-methylnaphthyl radicals directly gives the difference in homolytic C-H bond dissociation energies. The similarity observed for the reaction rates with the series of bases studied in this work suggests that the α-methylnaphthyl and β-methylnaphthyl radicals have C-H bond dissociation energies that are within 1.0 kcal mol^{-1} of each other. This result is reasonable, since the experimentally observed difference in H-atom abstraction rates by trichloromethyl radicals (β-methylnaphthalene reacts a factor of 0.682 slower than α-methylnaphthalene)[3] can be explained by a difference in activation energy of only 0.25 kcal mol^{-1}. The bond energy derived from the proton affinity is 87.1 ± 1.5 kcal mol^{-1}, which is 1.8 kcal mol^{-1} lower than the benzyl C-H bond energy in toluene.[29] This is in reasonable agreement with an earlier study which found that the C-C bond energy in α -

ethylnaphthalene is lower than the benzyl C-C bond energy in ethylbenzene by 2.9 kcal mol^{-1}.[6]

Since the ionization potentials of α-methylnaphthyl and β-methylnaphthyl radicals are nearly equal, the heterolytic C-H bond energies and carbonium ion heats of formation of the corresponding carbonium ions are calculated to be the same within experimental error. This result rules out estimates of the difference in carbonium ion stabilities that are greater than 3 kcal mol^{-1}.[30] The near equality of the ionization potentials obtained in this work show that if the carbonium ions are different by more than 2 kcal mol^{-1}, the radical heats of formation must differ by at least 1 kcal mol^{-1}. Further studies on the equilibrium between isotopically labelled α-methylnaphthyl and β-methylnaphthyl carbonium ions would determine the differences in heterolytic C-H bond energies with more precision.

1. Gleicher, G. J. *ACS Symp. Ser.* 1977, *69*, 227.

2. Olson, D. B.; Calcote, H. F. *Symp. (Int.) Combust. [Proc.]* **1980**, *18th*, 453.

3. Unruh, J. D.; Gleicher, G. J. *J. Am. Chem. Soc.* **1971**, *93*, 2008.

4. Huyser, E. S. *Ibid.* **1960**, *82*, 394.

5. (a) Herndon, W. C. *J. Org. Chem.* **1981**, *46*, 2119, and references therein. (b) Reference 3.

6. McMillen, D. F.; Trevor, P. L.; Golden , D. M. *J. Am. Chem. Soc.* **1980**, 102, 7400.

7. Streitwieser, A. Jr.; Hammond, H. A.; Jagow, R. H.; Williams, R. M.; Jesaitis, R. G.; Chang, C. J. Wolf, R. *Ibid.* **1970**, 92, 5141.

8. Greenberg, A.; Silverman, D. B. *J. Org. Chem.* **1982**, *47*, 3076.

9. Harrison, A. G.; Lossing, F. P. *J. Am. Chem. Soc.* **1960**, *82*, 1052.

10. (a) Hayashibara, K.; Kruppa, G. H.; Beauchamp, J. L. *J. Am. Chem. Soc.* **1986**, *108*, 5441. (b) Kruppa, G. H.; Beauchamp, J. L. *Ibid.* **1986**, 108, 2162.

11. (a) Solomon, J J.; Field, F. H. *J. Am. Chem. Soc.* **1975**, *97*, 2624. (b) Solomon, J. J.; Field, F. H. *Ibid.* **1976**, *18*, 1567. (c) Meot-Ner, M.; Solomon, J. J.; Field, F. H. *Ibid.* **1976**, *98*, 1025. (d) Sharma, R. B.; Sen Sharma, D. K.; Hiraoka, K.; Kebarle, P. *Ibid.* **1985**, *107*, 3747.

12. Meot-Ner, M. *J. Am. Chem. Soc.* **1982**, *104*, 5.

13. Kornblum, N.; Oliveto, E. P. *J. Am. Chem. Soc.* **1947**, *69*, 465.

14. Wolfrom, M. L.; Konigsberg, M.; Weisblat, D. I. *J. Am. Chem. Soc.* **1939**, *61*, 574.

15. Houle, F. A.; Beauchamp, J. L. *J. Am. Chem. Soc.* **1978**, *100*, 3290.

16. (a) Beauchamp, J. L. *Annu. Rev. Phys. Chem.* **1971**, *22*, 527. (b) Lehman, T. A.; Bursey, M. M. *Ion Cyclotron Resonance Spectrometry*; Wiley: New York, 1976.

17. (a) Comisarow, M. B.; Marshall, A. G. *Chem. Phys. Lett.* **1974**, *25*, 282. (b) Ledford, E. B., Jr.; Gharderi, S.; White, R. L.; Spencer, R. B.; Kulkarni, P. S.; Wilkins, C. L.; Gross, M. L. *Anal. Chem.* **1980**, *52*, 463. (c) Marshall, A. G. *Acc. Chem. Res.* **1985**, *18*, 316, and references contained therein.

18. Comisarow, M. B. *Int. J. Mass. Spectrom. Ion Phys.* **1981**, *37*, 251.

19. *Bio-Med* Tech, 2001 E. Galbreth, Pasadena, CA 91104.

20. Schulz, G. J.; Phelps, A. V. *Rev. Sci. Instrum.* **1957**, *28*, 1051.

21. Blint, R. J.; McMahon, T. B.; Beauchamp, J. L. *J. Am. Chem. Soc.* **1974**, *96*, 1269.

22. Lias, S. G.; Levin, R. D. *Natl. Stand. Ref. Data Ser., Natl. Bur. Stand.* **1982**, No. 71.

23. Cody, R. B.; Burnier, R. C.; Freiser, B. S. *Anal. Chem.* **1982**, *54*, 96.

24. Lias, S. G.; Liebman, J. G.; Levin, R. D. *J. Phys. Chem. Ref. Data* **1984**, *13*, 695.

25. Bowers, M. T. Ed., *Gas Phase Ion Chemistry*, Academic Press: New York, 1979; Volume 1.

26. Lossing, F. P. *Can. J. Chem.* **1971**, *49*, 357.

27. (a) Speros, D. M.; Rossini, F. D. *J. Phys. Chem.* **1960**, *64*, 1530. (b) Pedley, J. P.; Naylor, R. D.; Kirby, S. P. *Thermochemical Data of Organic Compounds*, Chapman and Hall: New York, 1986. (c) Karyakin, N. V.; Rabinovich, I. B.; Pakhomov, L. G. *Russ. J. Phys. Chem.* **1968**, *42*, 954.

28. Heilbronner, E.; Hoshi, T.; von Rosenberg, J. L.; Hafner, K. *Nouv. J. Chim.* **1976**, *1*, 105.

29. See references 10a and 12, and the references contained therein for a discussion of the value for the benzyl C-H bond dissociation energy in toluene.

30. See the discussion in reference 8, and references therein.